Unione Europea

Ministero dell'Istruzione, dell'Università e della Ricerca

UNIVERSITÀ DEGLI
STUDI DI SALERNO

FONDO SOCIALE EUROPEO

Programma Operativo Nazionale 2000/2006

"Ricerca Scientifica, Sviluppo Tecnologico, Alta Formazione"

Regioni dell'Obiettivo 1 – Misura III.4

"Formazione superiore ed universitaria"

Intelligent monitoring of the injection moulding process.

Umberto Vietri

Unione Europea

Ministero dell'Istruzione, dell'Università e della Ricerca

UNIVERSITÀ DEGLI STUDI DI SALERNO

FONDO SOCIALE EUROPEO

Programma Operativo Nazionale 2000/2006

"Ricerca Scientifica, Sviluppo Tecnologico, Alta Formazione"

Regioni dell'Obiettivo 1 – Misura III.4

"Formazione superiore ed universitaria"

Department of Chemical and Food Engineering

Ph.D. Course in Chemical Engineering
(IX Cycle-New Series)

INTELLIGENT MONITORING OF THE INJECTION MOULDING PROCESS

Supervisor
Prof. Roberto Pantani

Ph.D. student
Umberto Vietri

Scientific Referees
Prof. Giuseppe Titomalio
Prof. Antonio J. Pontes

Ph.D. Course Coordinator
Prof. Paolo Ciambelli

Publications list

U. Vietri, V. Speranza, R.Pantani, “Monitoring of injection moulding of thermoplastics: average solidification pressure as a key parameter for quality control” – Macromolecular Research – 2010 – in press (to appear in June 2011).

U. Vietri, A. Sorrentino, V. Speranza, R. Pantani, “Improving accuracy of injection moulding simulation software” – Polymer Engineering and Science 2010– in press (to appear in September 2011).

R. Pantani, U. Vietri, F. De Santis, A. Sorrentino, V. Speranza and G. Titomanlio, “Monitoring of Injection Molding of Thermoplastics and Identification of Key Parameters for Quality Control”. Proceedings of the Polymer Processing Society Europe/Africa Regional Meeting, PPS-2009, Larnaca (Cyprus), Ottobre 2009, Atti su CD su tre pagine.

R. Pantani, U. Vietri, F. De Santis, A. Sorrentino, V. Speranza, G. Titomanlio, “Monitoring of injection moulding of thermoplastics: average solidification pressure as a key parameter for quality control” – Proceedings in 26th Annual Meeting of the Polymer Processing Society – Banff, Canada – July 2010.

R. Pantani, F. De Santis, A. Sorrentino, V. Speranza, U. Vietri, G. Titomanlio, “Metodo e dispositivo per la determinazione dell'accuratezza dimensionale di manufatti stampati ad iniezione” Italian Patent n°SA2010A000009 22th March 2010 - Type: Inventions

Contents

Figures Index

Tables Index

Abstract

The quality requirements of injection-moulded components have become more stringent because of the growing s applications of plastics and increasing customer demands. The quality of the moulded parts depend on the processing conditions and this creates a continuous demand for developing advanced techniques for monitoring and controlling the process The current practice in industry is to adjust the parameters based on the product defects through trial and error, starting from information from the material supplier, mould designer, and, largely, on the basis of the moulding engineer's (or setup person's) own experience. Nevertheless, defects can occur in moulded parts due to, for instance, the variation in material properties (particularly when reground or biodegradable resins are used), the change in environmental conditions (e.g., humidity or temperature in the surroundings), and the machine characteristics (particularly those using hydraulic power). In this case, the process conditions have to be readjusted in order to re-establish the part quality targets. To overcome these difficulties, injection moulding quality control has been the subject of many off-line and on -line quality control studies. The purpose is to achieve automatic and adaptive quality control able to guarantee a stable and repeatable process, from the part quality point of view.

Temperature and pressure transducers are increasingly employed in the industry; therefore the use of their measurements to obtain indications concerning the product quality could overcome the traditional resistance of industry to introduce new sensors in their production. Cavity pressure is often considered the dominant factor determining the quality of the final product in injection moulding. A great deal of software for the control of quality and of cycle reproducibility is based on the comparison of the cavity pressure profile with a reference: when the profile substantially diverges

from the one chosen as a reference, the cycle is considered not consistent with the specification and the part is often rejected.

In this work, an attempt is made to identify a single parameter (using the cavity pressure and temperature signals) satisfactorily correlated with chosen quality parameters (i.e. in-plane shrinkage), in order to give a useful approach regarding on-line quality control in the injection moulding process. To reach this goal, a series of injection moulding tests have been conducted on several polymers, changing holding pressure and time, injection time, mould and injection temperature, nozzle length, gate and cavity thickness. The pressure histories and the temperature evolution at the interface with the mould at several positions along the flow-path were measured by means of pressure-temperature transducers. The samples were measured after moulding, in correspondence to the transducer positions and width shrinkage was assumed to be the target quality parameter. It was demonstrated that even the complete pressure curve cannot be adopted as a suitable parameter correlated with these quality features, and a criterion based on the reproducibility of the pressure profiles can cause the rejection of parts which are consistent with quality parameters. A different approach was thus considered, which basically consists in the determination of a single parameter, namely the local average solidification pressure Ps_av (the average over the thickness of the pressures at which each layer solidifies locally) which requires knowledge of both the local pressure history and the local solidification history. By plotting width shrinkage data versus the average solidification pressure values, Ps_av, it was demonstrated that this parameter is adequate for describing the quality of moulded parts.

Since the solidification history is not experimentally obtainable, a procedure was developed to obtain it directly with the local experimental pressure profile. The analysis was carried out using different materials: a Polystyrene, a Polycarbonate and Polypropylene.

A different parameter was detected for correlating with the part weight data. In fact it was observed that for samples having a positive average width shrinkage, weight is directly related to width shrinkage, and thus to $P_{sav.}$ *However , for samples showing an expansion, the correlation was poor and a further analysis was needed. With regard to this, as suggested in the literature, it was shown that cavity deformation plays a pivotal role, so the normalized part weight can be directly correlated with the average pressure inside the cavity at the instant when the gate solidifies, namely,* P_{gf}*. This approach used for analyzing sample weight data was adopted for all polymeric materials considered and led to a satisfactorily result for our purpose.*

Chapter One

Introduction

In this chapter a brief description of the injection moulding process is made with particular regard to the main operative variables involved in the process. Furthermore, on the basis of the indications of the scientific literature, the guide lines are given for implementing a system for monitoring and controlling the process from the quality of moulded product point of view.

I.1 Introduction

I.1.1 Injection Moulding process: generalities.

Injection moulding is one of the most versatile and important manufacturing processes, capable of mass-producing complicated plastic parts in net shape with excellent dimensional tolerance.

The process consists of three main phases: filling, packing and holding, and cooling. Raw material (resin), placed in the form of pellets inside the hopper, is fed into the barrel by the screw revolution. The solid resin is heat-melted by means of band heaters and by the frictional heat generated on the inside of the barrel too. When a sufficient amount of the molten resin accumulates in a pre-injection chamber, the screw moves quickly forward, along the axis of the barrel, injecting the molten resin into the mould through the nozzle. As the resin begins to cool, a holding pressure on the screw is imposed, in order to force more resin into the mould, compensating for volume reduction due to contact with the mould walls, and avoiding at the same time the backflow of material as well. After the resin at the gateway to the mould solidifies, the holding pressure is removed and the part remains in the mould to cool. When the part has sufficiently cooled, the mould opens and ejects the solid plastic part. In **Fig. 1** the injection moulding cycle is depicted showing the main phases until the product is obtained: injection, holding, plasticizing, cooling, and ejection.

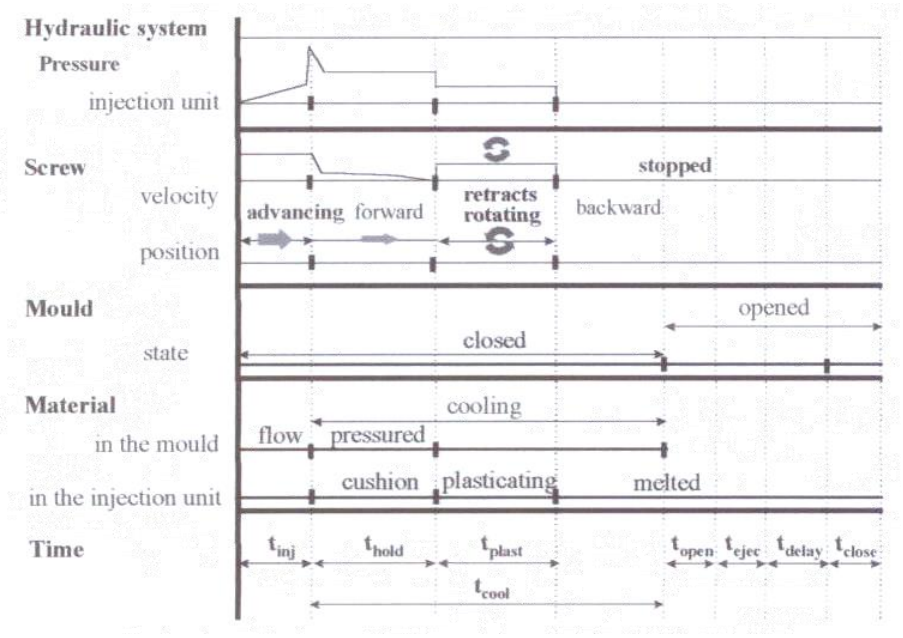

Fig. 1 Injection moulding cycle: (t_{inj}-injection time, t_{hold}-holding time, t_{plast}-plasticating time, t_{cool}-cooling time, $t_{open/close}$-mould opening/closing time, t_{ejec}-ejection time, t_{delay} delay time) **(Pontes 2002).**

I.1.2 The Injection Moulding process: the operative variables involved

The quality requirements of injection-moulded components have become more stringent because of the growing applications of plastics and increasing customer demands. Product quality takes into account both internal and external properties. The internal properties refer to the characteristics of the inner structure of a moulded part, including internal stresses, morphology (in terms of distribution of orientation, crystallinity, size of crystal structures) and the distribution of fillers and reinforcements. The external properties include weight, shrinkage and warpage, surface finishing, mechanical, optical and electrical properties of moulded parts. External properties are the main concern of producers and end-users and are usually monitored for quality control in the injection moulding industry.

During the process the polymeric material undergoes complicated thermo-mechanical histories, which, coupled to the large pressure values and rapid cooling imposed, involve modifications in its rheological, mechanical, and thermodynamic properties.

To guarantee that the mould part can be filled volumetrically, one has to take in account various factors regarding the part and mould designs as well as the material selection and process setup. The process parameters have a

pivotal role in determining the qualitative conformity of the injection moulded product. For example, larger holding pressures usually cause larger pressures inside the cavity and these, in their turn, give rise to larger product size. The effects are relatively small (for amorphous materials typically less than 1% deviation from mould dimensions) and for ordinary products do not cause serious problems. However, nowadays the trend is to attempt to produce by injection moulding products with very small tolerances. In this case, the exact knowledge of the final product dimensions is a strategic challenge, but on the basis of the abovementioned observations, one can understand that it is difficult to predict or control the quality of the injection-moulded products, without employing sophisticated computer simulation software during the design stage and frequent intervention by the machine operator during the manufacturing stage.

A proper setting of the optimal process parameters for injection moulding to minimize moulded part defects, and to match the design specifications consistently is very difficult to achieve due to the large number of factors involved. Current practice in industry is to adjust the parameters based on the product defects through trial and error, starting from information from the material supplier, mould designer, and, largely, on the basis of the moulding engineer's (or setup person's) own experience. This procedure, however, is both time consuming and costly and has to be repeated for each specific material/mould/machine configuration. Furthermore, even when the machine is properly set up, periodical checks of part quality are still necessary as a measure of quality assurance. In fact, defect occurrence in the moulded part can always take place due to, for instance, the variation in material properties (particularly when reground or biodegradable resins are used), the change in the environmental conditions (e.g., humidity or temperature in the surroundings), and machine characteristics (particularly those using hydraulic power). In this case, the process conditions have to be readjusted in order to re-establish the part quality targets. To overcome these difficulties, injection moulding quality control has been the subject of many off-line and on-line quality control studies. The purpose is to achieve automatic and adaptive quality control able to guarantee a stable and repeatable process, from the part quality point of view.

Because of the numerous variables involved in the complex injection moulding process, it is impossible to develop a suitable control strategy without a thorough understanding of the relationship and dependency among those variables (Chen and Turng 2005).

Wang et al. suggested identifying and dividing the important variables involved into three levels namely level 1 machine variables, level 2 process variables, and level 3 quality variables, as tabulated in **Fig. 2** (Wang, Zhou and Sakurai 1999), (Wang, Hieber, et al. 2000). These variables have a direct impact on the final part quality and process economics.

Level 1—Machine variables (independently controllable)
- Temperature
  - Barrel temperature (in several zones)
  - Nozzle temperature
  - Coolant temperature
- Pressure
  - Pack/hold pressure
  - Back (recovery) pressure
  - Maximum injection pressure
- Sequence and Motion
  - Clamp/fill/pack/hold/recovery/eject switchover point
  - Injection (ram) speed (constant or profiled)
  - Screw (rotation) speed
  - Shot volume and cushion (via screw displacement)

Level 2—Process (dependent) variables
- Melt temperature (in the nozzle, runner, or mold cavity)
- Melt pressure (in the nozzle, cavity)
- Melt-front advancement
- Maximum shear stress
- Rate of heat dissipation and cooling

Level 3—Quality definitions (final response)
- Part weight and part thickness
- Shrinkage and warpage
- Sink marks
- Appearance and strength at the weld lines
- Other aesthetic defects: burn marks, gate blushes, surface texture, etc.

Fig. 2 List of the three level variables (Chen and Turng 2005)

Level 1 variables are named "machine variables" because setting and control, are generally referred to the machine, which allows us to obtain these by means of proper sensors and controllers (working in feedback loop logic) such as the programmable logic controller (PLC) and proportional, integral, and derivative (PID) one.

The level 2 variables (process or dependent variables) depend both on the process conditions (the level 1 variables) and on the material, machine, and mould configuration chosen. They reflect the characteristics of the resin being processed and the machine dynamics, among other process and design parameters. Even if the majority of the modern injection moulding machines are predisposed for measuring this type of variable, in any case it is necessary to plan suitable facilities (for instance mould instrumentation for cavity pressure and temperature measurements) as reported in numerous publications (for instance: (Titomanlio, Brucato and Kamal 1987) (Harry 1992) (Jansen, Pantani and Titomanlio 1998) (Kamal, Varela and Patterson 1999) (Rawabdeh and Petersen 1999) (Pantani 1999) (Pontes 2002) (De Santis, et al. 2010)).

The quality variables, level 3, take into account different quality criteria. Depending on the applications and functional requirements of the part, different quality indices may be selected. Their control, became the main

goal for the expert in the injection moulding process, therefore many efforts have been carried out to establish a methodology to correlate machine, process and quality variables. Even though many works are available about process and machine controls, adequate knowledge about quality control, is still lacking. Authors (Chen and Turng 2005) recognize that real quality control without human intervention has not yet been realized, primarily due to the unsuitability of commercial transducers to measure quality in real time, and to the lack of a robust model able to correlate the checked variables with quantitative data of quality measures. Two major difficulties in implementing an on-line quality control in the injection moulding process are, first of all, the poorness of quantitative information concerning the relationship among machine, process, and quality variables and secondly the lack of online quality feedback information.

I.2 Objective of this thesis, and work done.

In-mould sensors can be obviously a valuable help for on-line measurements and hence for monitoring and control purposes. As a matter of fact, traditional hardware-based temperature and pressure transducers have been widely employed in the injection moulding field; however, the correlation between the measured evolution of temperature and pressure and product quality is not immediate. In this work an attempt is made to identify a single parameter which can be satisfactorily correlated with the chosen quality parameters (i.e. in-plane shrinkage) in order to give a useful approach regarding an on-line quality control in the injection moulding process. For this purpose, a series of injection moulding tests were conducted using a general purpose Polystyrene, changing holding pressure and time, injection time, mould and injection temperature, nozzle length, gate and cavity thickness. These tests have been performed using an instrumented research mould (equipped by pressure and temperature transducer), connected to a DAQ device for acquiring their signals along the flow path in the mould cavity. The aim was to find a suitable feature of the experimental pressure profile (single value of the pressure, time) which correlated with the parameter chosen as quality target for the moulded product. Consistently with this, the width dimensions of the moulded specimens were measured at the positions where the sensors were located, and the shrinkage values of the injected moulded specimens, were considered for analysis. Initially, an attempt was made to correlate the width shrinkage data with several machine parameters like hydraulic pressure and also the holding pressure and time. Similar analysis was extended to the experimental pressure and width shrinkage data referring to Polycarbonate and semicrystalline material like Polypropylene. Since the resulting correlations appeared to be very poor, a different approach was considered, based on the knowledge of both the local pressure history and the local solidification history, which determine the

local average solidification pressure Ps_av. Since the solidification history is not experimentally obtainable, it was necessary to perform the simulation of the whole injection moulding tests in order to obtain it. This operation involved only the Polystyrene cases and it allowed us to calculate the Ps_av values on the base of a jointly simulated-experimental calculus approach.

Furthermore, a different approach based on the use of the experimental pressure profile alone, to obtain local thermal solidification history, and thus the experimental average solidification pressure, was developed. For this activity an automatic calculus procedure based on Labview© platform was also developed. It was a very helpful tool since it allowed us to obtain Ps_av directly by the local experimental pressure acquired, and no simulation of the injection moulding test was required.

By implementing the approach and analyzing the results for each operative condition investigated, it was observed that the values of Ps_av obtained were fairly consistent with the ones obtained by means of the simulated solidification history, and this ensures the reliability of this approach towards our aim. Finally it was demonstrated how the Ps_av is able to describe width shrinkage data, regardless of the operative conditions adopted. Another important qualitative target which was considered for our purpose is the part weight of moulded product. In an attempt to correlate part weight of moulded samples with Ps_av, no satisfactorily relationship was obtained, for all the polymers considered. Following the suggestions of scientific literature, a different pressure feature, namely, the local pressure at the gate freeze off instant P_{gf} was considered for our aim. It will be demonstrated that in a certain hypothesis, it represents a suitable parameter for the part weight description.

I.3 Monitoring of Injection Moulding process: the state of the art

For precise and consistent part production, it is very important to be able to accurately monitor the suitable variables in injection moulding process, during each phase, in order to establish a key parameter for on-line quality control. Over the years, the attention in research and development in injection moulding process and quality control has shifted from control machine (machine control), to process (process control), and finally printed object through quality control (quality control). Referring to **Fig. 2**, the level 1 (machine control) has been recognized as a standard patent since the late 70s based on cycle time control. The first one (US3784657) was a system in which the viscosity of plasticized material being prepared in a shot was monitored as a function of a ram injection speed at constant hydraulic pressure. The time-interval was measured during ram advancement between the time at which a pressure relief valve was opened and the time that the cavity became substantially filled. If the time exceeded or fell below

predetermined limits, either the heat input to subsequent shots being prepared may be respectively raised or lowered in increments, high pressure injection time could be respectively added or subtracted in increments to increase the point in time at which lower secondary hydraulic pressure was applied, or injection pressure could be respectively raised or lowered. The second one (US4208176)was a system which provides for cycle time control by means of a response to actual material properties in the mould, rather than in response to elapsed interval time. In fact in this system, means were provided for reducing the injection pressure to the hold pressure when the measured or dynamic pressure in the cavity reached a pre-determined value; ending the hold pressure and initiating the cold / cure portion of the cycle by measuring the actual, physical condition of the plastic in the mould, such as pressure or temperature; opening the mould clamp to eject the moulded part and thus ending the cold /cure portion of the cycle in response to parameters based on actual, physical properties of the plastic in the mould such as pressure or temperature. The control machine cycle is thereby completely independent of time, thus minimizing cycle time.

All these type of systems were very helpful criteria which allowed industry to meet manufacturing deadlines and, in this case, provided indications about any failure in each part of the process, cycle by cycle.

Nowadays, there are many commercial control (Barber Colman Company 2003) (Milacron Inc. 2003) systems available on the market for machine control. These systems usually include function modules for controlling position/velocity, pressure, temperature, and motion sequences. The IMM, provides numerous electrical signals analogical/digital that can be used as a reliable input for programmable logic controller (PLC). Typically, a PLC sequence program or logic program is created for controlling a motion sequence such as clamping close/open, ejection, injection unit forward/ backward, and safety guard. The injection velocity, ram position, screw rotation speed, hydraulic system pressure at injection and backflow pressure, barrel temperature, and coolant temperature can be controlled via a conventional PID embedded in the intelligent modules.

To achieve consistent quality, the controller should be able to repeat the process conditions consistently with high accuracy. There are plenty of unpredictable disturbances, including those coming from polymer pellets and melt, which are very difficult to model and predict and, notwithstanding technological progress made in this field, traditional PID control sometimes cannot guarantee high standard machine performance. Moreover, it is well known to experts that the same mould, mounted on different machines operating with the same parameters (and hence the control of level 1) may produce different results from the quality moulded part point of view. Kelly et al. released an interesting work in which a comprehensive study into the performance of four different injection moulding machines is reported, using identical mould, polymer, and processing conditions (Kelly, Woodhead and

Coates 2005). It highlighted the difficulties in developing a rational system that would permit the use of the same mould on machines that could be very different. Mainly this study was about the analysis of both, start-up dynamics and the repeatability of the process. Authors showed that the modern machines guaranteed higher performance from the quality moulded properties point of view, notwithstanding the fact that the same mould and process condition were used. They supposed that this occurrence was due to better operative parameter control obtainable using modern machines rather than older ones, since, even small disturbances with respect to the set point of a certain variable, can produce unconformity in the quality of the moulded product. The authors considered the maximum tensile strength of sample as reference property, and observed variations of up to 10% depending on the press used to mould them. They attributed this event to the inability of older machines to keep the temperature unchanged either during the injection stage or in the post-injection one. As well, corresponding pressure cavity profile was different in any case. On the basis of these occurrences, and consistently with the directions of the scientific literature since the late '80s, the authors identified two proper critical parameters concerning the basic quality control in the injection moulding process: pressure cavity and temperature histories. Agralwal et al. set out to control the process variables rather than the machine variables in order to achieve desirable and consistent part quality since they represent the true indicators of the condition of the plastic inside the mould (Agralwal, Pandelidis and Pecht 1987). The characteristics of cavity pressure throughout all phases of injection moulding play a dominant role in determining part quality, which can be characterized by part weight, thickness, or other dimensional features like shrinkage and warpage. In addition to cavity pressure, other process variables, such as nozzle pressure, melt temperature, melt viscosity, and mould separation (in particularly when a high aesthetic performance is required for the moulded part), are widely employed in injection moulding process control. The validity of the suggestion has been proven in numerous research efforts which show that the polymer melt temperature and pressure have a very strong influence on the quality of the moulded part. In fact, even Harry suggested using cavity pressure as the best factor to correlate with the quality parameters properties of the product (Harry 1992). A few years later Rawabdeh and Petersen stated that on-line monitoring of the injection moulding operations required continuous measurements of different parameters while the machine was running (Rawabdeh and Petersen 1999). These measurements could be performed by direct contact between sensors and the molten material, such as in the case of pressure and temperature, or by monitoring the material through an optical window (as in the case of use of the infrared sensors), optical technique, or by indirect contact with the plastics, such as with ultrasound. Due to the inability of the current sensors to measure and interpret material physical properties, there is limited extent

of monitoring of the physical material properties, mainly limited to pressure and temperature measurements. Moreover the utilization of the infrared probe for use in injection moulding for nozzle, mould, and barrel applications has significant limitations. Hardware related that limitations are due to the need for a direct access to the polymer, which is not recommended in most cases (for instance in the case of the manufacturing of the moulded product with relevant aesthetic requirements (class 1 surface)). On the other hand, this occurrence does not allow us to obtain accuracy in performing some measurements (i.e.the temperature inside the moulded part). Also, the collection, interpretation, and analysis of the infrared signals due to low conductivity, radiation, and the optical properties of the polymers cause difficulties. In some cases, the infrared emissions from the molten polymer are corrupted by, and cannot be isolated from, the stray infrared emission from the hot mould. As far as the optical techniques are concerned, they were found to be highly sensitive in measuring material property variations, despite the fact they appear limited in this scope. In addition, the optical signals always come from the surface of the molten material and do not penetrate the material. Finally, the use of ultrasonic for monitoring polymer processing has been investigated by several researchers. Notwithstanding the fact there has been the recent development of high speed digitizers, and improvements in sensing capabilities, their use in monitoring polymer processing has been limited to the laboratory environment. On the basis of these observations, as a matter of fact, authors showed that the cavity pressure control and the melt temperature could be conveniently used as the best indicator of the moulding operation's performance, and as indirect indicators of the part final quality. MacFarlane and Dubay, provided useful information on the effect of changing moulding conditions on moulded part mass and cavity pressure for a two-phase screw –plunger injection moulding machine (Macfarlane e Dubay 2000). They showed that the variation of machine parameters, while the melt temperature was held constant, gave rise to the inconsistent part mass due to the varying amounts of backflow of material out of the mould cavity. In ensuring that the cavity's gate was sealed before the holding stage (plunger of screw is pulled forward) was finished, has resulted to maintaining a consistent part mass.

On the contrary the effect of melt temperature variation, resulted in changes in the part mass due to the change in polymer density. Moreover, they analyzed the effect on moulded part mass resulting from changing, one at a time, the injection rate, the hold time, and hold pressure. The results outlined in this paper demonstrated the general effects on cavity pressure by varying moulding variables. Substantially, they indicated that the cavity pressure profile can be used to explain variations in part mass. Many attempts have been made to model the volumetric shrinkage using PVT (pressure-volume temperature) diagrams (US-4767579; US-4850217; US-6019917). In practice, following the volume dependency on pressure and

temperature, the quality of the injection moulding process was guaranteed by controlling pressure and temperature precisely. To obtain constant size and mass for the moulded part, one had to ensure that the ejection of the moulded part should happen at atmospheric pressure and always at the same specific volume value. This was achieved by varying continuously the holding pressure, the screw rate, and both injection and mould temperature. On the basis of this approach, a method in which the parameters necessary for process control are recorded automatically during a "self learning" stage for the machine, has been realized. In this way, adjusting accurately the amount of material introduced into the mould cavity by means of a suitable valve, one could control the process without knowing beforehand the volumetric behaviour of the material. Similar approaches can be found in the literature of those years, which may be exemplified by the work published in 1999 (Kamal, Varela and Patterson 1999). The authors, (referring to Titomanlio, Brucato and Kamal 1987) stated that the key parameter for high performance of part quality in the injection moulding process was the average solidification pressure of the polymer, that was the combination of the entire history of temperature and pressure which the polymer had undergone inside the mould.

For the purposes of control, the bulk melt temperature was estimated from measurements by surface thermocouples at strategic locations in the cavity. A cascade scheme was implemented for the control of bulk temperature from cycle to cycle. A self-tuning algorithm, with an observer, was employed for controlling the cavity pressure-time profile, so that it followed a set point trajectory during a cycle. The factor of variation for pressure was related to the volumetric parameters of the polymer processed, which, depending if the volume of the part was too small or too large, was increased or decreased respectively. More recently other approaches have been proposed in the literature which is based on cavity pressure control; for instance, Gao et al. (Gao, Patterson and Kamal 1993) presented an algorithm to control the pressure in the cavity using the mould temperature. Pramujati et al. in their paper presented the design and implementation of a strategy to control the cavity pressure profile during the cooling stage (Pramujati, Dubay and Samaan 2006). The control strategy used a time constant τ as the controlled variable to represent the cavity pressure profile and coolant flow rate as the manipulated variable. The control simulation and real-time application results showed that the shape of the cavity pressure profiles could be controlled effectively and efficiently using τ and a predictive controller. Better control performance could also be achieved by controlling the cavity pressure during filling and packing, which guaranteed consistent cavity pressure at the end of the packing from cycle to cycle. (Jansen, Van Dijk and Husselman 1998) and (Jansen, Pantani and Titomanlio 1998) studied the effect of processing conditions on shrinkage in the injection moulding process of different materials by means of a simple thermo-elastic

model. Apart from all other considerations, the most significant information which emerged was that the average over the sample cross section of the solidification pressure, appeared to be the most relevant feature in determining shrinkage behaviour. In fact whilst the effects of injection velocity and mould temperature on shrinkage were much smaller and differed for each material, the shrinkage of injection moulded products was, in any case, highly influenced by the holding pressure and the melt temperature, that defined, precisely, the average solidification pressure.

Chapter Two

Experimental procedures

The material and methods which have been used in the experiment will be described, with the equipment and mould arrangements. Furthermore, a preliminary description of the influence of the operating conditions on pressure profile, is provided

II.1 Relevance of cavity's pressure profile: influence of injection moulding variables

The main purpose of this thesis is to find a single processing parameter able to correlate the effect of processing conditions, on the product quality in terms of weight and in-plane shrinkage. In order to detect the properly processing parameter, a detailed analysis of some monitored signals, during the injection moulding tests (performed varying either, process conditions, or mould and nozzle geometry), has been done. At the same time the samples belonging to any experimental condition investigated were measured after moulding, and in turn, in-plane width shrinkage and part weight data were obtained. To determine the effect of each operative variable on the part quality target chosen, each monitored signal (or qualified feature), was correlated to the corresponding target quality data; on the basis of this approach, it was possible to detect the best parameter for quality part description in the injection moulding process.

As stated earlier, the monitoring of thermo mechanical history variables (like temperature and pressure) inside the mould can represent a useful approach for our purpose. In order to help our understanding of the following results, in Fig. 3 a typical qualitative pressure evolution inside the mould cavity is plotted with its main features.

.

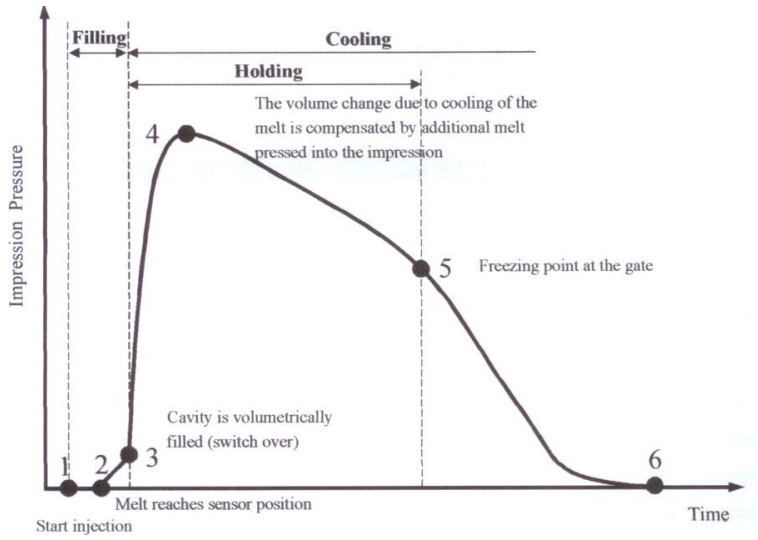

Fig. 3 Typical pressure evolution inside the mould's cavity (Pontes 2002)

Any changes in the injection moulding process due to temperature, flow rate, holding pressure and time, cause changes in this profile. In **Fig. 4** the qualitative effect caused by the changing of these variables in the cavity pressure profile is shown. It appears that an increase of both, the holding pressure, and time, lead to the higher level pressure in the mould cavity Where the effect of the flow rate increases, it pushes down the cavity pressure profile, since the injection stage, is reduced. Finally, the mould temperature increments, enlarge the cavity pressure profile, as the cooling stage is delayed.

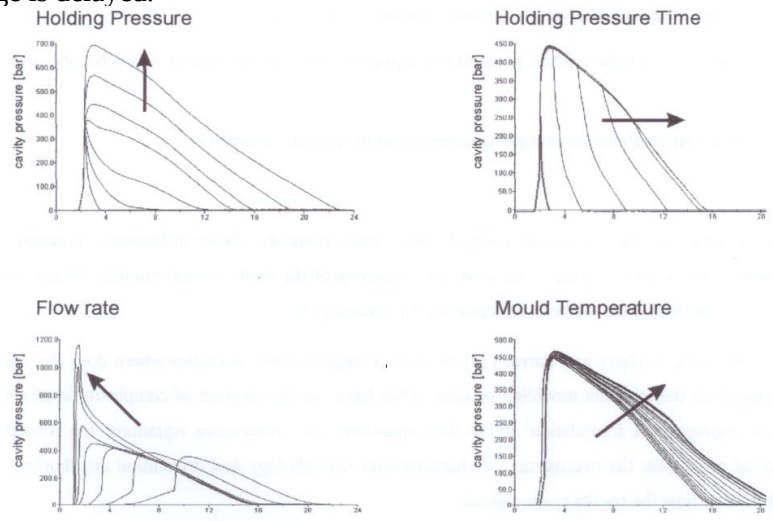

Fig. 4 The influence of some injection moulding variables on the pressure evolution profile inside the mould cavity (Pontes 2002)

II.2 Materials

In order to obtain a full investigation, making as general as possible any considerations about the subject through the present activity, three different thermoplastic polymers were used; a semi-crystalline polypropylene and two amorphous thermoplastics: atactic polystyrene and polycarbonate.

II.2.1 Polystyrene PS 678E

The material used was a general purpose Polystyrene (PS 678E) supplied by Dow Chemicals, with a molecular weight distribution characterised by Mn=(87±4) 10^3, Mw=(250±20) 10^3 and Mz=(490±60) 10^3. The resin was well characterized and relevant properties (Flaman 1990) (Laven 1985) (Pantani 1999) are summarized below.

The thermal conductivity of the resin is reported (Pantani, Speranza and Titomanlio 2001a) as essentially constant with the temperature; in particular at T = 343K and T = 473 K (i.e. above and below glass transition temperature) the values 0.165 W/m K and 0.18 W/m K were reported, respectively. The Specific heat of resin, as measured by (Flaman 1990) at different temperatures is given in **Table 1**.

Table 1 Specific heat of PS 678E (Flaman 1990)

Temperature [K]	Specific heat [J/Kg K]
523	2300
473	2150
423	2000
373	1900
363	1600
353	1500
343	1450
333	1400

Typical properties of solid PS 678E are resumed in **Table 2**.

Table 2 Properties for PS 678E

	Method	Value	Unit	Reference
Physical property				
Density	ISO 1183	1050	Kg m^{-3}	[1]
Mechanical Property				
Elasticity Modulus, 23°C	ISO 178	3255	MPa	[1]
Yield Stress	ISO 527-1/-2	43	MPa	[2]
Strain at break	ISO 527-1/-2	2	%	[1]
Poisson's coefficient ν	-	0.33	[-]	[1]
Ball indentation hardness	ISO 2391/-1	150	MPa	[2]
Thermal Property				
Thermal Conductivity	ASTM C177	0.17	W m^{-1} K^{-1}	[3] [4]
Specific Heat	ASTM C351	See **Table 1**	J Kg^{-1} K^{-1}	[3]
Vicat softening point (50°C/h 50N)	ISO 306	86	°C	[2]
Coefficient of linear thermal expansion α_L	ASTM D696	7.5 10^{-5}	K^{-1}	[1]
Linear Compressibility β_L	ASTM D696	1.04 10^{-4}	MPa^{-1}	[1]
Processing characteristics				
Melt Flow Index (200°C, 5 Kg)	ISO 1133	11	g 10 min^{-1}	[2]
Injection temperature range		200 ÷ 240	°C	[5]
Mould temperature range		20 ÷ 70	°C	[5]
Maximum shear stress		0.25	MPa	[5]
Minimum shear rate		40000	s^{-1}	[5]

[1] (Pantani, Analysis of Shrinkage Development" Ph.D Thesis¬ 1999)
[2] (www.materialdatacenter.com n.d.)
[3] (Flaman 1990)
[4] (Pantani, Speranza and Titomanlio, Relevance of mold-induced thermal boundary conditions and cavity deformation in the simulation of injection molding 2001a)
[5] (MoldFlow Plastic Insight 2006)

II.2.2 PolyCarbonate Lexan 141R (Pontes 2002).

A second amorphous thermo-plastic polymer was used: polycarbonate PC Lexan 141R supplied by GE Plastics (Europe) with a molecular weight distribution characterised by M_n=10.7 10^3, and M_w=25.6 10^3 (General Electrics Plastic Europe 1999). Some relevant physical, mechanical, thermal and processing characteristics of the material are reported in **Table 3**

Table 3 Properties for PC Lexan 141R

	Method	Value	Unit	Reference
Physical property				
Density	D 792	1190	Kg m^{-3}	[6] [7] [8]
Mechanical Property				
Flexural Modulus, 23°C	D 790	2343	MPa	[6, 7,8]
Tensile Strength	D 638	69	MPa	[6] [7] [8]
Elongation at break	D 638	130	%	[6,7,8]
Poisson's coefficient ν	-	0.417	[-]	[9]
Charpy impact strength	D256	31.8	KJ m^{-2}	[7]
Thermal Property				
Thermal Conductivity	ASTM C177	0.25	W m^{-1} K^{-1}	[6]
Specific Heat	ASTM C351	1300	J Kg^{-1} K^{-1}	[6]
Vicat softening point (50°C/h 50N)	ASTM D1525	154	°C	[6,7]
Coefficient of linear thermal expansion α_L	ASTM D696	6.84 10^{-5}	K^{-1}	[6]
Linear Compressibility β_L	ASTM D696	-	-	-
Processing characteristics				
Melt Flow Index (300°C,1.2 Kg)	ASTM D1238	10.5	g *10 min^{-1}	[6,7]
Injection temperature range		270 ÷ 310	°C	[7]
Mould temperature range		70 ÷ 100	°C	[7]
Maximum shear stress		0.5	MPa	[9,7]
Minimum shear rate		40000	s^{-1}	[9,7]

[6] (www.materialdatacenter.com n.d.)
[7] (Pontes 2002)
[8] (General Electrics Plastic Europe 1999)
[9] (MoldFlow Plastic Insight 2006)

II.2.3 Polypropylene HIFAX BA 238 G3 (De Santis, et al. 2010)

Finally, a semi-crystalline thermo-plastic polypropylene with increased isotactic index supplied by Montell M_n=55.6 10^3, and M_w=37.6 10^4 (Montell Polyolefins (1998)) was used. This grade of polypropylene is compounded with about 26% in weight of ethylene-propylene rubber, which gives high impact strength, and 1.5% talc employed as a nucleating agent. The relevant physical, mechanical, thermal and processing characteristics are summarized in the following **Table 4**.

Table 4 Properties for HIFAX BA 238 G3

	Method	Value	Unit	Reference
Physical property				
Density	D 792	900	Kg m^{-3}	[10]
Mechanical Property				
Flexural Modulus, 23°C	D 790	1000	MPa	[11]
Tensile Strength	D 638	20	MPa	[10,11]
Elongation at break	D 638	400	%	[10,11]
Poisson's coefficient ν	[-]		[-]	
Notched Izod impact strength	D 256	80 (-30°C) 140 (0°C) >600 (23°C)	J m^{-1}	[10,11]
Thermal Property				
Thermal Conductivity	ASTM C177	0.172	$Wm^{-1}K^{-1}$	[12]
Specific Heat	ASTM C351	2620	J Kg^{-1} K^{-1}	[11,12]
Vicat softening point (50°C/h 50N)	ASTM D1525	55	°C	[10,11]
Latent Heat of crystallization		1.88 10^5	J Kg^{-1}	[12]
Coefficient of linear thermal expansion α_L	ASTM D696	2 10^{-4} (crystalline 72.5%)	K^{-1}	[10]
	ASTM D696	6.55 10^{-4} (amorphous 72.5%)	K^{-1}	[10]
Linear Compressibility β_L	ASTM D696	1.0 10^{-5} (crystalline 72.5%)	MPa^{-1}	[10]
	ASTM D696	9.8 10^{-4} (amorphous 72.5%)	MPa^{-1}	[10]
Processing characteristics				
Melt Flow Index (230°C,2.2 Kg)	ASTM D1238	13	g/10min	[10]
Injection temperature range		180÷290	°C	[11]
Mould temperature range		20÷60	°C	[11]
Maximum shear stress		0.26	MPa	[11,13]
Minimum shear rate		24000	s^{-1}	[11]

[10] (De Santis, et al. 2010)
[11] (Pontes 2002)
[12] (Pantani, Speranza and Titomanlio 2001 b)
[13] (Moldflow Plastic Insight data base ver. 6.1)

II.3 Rheology description

The viscosity of all the materials used in this work is well described by a simple Cross WLF viscosity model which is given by the following equations (2.1):

$$\eta(\dot{\gamma},T,P)=\frac{\eta_0(T,P)}{1+\left(\frac{\eta_0(T,P)\dot{\gamma}}{\tau^*}\right)^{1-n}} \qquad (2.1)$$

In eq.(2.1) η is the viscosity (Pa. sec.), $\dot{\gamma}$ is the shear rate (1/sec.), T is the temperature (deg.K), P is the pressure (Pa). Finally η_0 is the zero shear rate viscosity which is given by the modified-WLF equation.

$$\eta_0(T,P)=D_1\cdot\exp\left[\frac{-A_1\cdot(T-D_2-D_3P)}{A_2+T-D_2}\cdot\right] \qquad (2.2)$$

The terms τ*, D_1, D_2, D_3, A_1, A_2 are data-fitted coefficients. In the rheological model τ* is related to the relaxation time of the material, whereas D_2 and D_3 respectively represent, the glass transition temperature T_g, and the pressure effects on viscosity.

The Cross-WLF model constant values are given in **Table 5**.

Table 5 Constant values of Cross-WLF model.

Parameters	PS 678E[14]	PC Lexan 141R [15]	PP Hifax 238 GE [16]	Unit
n	0.252	0.17	0.2992	[-]
τ	30.8	716.5	23.25 (**)	kPa
D1	47.6	$2.68\ 10^3$	$168\ 10^3$	GPa s
D2	373.15	417.15	263.15	K
D3	0.51	0.2	0.5	K MPa^{-1}
A1	25.74	31.67	13.75	[-]
A2	61.06	51.6	51.6	K
f	0	0	1015	[-]
h	0	0	250	[-]
m	0	0	0.09	[-]

With regard to PP Hifax 238 GE, Authors (Pantani, Speranza and Titomanlio 2001 b) observed that the effect of crystallinity degree χ on material viscosity was very meaningful (taking an increase of viscosity by one order of magnitude as a non-flow condition). Accordingly, a modified Cross model describing the rheological behaviour which takes into account this occurrence, was adopted.

$$\eta(\dot{\gamma},T,P,\chi)=\frac{\eta_0(T,P)}{1+C\left(\eta_0(T,P)\dot{\gamma}\right)^{1-n}}\left[1+f\exp\left(\frac{-h}{\chi^m}\right)\right] \qquad (2.3)$$

Furthermore, PVT behaviour in equilibrium conditions, for all the materials, referred to a characterisation procedure based on isothermal compression volume changes, measurements starting at each temperature from atmospheric pressure. The PVT behaviour explored as specified above, is described by the modified form of the Tait equation.

$$v(T,P)=v_0(T)\left(1-c\ln\left(1+\frac{P}{B(T)}\right)\right)+v_r(T,P) \qquad (2.4)$$

[14] (MoldFlow Plastic Insight 2006)
[15] (Pontes 2002)
[16] (Pantani, Speranza and Titomanlio 2001 b)
(*)This value was not included in the MoldFlow data base ver. 6.1 (MoldFlow Plastic Insight 2006) which originally has taken 0; the same value was estimated by (Zoetelief 1995).
(**) (Pontes 2002)

Where $v(T,P)$ is the specific volume [m^3/Kg] at temperature T [K] and pressure P [Pa], v_0 is the specific volume at zero gauge pressure, c is a universal constant 0.0894 (Flaman 1990). Instead, B takes into account the pressure sensitivity of the material and $v_r(T,P)$ which is the value for crystalline resins only applies to temperature values below the transition one (clearly for the amorphous ones). Both are defined below in **Table 6**.

Table 6 Summary of modified Tait Model Coefficient used.

	Upper temperature region (T > Tr(P))	Lower temperature region (T < Tr(P))
vo(T)=	$B_{1m}+B_{2m}\,T_c$	$B_{1s}+B_{2s}\,T_c$
B(T)=	$B_{3m}\exp(-B_{4m}\,T_c)$	$B_{3s}\exp(-B_{4s}\,T_c)$
$v_r(T,P)$=	0	$B_7\exp(B_8\,T_C - B_9\,P)$
T_c =	$T - B_5$	
$T_r(P)$=	$B_5 + B_6\,P$	

Where B_{1m}, B_{2m}, B_{3m}, B_{4m} and B_5 (which represent the volumetric transition temperatures, T_r, at zero gauge pressure) are data-fitted coefficients. Similarly B_{1s}, B_{2s}, B_{3s}, B_{4s}, B_7, B_8, and B_9 are data-fitted coefficients for modelling in the lower temperature region. The dependence of T_r on pressure is described in the bottom line of the table in which B_6 is a corresponding data-fitted coefficient. The values of the parameters to be used in eq.(2.4) values are given in **Table 7**.

Table 7 Values of Tait Model Coefficient appearing in eq.(2.4).

Parameters	PS 678 E [17]	PC Lexan 141R [18]	PP Hifax 238 GE [19]	Unit
B5	377.23	417.15	428.15	K
B6	0.3495	0.348	0.0715	$K\ MPa^{-1}$
B1m	$0.972\ 10^{-3}$	$0.854\ 10^{-3}$	$1.275\ 10^{-3}$	$m^3\ kg^{-1}$
B2m	$6.044\ 10^{-7}$	$5.66\ 10^{-7}$	$1\ 10^{-6}$	$m^3\ kg^{-1}\ K^{-1}$
B3m	**42.8 (*)** (thinner cavity) **76.8(**)** (thicker cavity)	182	86.6	MPa
B4m	**$2.48\ 10^{-3}$(*)** (thinner cavity) **$3.14\ 10^{-3}$(**)** (thicker cavity)	$4.041\ 10^{-3}$	$5.181\ 10^{-3}$	K^{-1}
B1s	$0.972\ 10^{-3}$	$0.16\ 10^{-3}$	$1.184\ 10^{-3}$	$m^3\ kg^{-1}$
B2s	$2.248\ 10^{-7}$	$1.6\ 10^{-7}$	$6\ 10^{-7}$	$m^3\ kg^{-1}\ K^{-1}$
B3s	**48.1(*)** (thinner cavity) **89.8 (**)** (thicker cavity)	299	147	MPa
B4s	**$9.86\ 10^{-4}$(*)** (thinner cavity) **$1.43\ 10^{-3}$ (**)** (thicker cavity)	$1.711\ 10^{-3}$	$4.589\ 10^{-3}$	K^{-1}
B7	0	0	$0.907\ 10^{-3}$	$m^3\ kg^{-1}$
B8	0	0	0.1256	K^{-1}
B9	0	0	$12.1\ 10^{-3}$	MPa^{-1}

II.4 Moulding and Equipment.

II.4.1 Injection Moulding machine

With regard to PS678E, a 70-ton Negri-Bossi reciprocating screw, injection moulding machine was used for the experiments; whereas a 65-ton Pentatron Penta 65/185 reciprocating screw injection moulding machine was used for PC Lexan 141R, and PP Hifax BA238GE (De Santis, et al. 2010) tests. The main characteristics of the machines are summarized in **Table 8**.

[17] (MoldFlow Plastic Insight 2006)
[18] (Pontes 2002)
[19] (De Santis, et al. 2010)
(*) (**)These values were not included in the MoldFlow data base ver.6.1 (MoldFlow Plastic Insight 2006) which originally have taken B3m=185 [MPa] and B3s=264 [MPa] B4m=4.93 10^{-3} [K^{-1}] and B4s=3.51 10^{-3} respectively. The way of calculation of these parameter will be explained in § [IV.2].

Table 8 Technical data for the Injection Moulding Machines used

IMM		
Model	Negri-Bossi V70-150 h /65v	Pentatron Penta 65/185
Power	hydraulic press technology	hydraulic press technology
Screw diameter	25 [mm]	34 [mm]
Screw L/D ratio	22	22
Theoretical injection capacity	76 [cm^3]	155 [cm^3]
Shot weight PS	69 [g]	145 [g]
Injection rate	53 [cm^3/s]	75 [cm^3/s]
Max. pressure on material (injection stadium)	2160 [bar]	1475 [bar]
Screw speed	10-320 [min^{-1}]	10-350 [min^{-1}]
Plasticising capacity PS	32.4 [kg/h]	72 [kg/h]
Barrel heating zones	3	3
Installed Heating capacity	4.5 [kW]	5,29 [kW]
Nozzle contact force	19 [kN]	29 [kN]
Clamping force	700 [kN]	650 [kN]
Mould max. -opening stroke	310 [mm]	160-315 [mm]
Mould height min/max	120-320 [mm]	120-350 [mm]
Distance between tie bars HxV	360 x 315 [mm]	315 x 315 [mm]
Pump driving power	11 [kW]	11 [kW]

In some cases, a temperature controller unit was also provided to set mould temperature. A HAAKE thermo regulator K20 model (using water as the medium) was used for PS 678E injection moulding tests, whereas a PIOVAN TH 9/OCNOT (using oil as medium) was used for the other materials.

II.4.2 Nozzle and Mould

To perform the experiments regarding PS 678E, 70 ton- Negri-Bossi IMM was equipped with two different nozzles both having the same diameter 2.2 [mm], one 108 [mm] long (which will be indicated as short) and another one 300 [mm] long (which will be indicated as long). The 65 ton- Pentatron Penta 65/185, to perform the injection moulding tests for PC Lexan 141R and PP Hifax BA238GE, was equipped with a nozzle of diameter 2.2 [mm] and length 40 [mm] (Pontes 2002), (De Santis, et al. 2010). No other different technical issues were considered as regards the equipment used for performing the tests. The sprue tapered from a diameter of 7 [mm] (at mould side) to a diameter of 4.7 [mm] (at nozzle side) over a length of 80 mm. The runner had a diameter of 8 [mm] and was 68 [mm] long. The material was injected into a line gated rectangular cavity of 120

[mm] x 30 [mm] x 2L, where 2L was the cavity thickness. Two different values for cavity thickness 2 [mm] and 4 [mm] were considered in performing the tests. Special dies containing different gates could be assembled in the mould, in particular use was made of three gates having the same width of the cavity, length of 6 [mm] and three different thickness 2 [mm] 1.5 [mm] or 0.5 [mm]. All these features will be considered in the settings of the project for the injection moulding test simulation [Chapter IV]. The moulding machine and the mould were equipped with five piezoelectric transducers for pressure measurement, which were located along the flow path: one in the injection chamber, one just before the gate and three in the cavity at 15 [mm], 60 [mm] and 105 [mm] from the gate. These positions will be referred to as P0, P1, P2, P3 and P4, respectively. The transducers signals were acquired by a data acquisition system and stored in a desktop computer. A complete description of cavity geometry is given in **Fig. 5**.

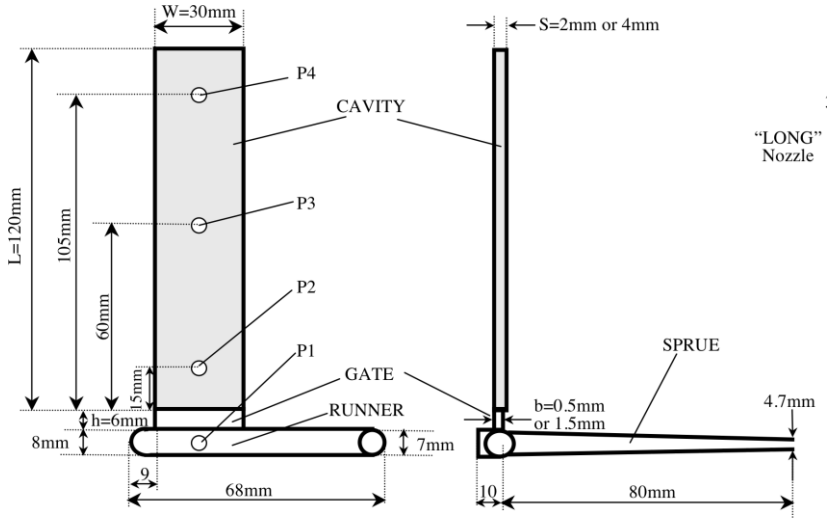

Fig. 5 Cavity Geometry

II.4.3 Moulding condition for PS 678E plates.

The moulding experiments were carried out by changing holding pressure, holding time, mould temperature and injection temperature. The time after holding (cooling time) was constantly kept at 30 [s]. In **Table 9** processing conditions for PS678E are summarized.

Table 9 Summary of Injection Moulding processing conditions for PS678E

Series	Holding Pressure, Ph [bar]	Holding time, th [s]	Injection time [s]	Melt temp., T_{inj} [°C]	Mould temp, T_{mould} [°C]	Gate thickness [mm]	Cavity thickness [mm]	Nozzle
A	80 to 1100	12	0.45	**220**	25	1.5	2	short
	800 to1100 (*)([20])	30						
B	80 to 1300	12	0.45	**200**	25	1.5	2	short
	900 to 1300 (*)	30						
C	330 to 1300	12	**2.2**	220	25	1.5	2	short
	980 to 1300 (*)	30						
D	80 to 1300	12	0.6	220	25	**0.5**	2	short
	1100 to 1300 (*)	30						
E	80 to 900	12	0.45	220	**55**	1.5	2	short
	800 to 900 (*)	30						
F	1000	**1 to 30**	0.45	220	25	1.5	2	short
G	90 to 1050	12	0.56	220	25	1.5	**4**	short
	950 to 1050 (*)	30						
H	80 to 1050	12	0.45	220	25	1.5	2	**long**
	900 to 1050 (*)	30						

As can be observed, each series test, has been performed imposing two different holding time values, keeping the same value for the other operative conditions. In the following sections [§ V.2] dedicated to the results, the necessity to perform some tests using a very long holding time will be explained.

(*) Long holding time injection molding tests for determining the solidification history of polymer

II.4.4 Moulding condition for PC Lexan 141R (Oliveira 1999) .

Experimental pressure data regarding the injection moulding tests for Polycarbonate supplied by (Oliveira 1999) were considered in this study. (Width shrinkage measurements on moulded specimens were performed referring to the method which will be illustrated in the following § II.4.6). The moulding experiments were carried out by changing holding pressure, holding time, and setting a constant value for both mould and injection temperature. In **Table 10** processing conditions for PC Lexan 141R are summarized.

Table 10 Summary of Injection Moulding processing conditions for PC Lexan 141R (Oliveira 1999)

Holding Pressure, Ph [bar]	Holding time, th [s]	Injection time [s]	Melt temp., T_{inj} [°C]	Mould temp, T_{mould} [°C]	Gate thickness [mm]	Cavity thickness [mm]	Nozzle
360 to 800	15	1.5	310	75	2	4	short
490	**0 to 15**	1.5	310	75	2	4	short

II.4.5 Moulding conditions for PP Hifax BA238GE (De Santis, et al. 2010).

Experimental data regarding the injection moulding tests for Polypropylene supplied by (De Santis, et al. 2010) (including width shrinkage measurements on moulded specimens) were considered in this study. The mouldings were produced setting a constant value for both the mould and injection temperature at 25 °C and an injection temperature of 230 °C; the flow rate was set up in the machine controller at 27 cm^3/s, resulting in an injection time of 0.5 [s]. The time after holding (cooling time) was constantly kept at 15 [s]. In the following **Table 11** the relevant processing conditions for PP Hifax BA238GE are reported.

Table 11 Summary of Injection Moulding processing conditions for PP Hifax BA238GE (De Santis, et al. 2010)

Holding Pressure, Ph [bar]	Holding time, th [s]	Injection time [s]	Melt temp., T_{inj} [°C]	Mould temp, T_{mould} [°C]	Gate thickness [mm]	Cavity thickness [mm]	Nozzle
180 to 700	10	1	230	25	1.5	2	Short
180 to 700	10	1	230	25	**0.5**	2	Short
400	**0 to 18**	1	230	25	1.5	2	Short

II.4.6 As-moulded width shrinkage measurements and error bars.

In this thesis, width shrinkage was calculated by means of the following relationship.

$$s_i = \left(d_{0i} - d_i\right) / d_{0i} \qquad (2.5)$$

where d is the product width and do is the corresponding local cavity width at 303 [K]. The subscripts indicate the position inside the cavity where width shrinkage was measured (s_i indicates the transducer position Pi). According to this definition, shrinkage is opposite to strain, and it will be negative if the part dimension becomes larger than the impression. After ejection, moulded specimens were allowed to equilibrate at room temperature (about 303 [K]) for 10 minutes. Then width dimensions at P2, P3 and P4 and of three successive samples were measured with digital callipers (accuracy 0.01mm). Average measurement scatter turned out to be close to instrument accuracy. The results of these measurements were corrected using the material coefficient of thermal expansion ($7.5\ 10^{-5}$ [K^{-1}]) in order to obtain sample dimensions all at the same temperature which, as already mentioned, was chosen as 303 [K]. Mould dimensions at 303°K (Pantani 1999) are given in Table 12.

Table 12 Mould dimensions at room temperature.

Nominal Cavity thickness 2 [mm] (Pantani 1999)			
Position	Length [mm]	d_0 Width [mm]	Thickness [mm]
P2	120.07	30.04	2.0385
P3		30.05	2.0387
P4		30.04	2.0372
Nominal Cavity thickness 4 [mm] (Oliveira 1999)			
Position	Length [mm]	d_0 Width [mm]	Thickness [mm]
P2	120.05	29.94	3.90
P3		29.96	3.91
P4		29.95	3.92

II.4.7 As-moulded normalized part weight.

For each case investigated, three consecutive samples were weighed after cutting out the scraps (i.e. considering only the part marked in gray in **Fig. 5**) by means of a balance (accuracy 0.01 [g]). For our purpose, the average value of the measurements were considered, in order to calculate the normalized part weight percentage which is defined in the equation (2.6):

$$\Delta M\% = \frac{M_0 - M}{M_0} \tag{2.6}$$

where M_0 is the product of cavity volume (V_0) and polymeric density (ρ) at room condition (reported in the previous section § II.2);

$$M_0 = \rho \cdot V_0 \tag{2.7}$$

If the density is constant, on the basis of the proportionality between mass and volume, the normalized part weight corresponds to the volumetric shrinkage. In **Table 13**, the values of M_0 calculated for the different cases, are summarized.

Table 13 Summary of M_0 values considered in eq.(2.6).

Polymer	Cavity volume V_0 [mm^3]	M_0 [g]
PS 678E	7482	7.35
	14964	14.7
PC Lexan 141R	15145	16.5
PP BA238GE	7482	6.5

II.5 Moulding identification.

It is useful to identify for the mouldings, a code corresponding to the processing variable used. With regard to Polystyrene, in the previous table (see **Table 9**), the different experimental cases have already been identified by a letter.

The whole code is completed by adding information about the process variable considered:

Series A _Ph500[bar]_th..

The first label **Series A** refers to a particular configuration (as reported in **Table 9**), whereas _Ph500 indicates the corresponding measured holding pressure value [bar].The third label indicates the holding pressure time imposed in performing the tests.

For Polycarbonate (Oliveira 1999) a single cavity and nozzle dimension were considered. Furthermore a single value either for injection, mould temperature, or for injection time was considered. Likewise the same was done for Polypropylene (De Santis, et al. 2010). Then for both a different code was considered, for instance:

PC_Ph500[bar]_th..

The first label refers to the material processed.

The second number indicates the particular measured holding pressure value [bar] to which the test refers. The third label indicates the holding pressure time imposed in performing the tests.

Chapter Three

Experimental procedures: results and discussion.

In this chapter, the experimental cavity pressure time profiles are reported, for several series which are representative of all the operative conditions considered. Furthermore, a preliminary attempt was made to find an adequate correlation between holding pressure/time and the quality parameters chosen for the moulded parts.

III.1 Moulding experimental pressure.

In this section the pressure evolution during the injection moulding of the sample will be presented. The experimental pressure evolution is used to obtain objective information about the flow rate , the extent of the filling, the holding and the cooling progress, and to validate some simulation. Furthermore the comparison between the experimental and simulated pressure curve will be analysed examining the effect of the pressure on viscosity and the mould deformation.

III.1.1 Experimental pressure for PS 678E tests

Particularly, for the case of PS 678E, a very wide range of process conditions (as recognizable in **Table 9**) was adopted, to explore an extremely wide range of situations that occur inside the cavity. In order to make the understanding of the results easier, we have reported in **Fig. 6-11** several pressure curves, belonging each to a different series of experiments, which gave rise to about the same sample weight and about the same width shrinkage. For the same holding time cases (except the F series), the pressure profiles are quite different from each other, but the width shrinkage was about the same. The faster the pressure decreased inside the cavity, the higher the pressure maxima had to be to assure the same width shrinkage: this is the case of series A, B, D and E. For series F, larger values of pressures are needed because the pressure is forced to zero in a short time. As shown , higher holding pressure induces higher pressure levels inside the cavity. Furthermore, just downstream from the gate, a residual pressure was still present at the mould opening. As already observed in the literature by Authors (Pantani 1999), (Pantani, Speranza and Titomanlio 2001a), this phenomenon is due to the fact that when the polymer is injected in the cavity at high pressure, it causes elastic deformation. At the end of packing phase, during cooling, the loaded mould gradually releases the stored deformation and maintains the pressure at a higher value. Regarding series F time varying series (**Fig. 8-10 F**), for which just one holding pressure was adopted, five tests having holding times of 15s,12s, 6s, 2s, and 1s are reported. As stated above, high holding pressure (like 950 bar) caused a residual pressure inside the cavity: the pressure reached a non-zero plateau value and, at ejection, the sample expanded in thickness. On the contrary, for lower holding pressures, the sample detached itself from the mould surface before ejection and cavity pressure became zero (**Fig. 8F** for P3 and P4 positions). The longer filling time for series C is clearly visible from the pressure curves (**Fig. 7C**): the cavity pressure profile began to increase after nearly 2.5[s] with respect to the start of the cycle. For series F, it can be observed that, for holding times shorter than 7[s], the holding pressure release caused a sudden pressure drop

in the cavity. This means that the gate wasn't solidified yet and some material left the cavity due to the inversion of pressure gradients. From this occurrence it was possible to state that the gate sealing time was within 6[s] and 7[s]. Regarding the effect of temperature: the comparison between **Fig. 6A** (melt temperature=220°C) and **Fig. 6B** (melt temperature=200°C) shows that a lower melt temperature, for the same holding pressure, causes a larger pressure value at longer times because of a lower width shrinkage; the comparison between **Fig. 6A** (mould temperature=25°C) and **Fig. 8F** (mould temperature=55°C) shows that, for the same reason, a higher mould temperature allows higher pressures at longer times (this is clearly shown for the lower holding pressure). The effect of a thicker cavity can be evinced by comparing **Fig. 6A** (cavity thickness=2mm) and **Fig. 11G** (cavity thickness=4mm): for the same holding pressure, the cavity pressure decrease is much steeper for a thinner cavity due to the larger pressure drops and the faster cooling. The effect of a thinner gate is made clear from the comparison of **Fig. 6A** (gate thickness=1.5 mm) and **Fig. 7D** (gate thickness=0.5 mm): for the same holding pressure the pressure drop between the position P0 (injection chamber) and position P3 (central in the cavity) is much higher for the thinner gate configuration. The effect of a longer nozzle (series H) is not evident from **Fig. 11H** and it is mainly limited to the filling step: the pressure drops during filling are much greater when the long nozzle configuration is adopted.

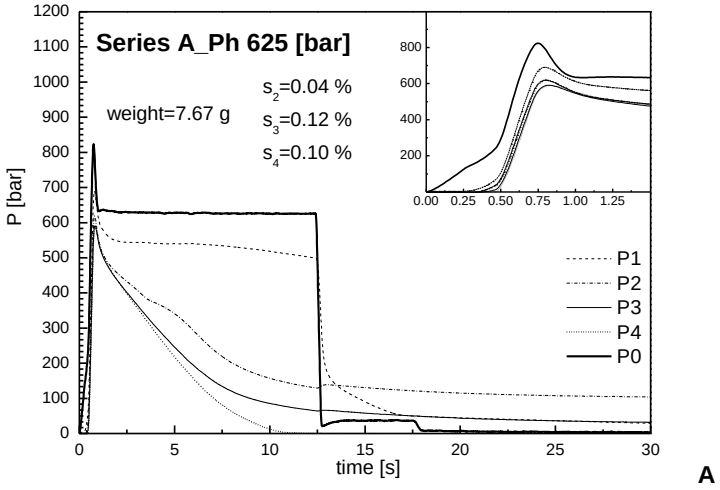

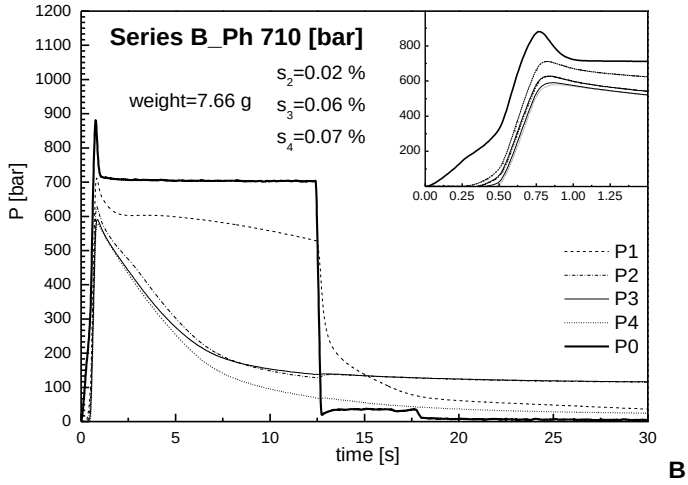

Fig. 6 Experimental pressure evolutions of PS 678E recorded in P0 (injection chamber), P1 just before the gate, and P2, P3 and P4 inside the cavity, for tests belonging to, respectively, A and B series (**Table 9**), (continued);

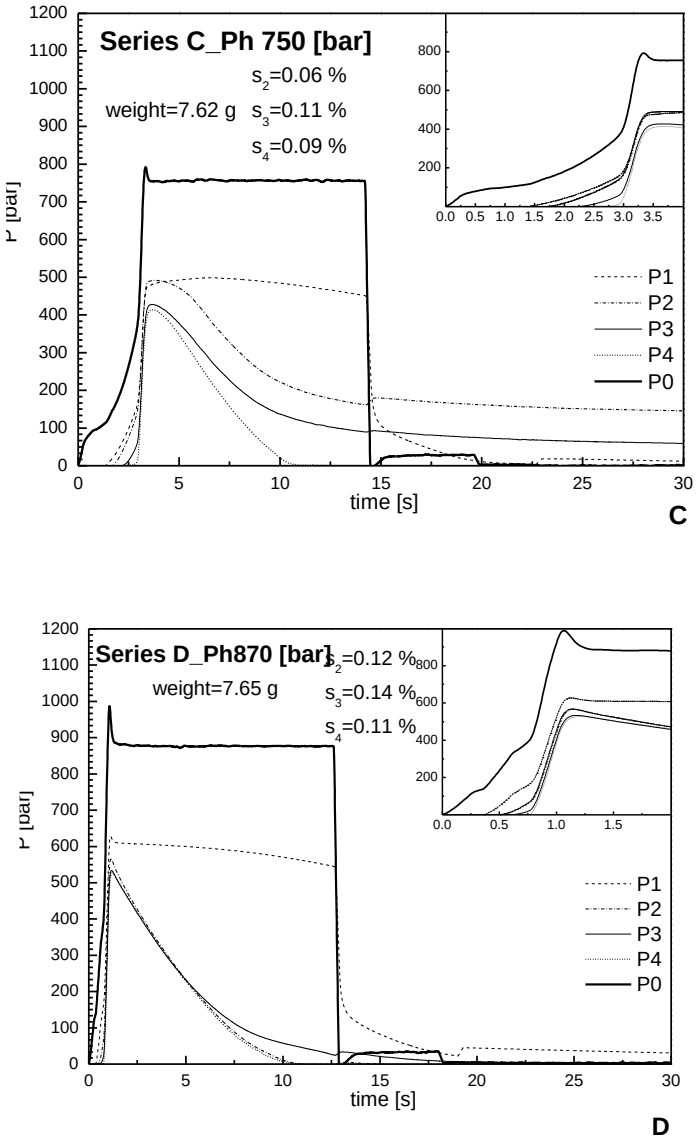

Fig. 7 Experimental pressure evolutions of PS 678E recorded in P0 (injection chamber), P1 just before the gate, and P2, P3 and P4 inside the cavity, for tests belonging to, respectively, C and D series (**Table 9**), (continued);

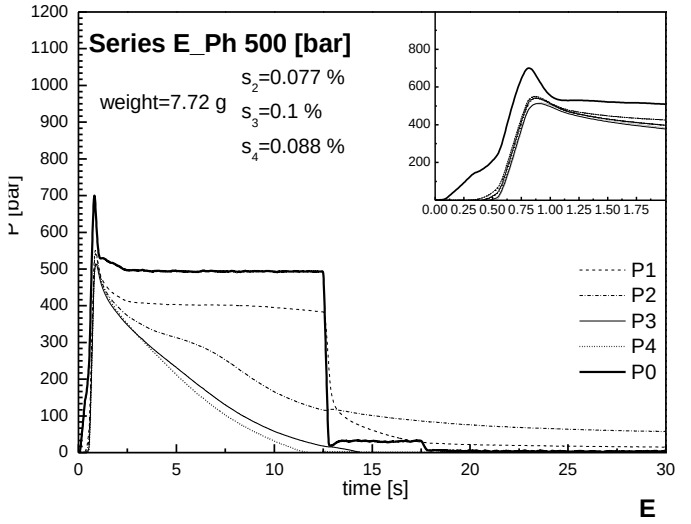

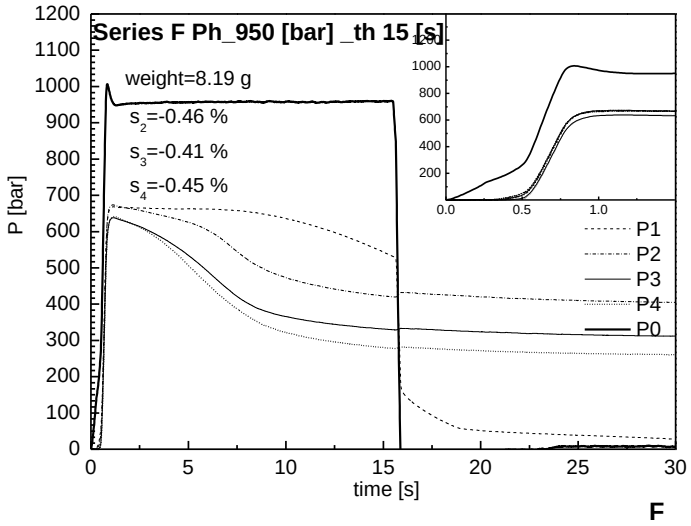

Fig. 8 Experimental pressure evolutions of PS 678E recorded in P0 (injection chamber), P1 just before the gate, and P2, P3 and P4 inside the cavity, for tests belonging to, respectively, E and F (holding time 15 [s]) series (**Table 9**), (continued);

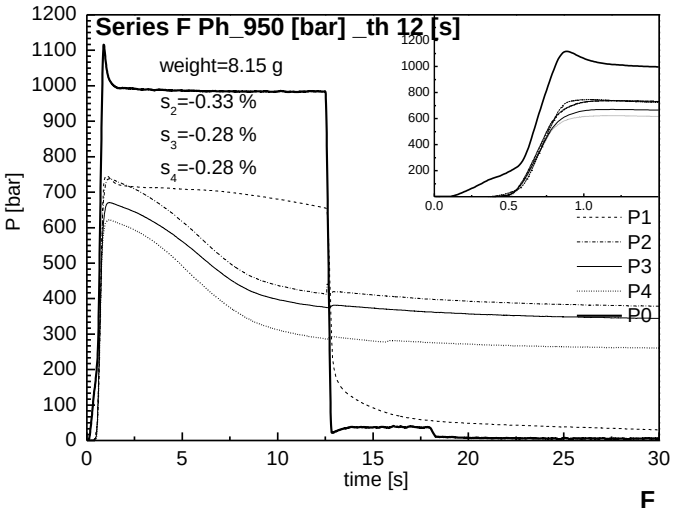

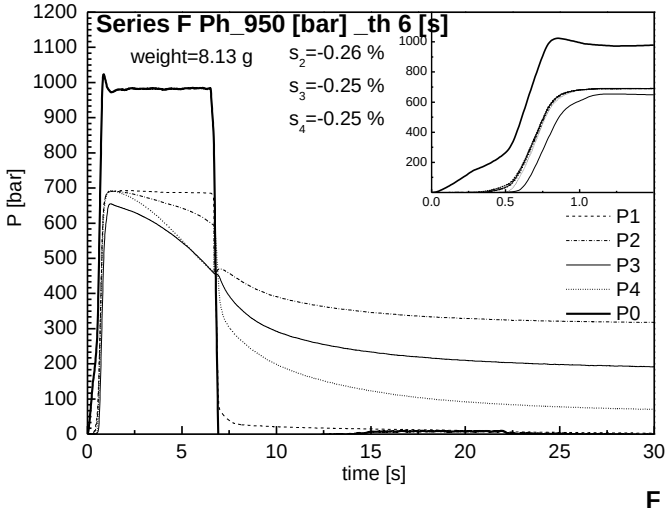

Fig. 9 Experimental pressure evolutions of PS 678E recorded in P0 (injection chamber), P1 just before the gate, and P2, P3 and P4 inside the cavity, for tests belonging to, F series (respectively holding time 12 [s] and 6 [s]) (**Table 9**), (continued);

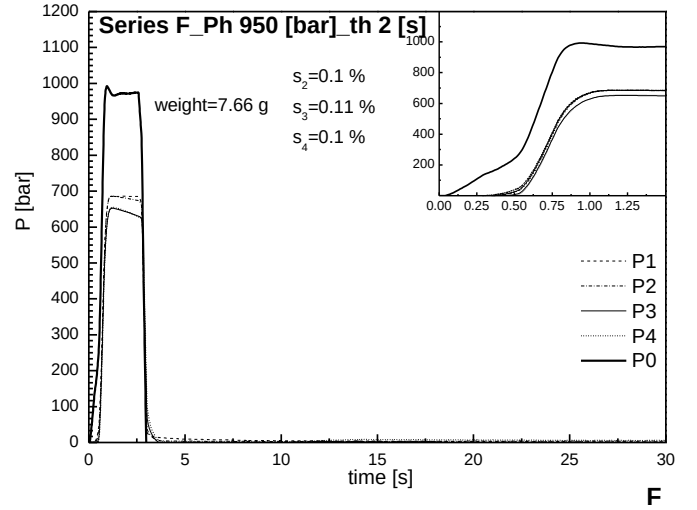

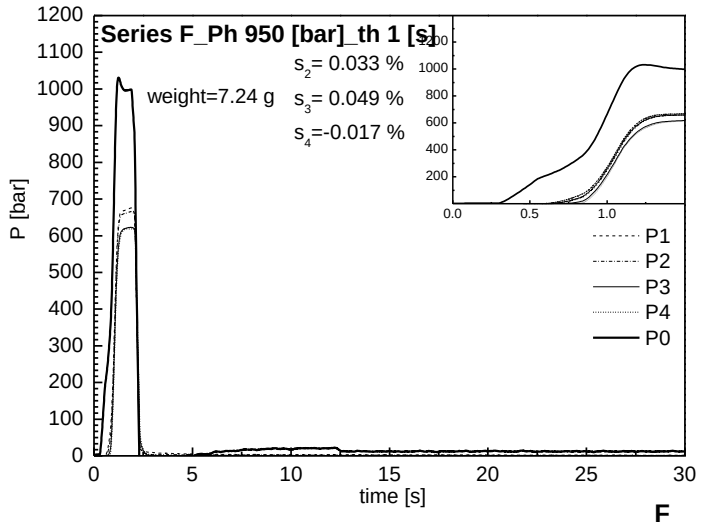

Fig. 10 Experimental pressure evolutions of PS 678E recorded in P0 (injection chamber), P1 just before the gate, and P2, P3 and P4 inside the cavity, for tests belonging to, F series (respectively holding time 2 [s] and 1 [s]) (**Table 9**), (continued);

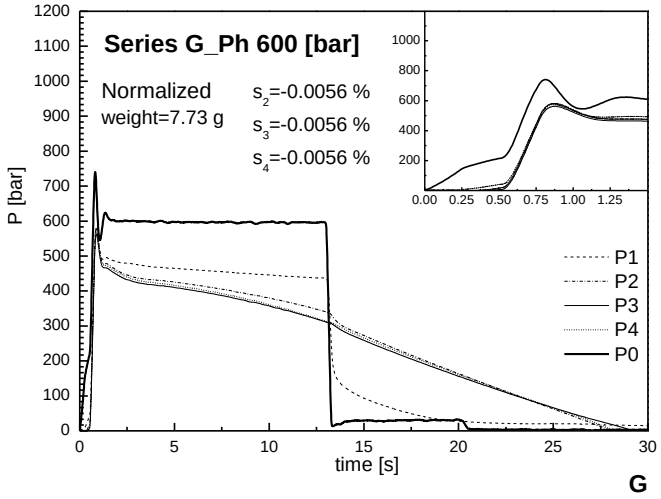

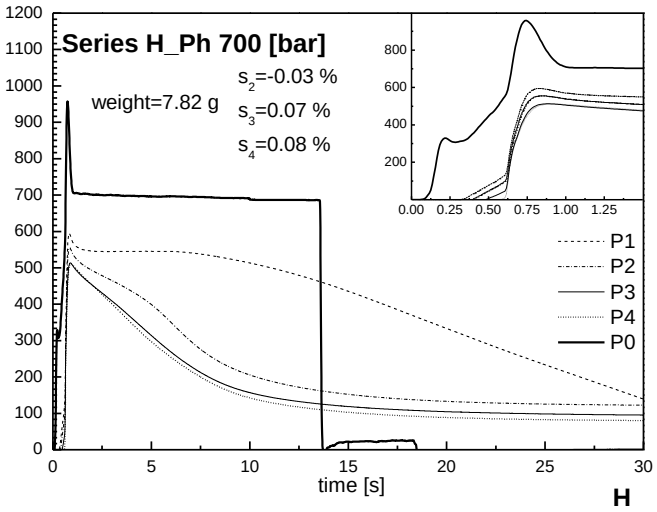

Fig. 11 Experimental pressure evolutions of PS 678E recorded in P0 (injection chamber), P1 just before the gate, and P2, P3 and P4 inside the cavity, for tests belonging to, respectively, G and H series (**Table 9**)

III.1.2 Experimental pressure for PC Lexan 141R tests

The pressure curves of PC Lexan 141R recorded by (Oliveira 1999) for some of the moulding settings are shown in **Fig. 12-17**. With regard to the P0 position (namely, nozzle pressure), the pressure spike which appears some seconds after the holding pressure is released, regardless of operative conditions, refers to the back pressure that the screw uses to fill the injection chamber for the following shot.

In each plot, both the width shrinkage and weight values resulting from the test are reported. In this case the only effect shown on pressure evolution is due to the holding pressure and holding time. As expected, higher holding pressures induce higher pressure levels inside the cavity. Furthermore, inside the cavity, just downstream from the gate, a residual pressure was still present at the mould opening when a holding pressure of 800 or 650 bar was adopted.

For a low holding pressure of 36 [MPa] **Fig. 13 D** the pressure in the cavity becomes zero between 17 and 20 [s]. At this point, the thickness shrinkage starts and the mouldings detach from the mould impression wall. For higher pressure **Fig. 12 A,B**, the over-packing of the polymer in the mould at the moment of gate freeze-off, is so high that thermal contraction due to cooling is not capable of overcoming the pressure effect, and the moulded part remains (in contact with)/(attached to) the mould wall impression . The gate sealing time was estimated by (Oliveira 1999) to be 10 [s] by observing both the pressure evolution in P1 and P2 in **Fig. 12 A**. Indeed it has been shown (Pantani, De Santis, et al. 2004) that an inflection point in the pressure evolution just upstream from the gate (P1) occurs when the gate solidifies. Correspondingly, the pressure curve just downstream from the gate (P2) changes its concavity from downwards to upwards. The reliability of this statement can be substantiated by comparison with the evolution of the pressure curves **Fig. 13 C** and **Fig. 15 E** (same holding pressure 470 [bar], and respectively for holding time 15 [s] and 10 [s]). During the holding phase, the mass flow rate through the gate counteracts the effect of the material volumetric decrease due to cooling, on the impression pressure evolution. If the holding pressure is released before the gate sealing time, the pressure decreases suddenly as appears comparing **Fig. 14 E,F** with **Fig. 15 G,H**. This occurrence called “backflow” determines lower sample weight as can be observed by comparing **Fig. 13 C** and **Fig. 16** which represent the test performed with the same holding pressure but increasing holding time to 15 [s]. Indeed, in this case, the pressure remains after the end of the holding phase and no back flow is involved, resulting in a heavier moulded part. Essentially, **Fig. 13 C** demonstrates that the cavity gate is solid after 15[s], whereas, it does not appear solid for times lower than 10[s] **Fig. 15 G,H**.

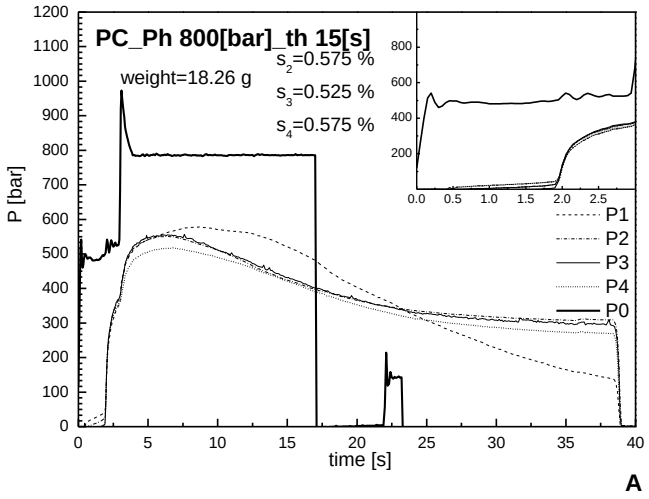

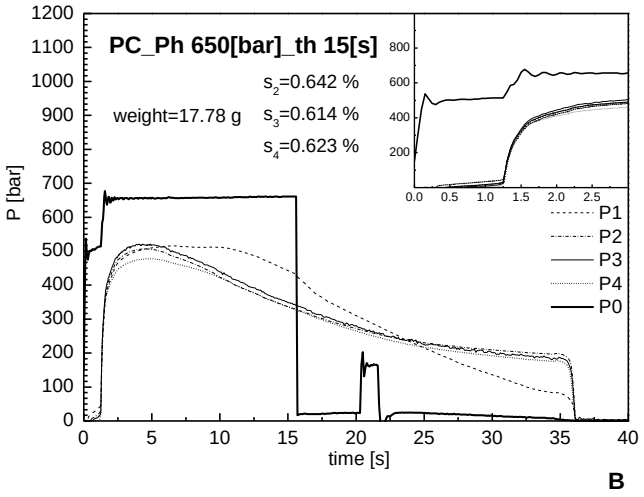

Fig. 12 Experimental pressure evolutions of PC Lexan 141R recorded by (Oliveira 1999) relating to P0 in the injection chamber, P1 just before the gate, and P2, P3 and P4 inside the cavity, referred respectively to P_{hold} 800 [bar] (A), and P_{hold} 650 [bar] (B) holding conditions (see **Table 10** in the previous section), (continued).

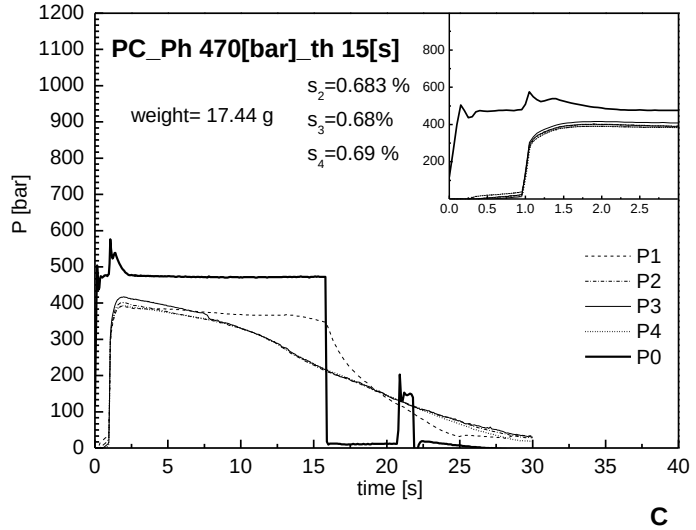

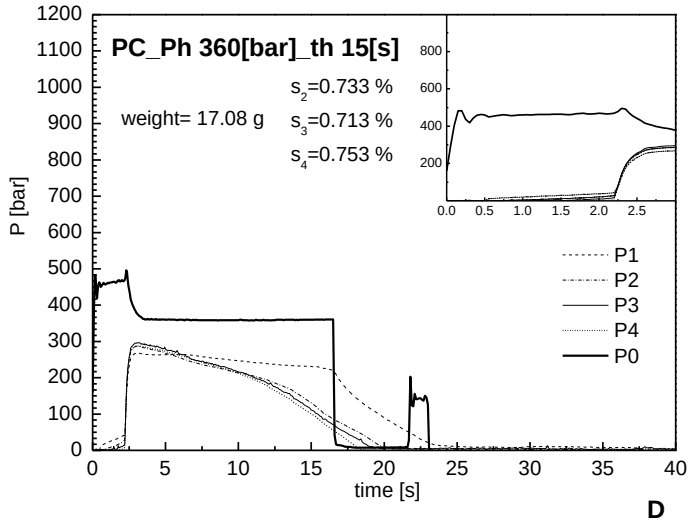

Fig. 13 Experimental pressure of PC Lexan 141R recorded by (Oliveira 1999) relating to P0 in the injection chamber, P1 just before the gate, and P2, P3 and P4 inside the cavity, referred respectively to P_{hold} 470 [bar] (C), and P_{hold} 360 [bar] (D) holding conditions (see **Table 10**), (continued).

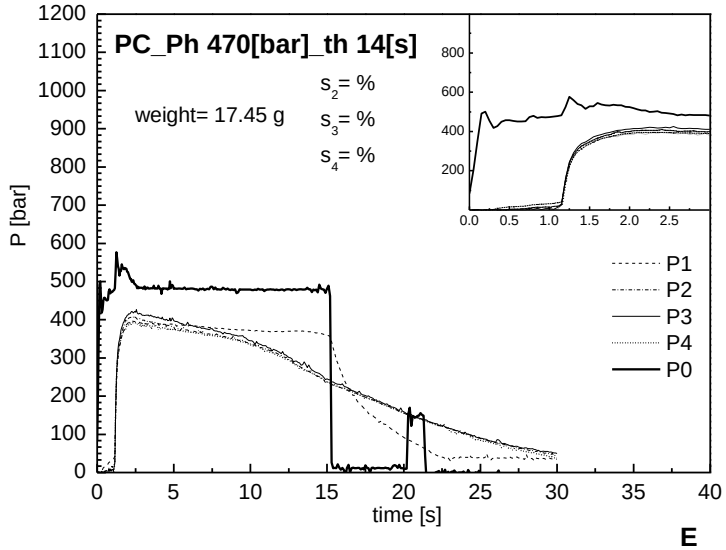

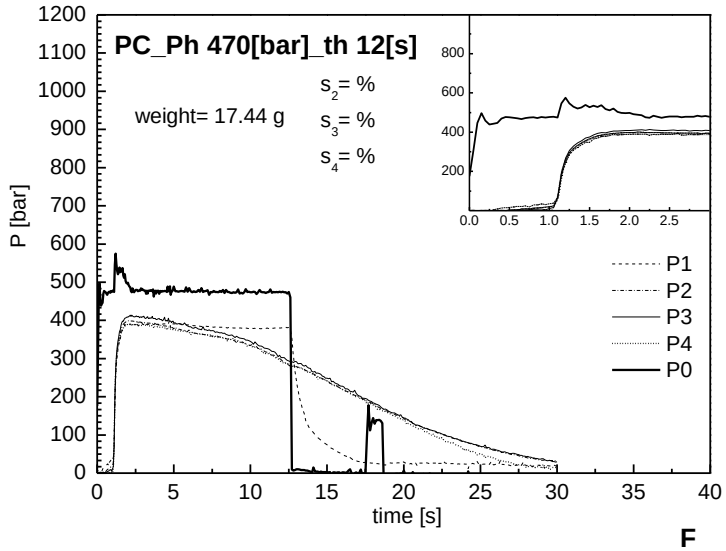

Fig. 14 Experimental pressure of PC Lexan 141R recorded by (Oliveira 1999) relating to P0 in the injection chamber, P1 just before the gate, and P2, P3 and P4 inside the cavity, referred respectively to P_{hold} 470 [bar]_th14 [s] (E), and P_{hold} 470 [bar]_ th12 [s] (F) holding conditions (see **Table 10**), (Continued).

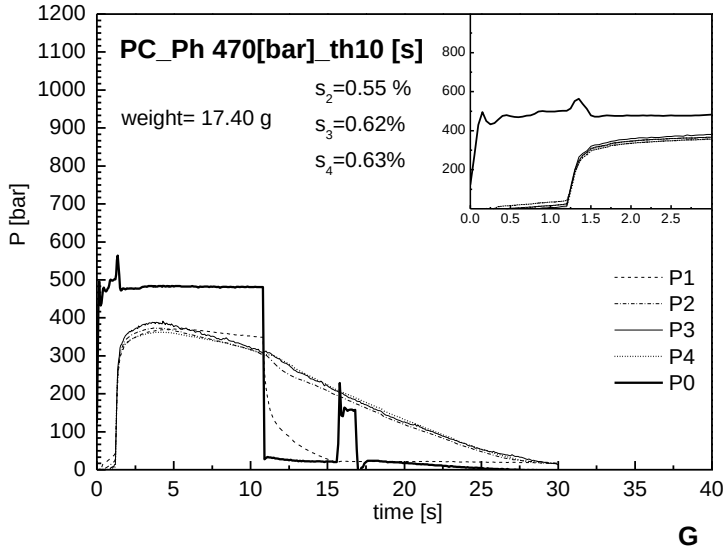

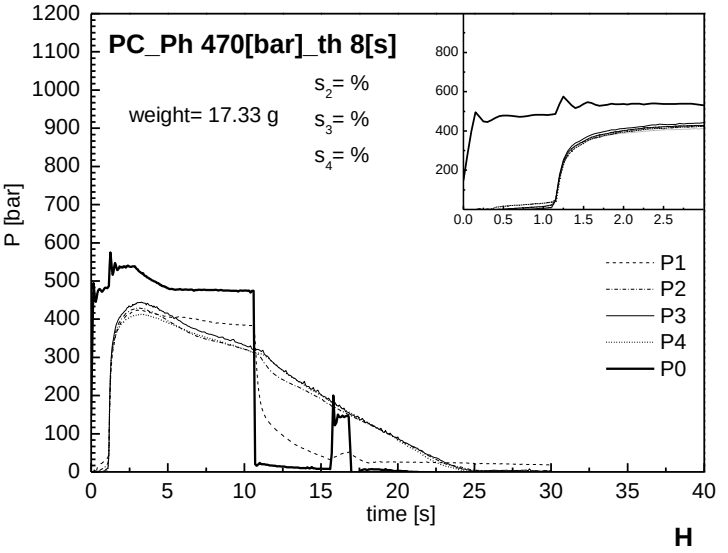

Fig. 15 Experimental pressure of PC Lexan 141R recorded by (Oliveira 1999) relating to P0 in the injection chamber, P1 just before the gate, and P2, P3 and P4 inside the cavity, referred respectively to P_{hold} 470 [bar]_th10 [s] (G), and P_{hold} 470 [bar]_ th 8 [s] (H) holding conditions (see **Table 10**), (Continued).

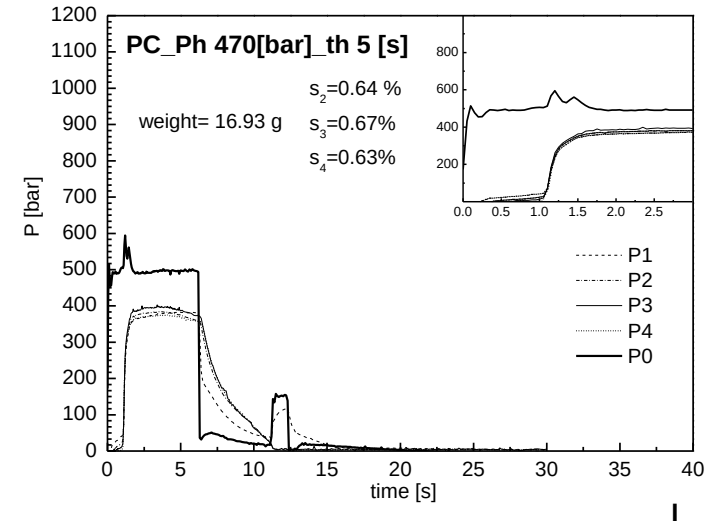

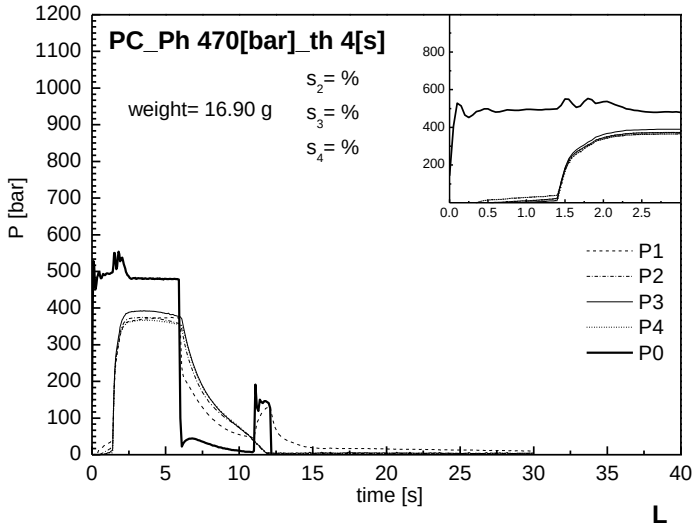

Fig. 16 Experimental pressure of PC Lexan 141R recorded by (Oliveira 1999) relating to P0 in the injection chamber, P1 just before the gate, and P2, P3 and P4 inside the cavity, referred respectively to P_{hold} 470 [bar]_th5 [s] (I), and P_{hold} 470 [bar]]_th4 [s] (L) holding conditions (see **Table 10**), (Continued).

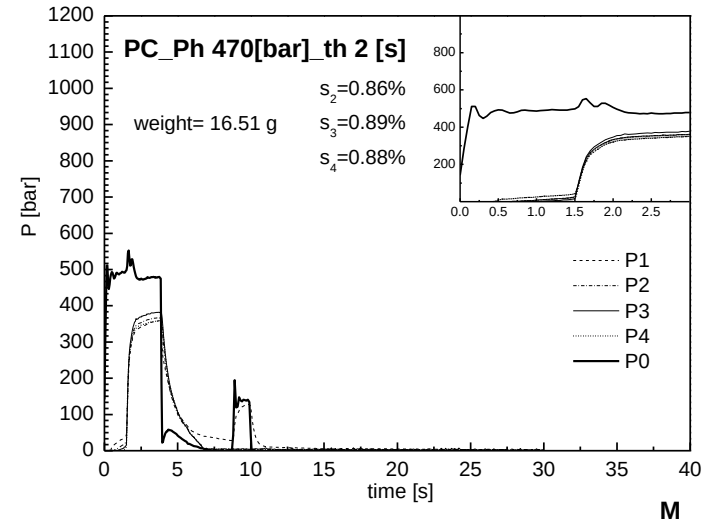

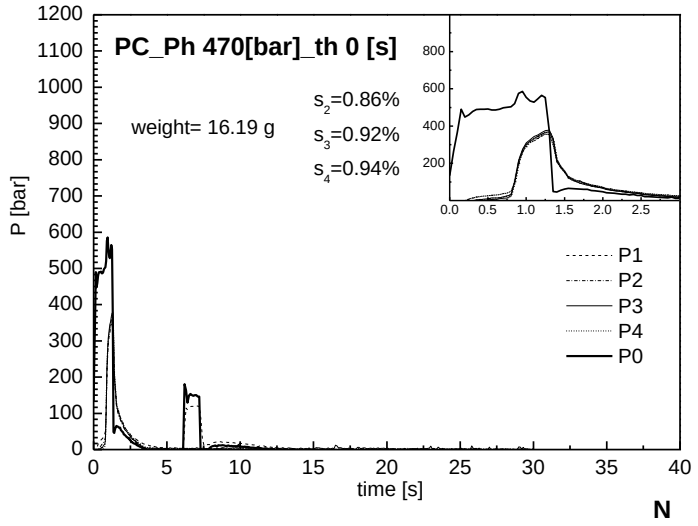

Fig. 17 Experimental pressure of PC Lexan 141R recorded by (Oliveira 1999) relating to P0 in the injection chamber, P1 just before the gate, and P2, P3 and P4 inside the cavity, referred respectively to P_{hold} 470 [bar]_th 2 [s] (M), and P_{hold} 470 [bar]]_th 0 [s] (N) holding conditions (see **Table 10**).

III.1.3 Experimental pressure for PP Hifax BA238GE tests

The pressure curves of PP Hifax BA238GE recorded by (De Santis, et al. 2010) for some of the moulding settings are shown in the **Fig. 18-Fig. 24**. In these plots both width shrinkage and weight values which were also measured by (De Santis, et al. 2010), are also reported. Regarding the P0 position (namely, nozzle pressure), the pressure spike which appears some seconds after the holding pressure is released, regardless of operating conditions, refers to the back pressure that the screw uses to fill the injection chamber for the following shot. Likewise with Polycarbonate cases, a higher holding pressure condition involves the over-packing of the polymer in the cavity, and consequently the moulded part remains in contact with the mould wall impression for a longer time, and a residual pressure is sometimes present at the mould opening (as is recognizable in **Fig. 18 A, B**). At the same time this involves small shrinkage values, and heavier moulded specimens.

As previously reported, (Pantani, De Santis, et al. 2004), from the experimental pressure evolution it is possible to identify a time interval in which the gate sealing time falls. In fact, observing **Fig. 18 A**, **Fig. 19 C,D Fig. 20 E** which refer to holding time t_h 10 [s] moulding tests, it appears that the inflection point in the pressure evolution just upstream from the gate (P1) occurs approximately between 6 [s] and 8 [s], regardless of the holding pressure values. This occurrence is confirmed in comparing **Fig. 20 E**, **Fig. 21 H**, and **Fig. 22 I**, which represent the test performed with the same holding pressure but increasing holding time to 12 [s]. It is clear that when the holding pressure is released before the gate sealing time, the pressure decreases suddenly and backflow takes place, determining a lower sample weight (**Fig. 22 I**). On the contrary, if the holding pressure is released after gate solidification, no back-flow is present and heavier moulded parts are involved as appears in **Fig. 20 E**, **Fig. 21 H**.

Finally, the effect of a thinner gate is made clear by the comparison between the tests performed in the same holding conditions, but using different gate thicknesses as in **Fig. 18 A,B Fig. 20 E,F Fig. 24 O,P** respectively. For the thinner gate configuration cases it appears that the cavity pressure quickly fades. Furthermore, no residual cavity pressure is detectable even in the case of imposing higher holding pressure.

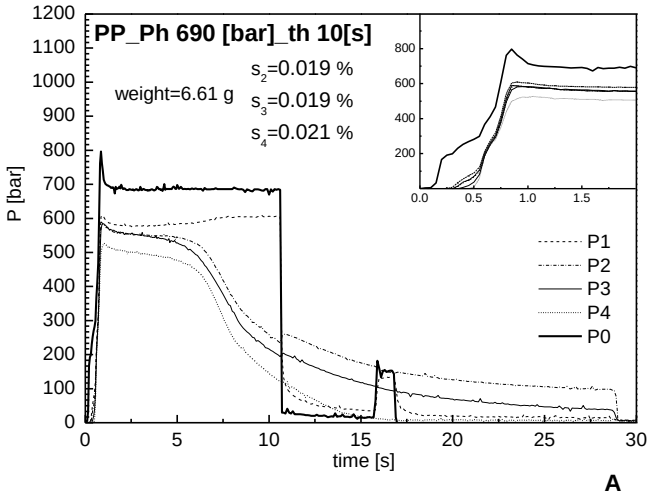

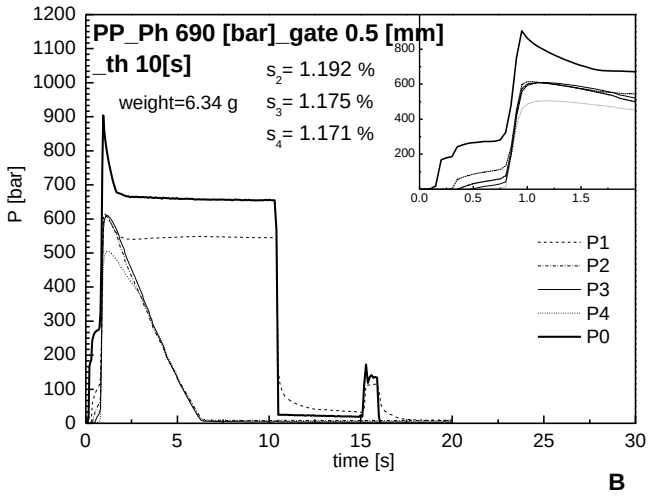

Fig. 18 Experimental pressure evolutions of PP Hifax BA238GE relating to P0 in the injection chamber, P1 just before the gate, and P2, P3 and P4 inside the cavity recorded by (De Santis, et al. 2010) referring respectively to P_{hold} 690 [bar] (A) and P_{hold} 690 [bar]_gate0.5 [mm] (B) (see **Table 11**), (Continued).

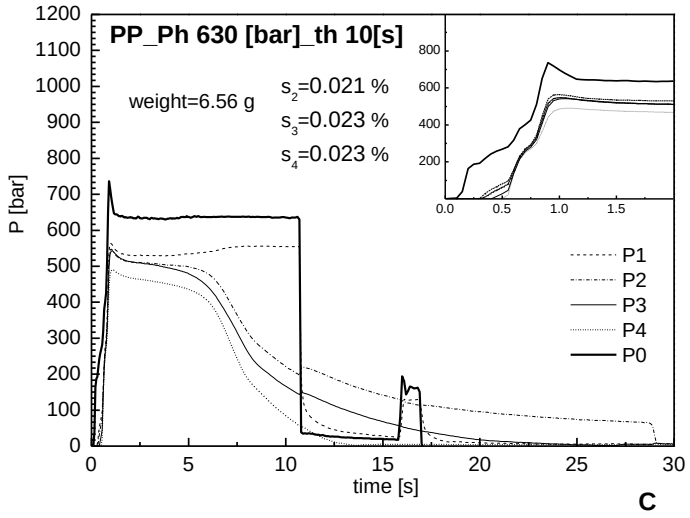

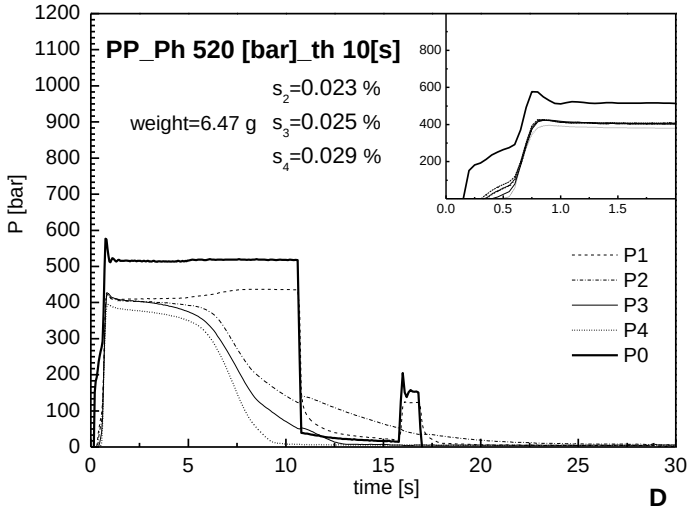

Fig. 19 Experimental pressure evolutions of PP Hifax BA238GE relating to P0 in the injection chamber, P1 just before the gate, and P2, P3 and P4 inside the cavity recorded by (De Santis, et al. 2010) referring respectively to P_{hold} 630 [bar] (C) and P_{hold} 520 [bar] (D) (see **Table 11**), (Continued).

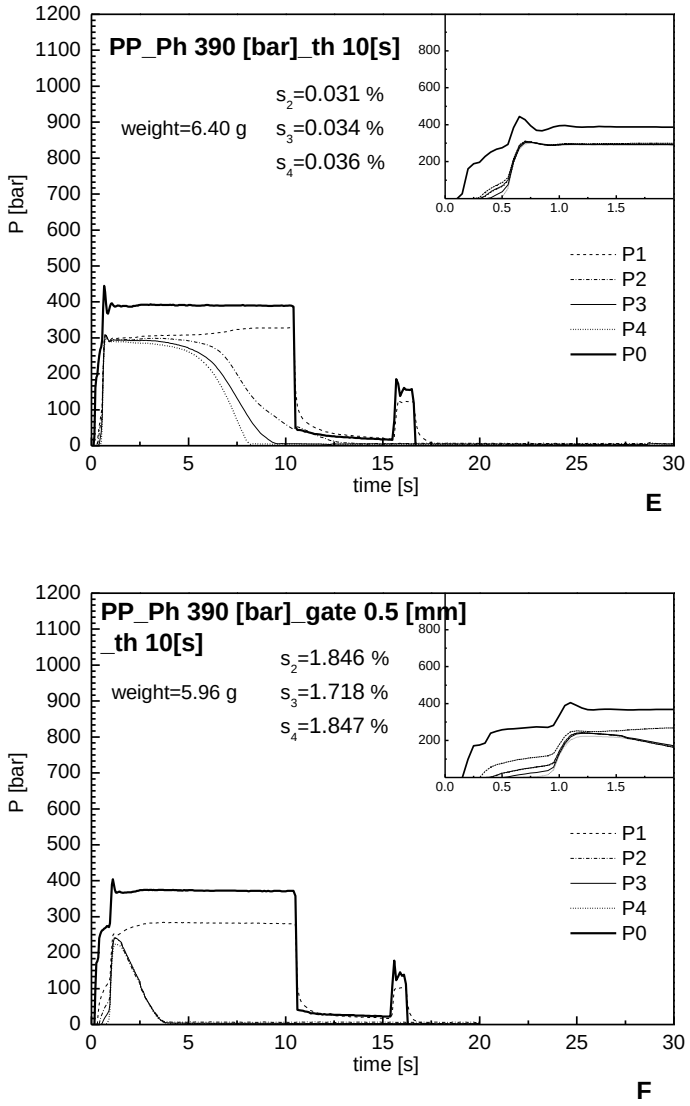

Fig. 20 Experimental pressure evolutions of PP Hifax BA238GE relating to P0 in the injection chamber, P1 just before the gate, and P2, P3 and P4 inside the cavity recorded by (De Santis, et al. 2010) referring respectively to P_{hold} 390 [bar] (E) and P_{hold} 390 [bar]_gate0.5 [mm] (F) (see **Table 11**), (Continued).

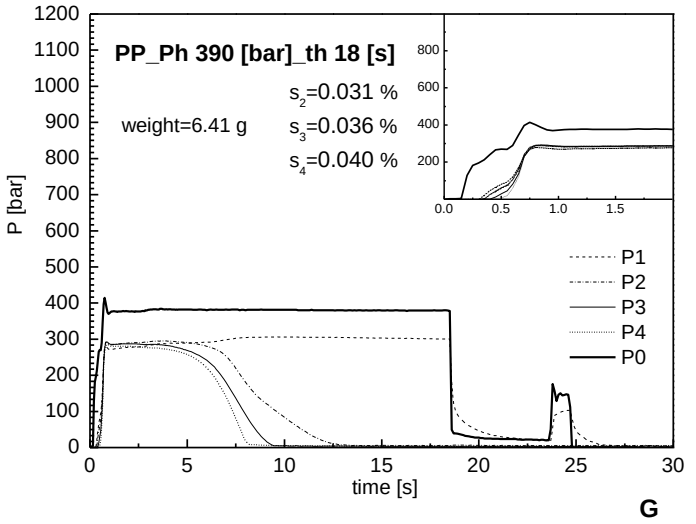

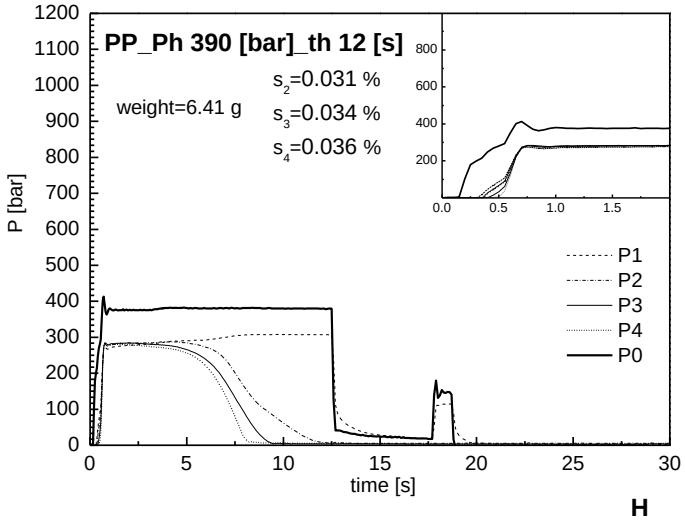

Fig. 21 Experimental pressure evolutions of PP Hifax BA238GE relating to P0 in the injection chamber, P1 just before the gate, and P2, P3 and P4 inside the cavity recorded by (De Santis, et al. 2010) referring respectively to P_{hold} 390 [bar]_th18[s] (G) and P_{hold} 390 [bar]_th12[s] (H) (see **Table 11**), (Continued).

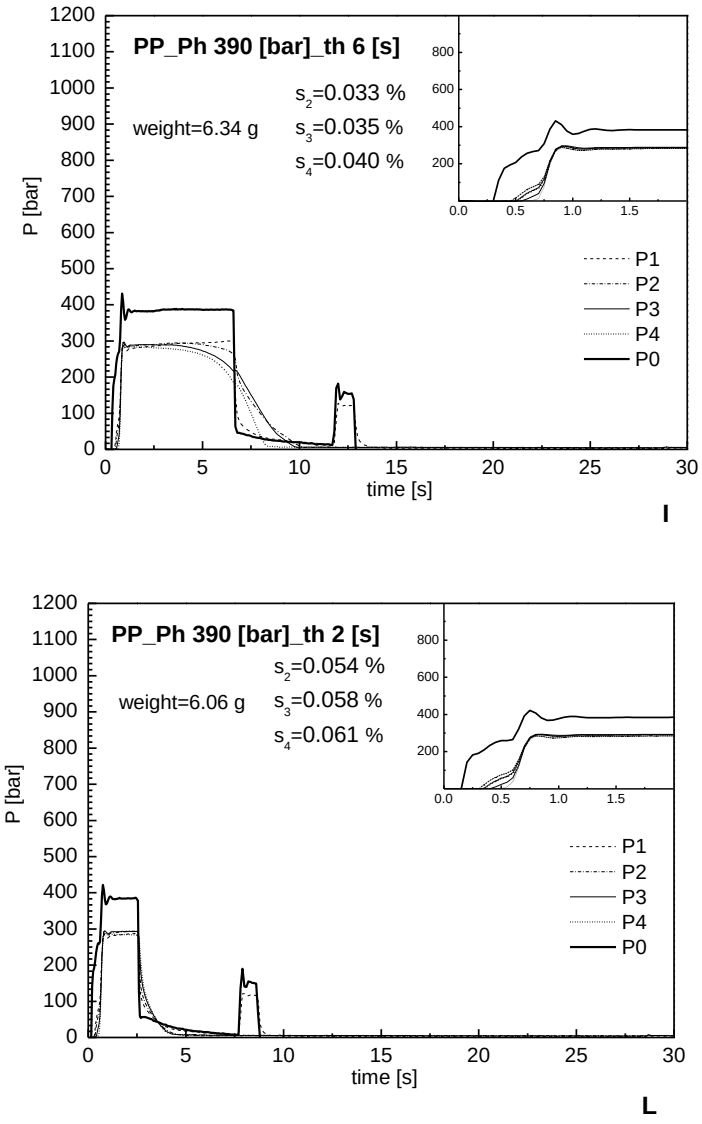

Fig. 22 Experimental pressure evolutions of PP Hifax BA238GE relating to P0 in the injection chamber, P1 just before the gate, and P2, P3 and P4 inside the cavity recorded by (De Santis, et al. 2010) referring respectively to P_{hold} 390 [bar]_th 6[s] (I) and P_{hold} 390 [bar]_th 2[s] (L) (see **Table 11**).

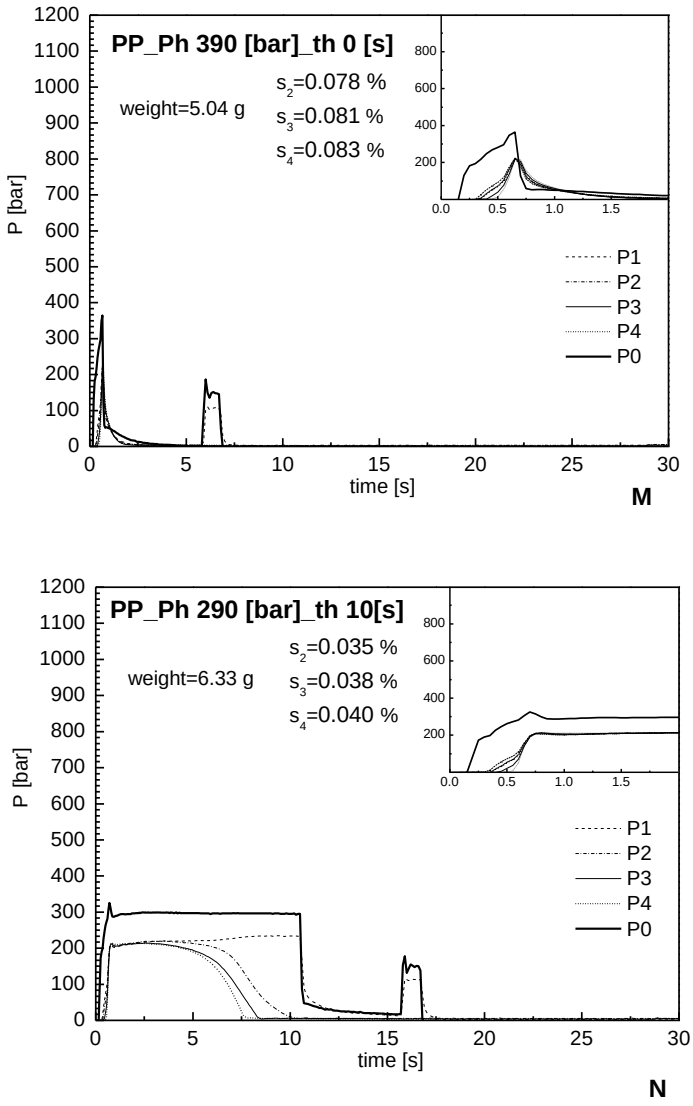

Fig. 23 Experimental pressure evolutions of PP Hifax BA238GE relating to P0 in the injection chamber, P1 just before the gate, and P2, P3 and P4 inside the cavity recorded by (De Santis, et al. 2010) referring respectively to P_{hold} 390 [bar]_th 0[s] (M) and P_{hold} 290 [bar] (N) (see **Table 11**), (Continued).

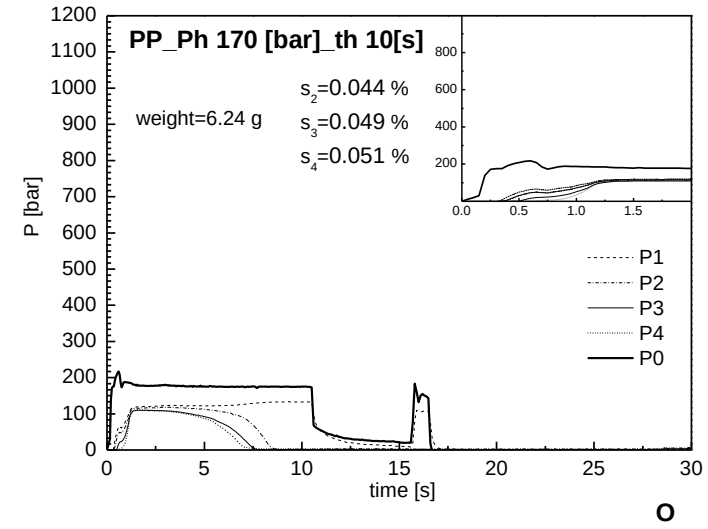

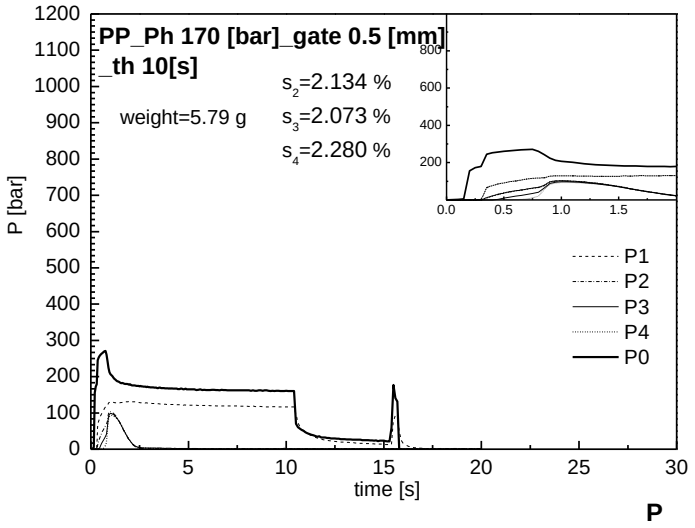

Fig. 24 Experimental pressure evolutions of PP Hifax BA238GE relating to P0 in the injection chamber, P1 just before the gate, and P2, P3 and P4 inside the cavity recorded by (De Santis, et al. 2010) referring respectively to P_{hold} 170 [bar] (O) and P_{hold} 170 [bar]_gate 0.5[mm] (P) (see **Table 11**).

III.2 Width shrinkage results.

The purpose of this thesis is to identify a single parameter which can be satisfactorily correlated to the chosen quality parameters. The most accessible parameter is obviously hydraulic pressure. This parameter is normally considered to be correlated by a unique relationship with the pressure of the melt inside the injection chamber measured during the holding step (which will be indicated in the following as holding pressure Ph). Thus a preliminary attempt was made to find a correlation between holding pressure/time and in plane-shrinkage data.

In **Fig. 25 A** the average width shrinkage data (over the three positions inside the cavity) for PS 678E moulded samples are reported, versus the hydraulic holding pressure (upper abscissa axis). In this plot, the average width shrinkage data belonging to series F (tests performed with a hydraulic pressure of 960 [bar]) are also plotted versus the holding time (bottom abscissa axis). Width shrinkage decreased on increasing holding pressure. A general decrease was also observed when increasing the holding time, until the achievement of a plateau value (in corresponding to 7s). This instant is considered to be the gate sealing time (Pantani, De Santis, et al. 2004) and gives a clearly indication about the part weight of the moulded sample. In **Fig. 25 B** the effect of the position is shown for all the series regarding PS 678E. In most of the cases the difference was of the order of reproducibility, even though in some others (series E, for instance) it was very significant, the width shrinkage being, nevertheless, always smaller in pos P2 (closer to the gate).

Obviously, apart from a general trend, it appears that both, the hydraulic and holding pressure (which are proportional to each other) are not appropriate parameters for describing width shrinkage: they do not take into account the width shrinkage differences inside the cavity, and the effect of holding time is disregarded. Indeed, as appears in **Fig. 25 B**, for the same holding pressure, width shrinkage differences as high as 0.4% (namely nearly equal to the whole range of data) have been found. The same plots are reported in (**Fig. 26 C, D**) for PC Lexan 141 R and in (**Fig. 27 E F**) for PP Hifax BA 238 GE tests. In Polycarbonate plots, only the effects of both holding pressure and time on width shrinkage were analyzed. In fact, due to the high viscosity of Polycarbonate, it was necessary to use a thicker mould cavity to perform injection moulding tests successfully. For the same reason it was not possible to perform any moulding test by using a longer nozzle and smaller gate dimension. For Polypropylene cases, a different gate dimension was also used in performing the injection moulding tests, and the results are also plotted. **Fig. 26** and **Fig. 27** suggest that the parameters used cannot be considered for a correct description of the width shrinkage, since very poor correlations were obtained.

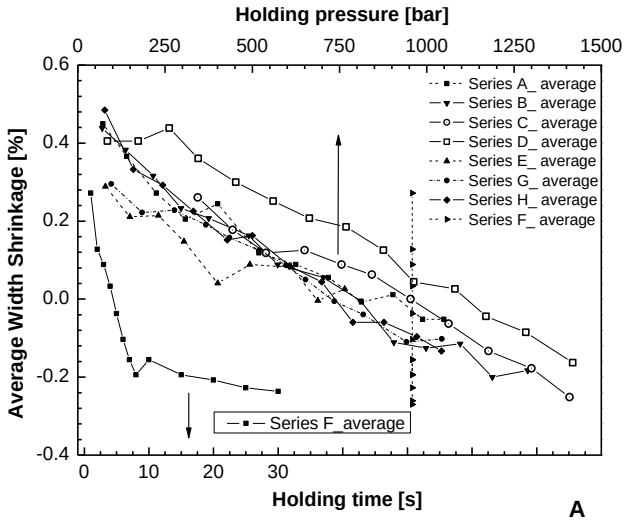

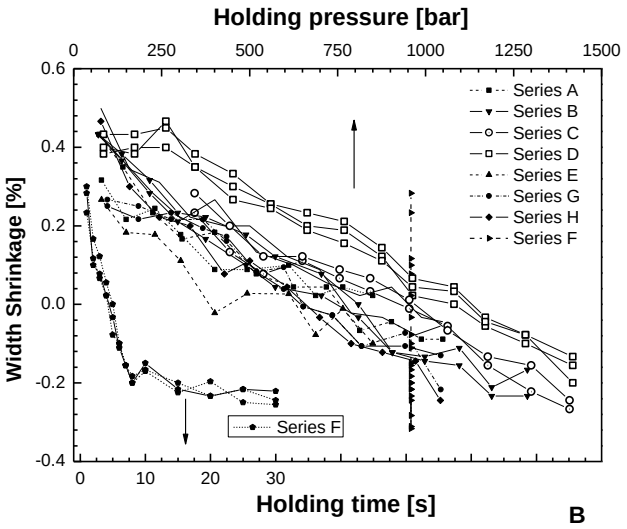

Fig. 25 Average Width Shrinkage vs. holding pressure and holding time (A). Width Shrinkage vs. holding pressure and holding time in all cavity positions (B). Data referring to PS678E series. (Continued)

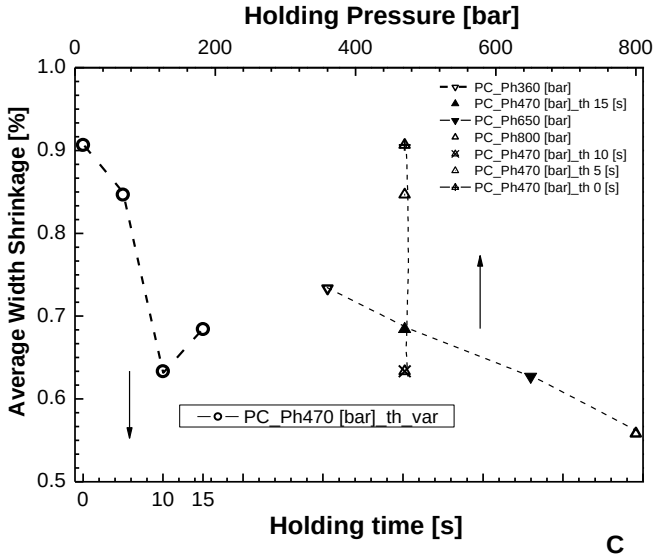

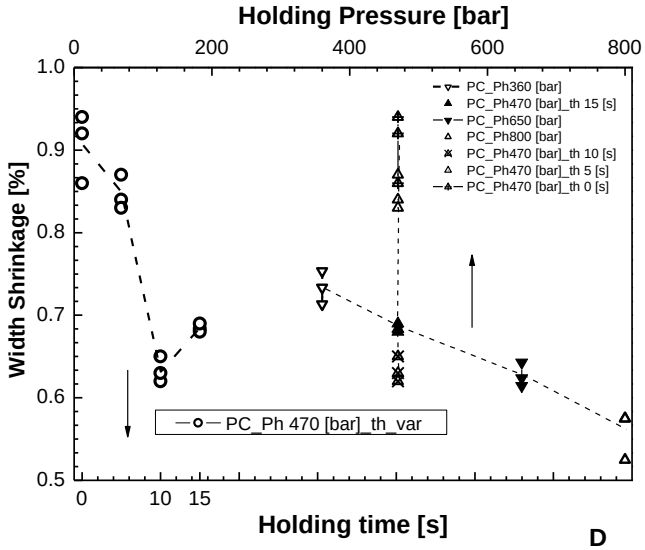

Fig. 26 Average Width Shrinkage vs. holding pressure and holding time (C). Width Shrinkage vs. holding pressure and holding time in all cavity positions (D). Data referring to PC Lexan 141R series. (Continued)

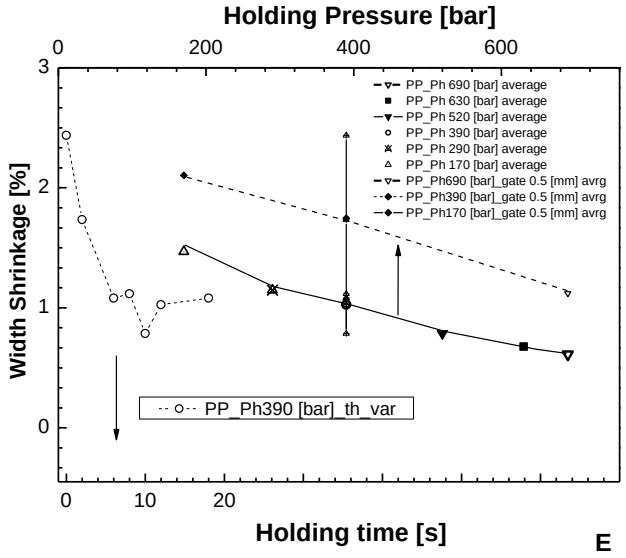

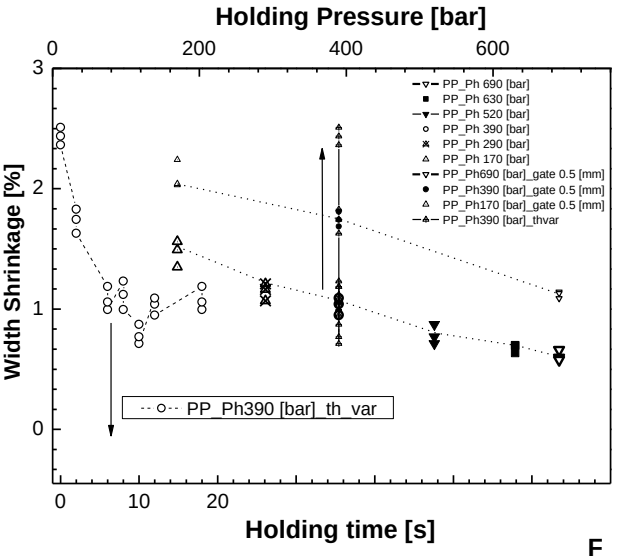

Fig. 27 Average Width Shrinkage vs. holding pressure and holding time (E). Width Shrinkage vs. holding pressure and holding time in all cavity positions (F). Data referring to PP Hifax BA238GE series.

III.3 Normalized part weight results

A similar approach was adopted in correlating normalized part weight data with holding pressure/time, as reported in **Fig. 28.**

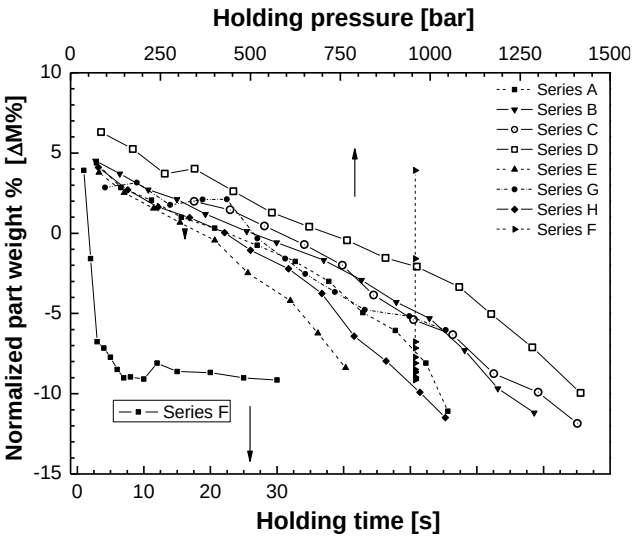

Fig. 28 Normalized part weight percentage vs. holding pressure and holding time in all cavity positions P2, P3 and P4 for PS 678E.

The data exhibit a very poor correlation with the hydraulic pressure. In fact, whereas for the samples having positive weight variations, most of the data lay on a single curve; on the contrary, for other samples affected by negative normalized weight, the data appear to lie aside from the trend. In addition the results worsen when considering series F. The plots reported in (Fig. 29 and Fig. 30) refer to PC Lexan 141 R and PP Hifax BA 238 GE respectively. No adequate correlation was identified, therefore, a different approach from holding pressure or time was necessary to detect an appropriate parameter which was descriptive of the part weight quality for injection moulded samples.

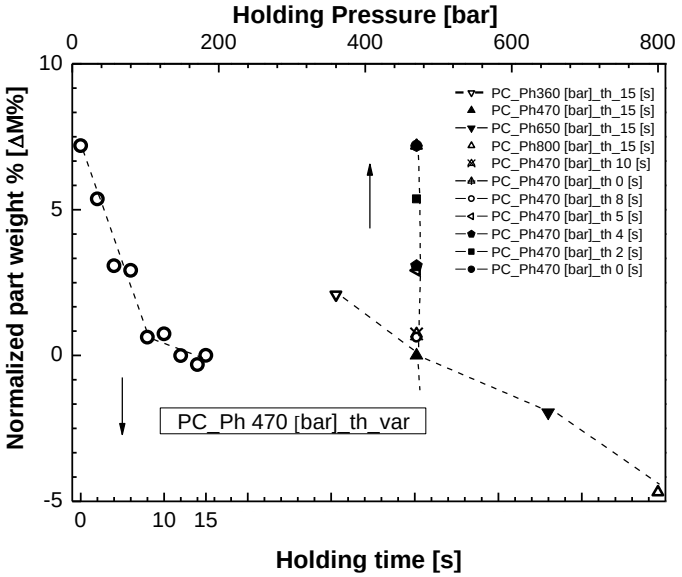

Fig. 29 Normalized part weight percentage vs. holding pressure and holding time in all cavity positions P2, P3 and P4 for PC Lexan 141R.

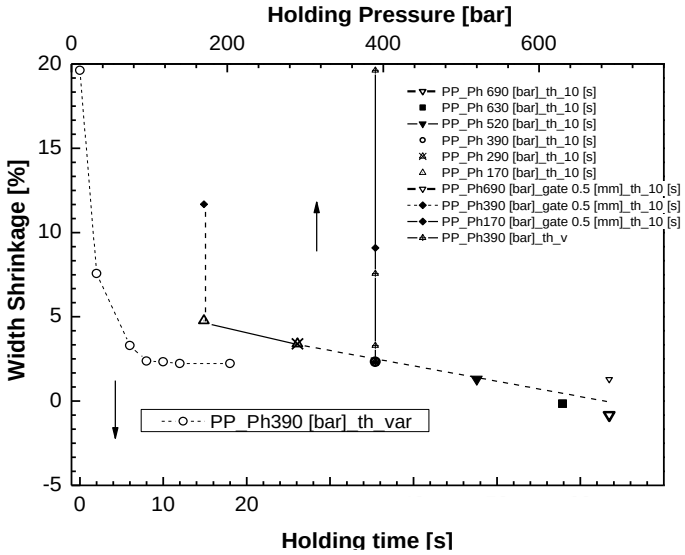

Fig. 30 Normalized part weight percentage vs. holding pressure and holding time in all cavity positions P2, P3 and P4 for PP BA 238 GE.

Chapter Four

Simulation of the injection moulding tests.

In this chapter, simulation procedures (tools, meshing and techniques) used in this work are described. The simulated pressure profiles are compared to the experimental ones in order to reproduce the experimental conditions in the best possible way. Also the corresponding solidification layer profiles are plotted as one of the results of the simulator software.

IV.1 Moldflow© simulations: tools, meshing and techniques.

Injection moulding tests for PS 678E, have been simulated using Moldflow Plastic Insight version 6.1. Each experimental test was simulated by imposing the geometry of nozzle, channels and cavity. Basically, the moulded part geometry was reproduced and adopted as the calculus domain by means of finite element meshing. The mesh provides the basis for a Moldflow analysis, where moulding properties are calculated at every node. It was necessary to use two different meshing types for the calculus domain. For nozzle and sprue geometries a beam element meshing was considered, which currently consists of a cylindrical shape element including two-nodes, with a longitudinal straight axis, so that when modelling curved beams, they provide a "faceted" approximation to the true geometry. Hot runner channels were chosen for the nozzle geometry mesh, and cold runner channels for meshing the sprue. To mesh the remaining moulded part we have chosen the mid-plane mesh element type which consists of tri-noded triangular elements that form a one dimensional representation of the part, through its centre. This mesh type is suitable in the case of thin-walled parts. The flow analysis type study was set up to predict material behaviour during the moulding cycle by analyzing the Mid-plane mesh part model **Fig. 31**.

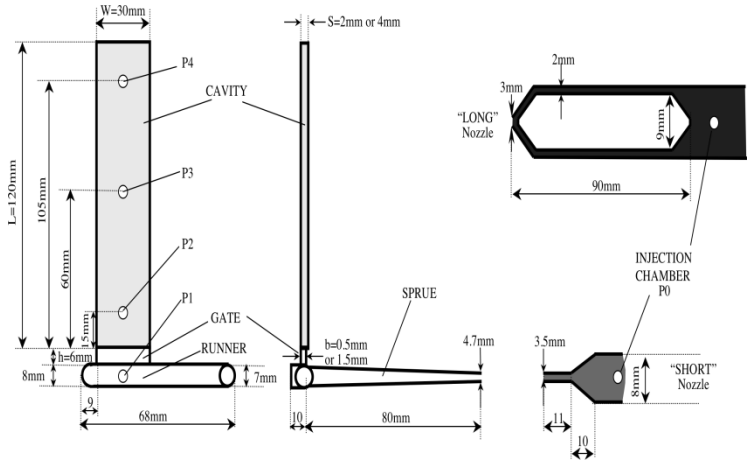

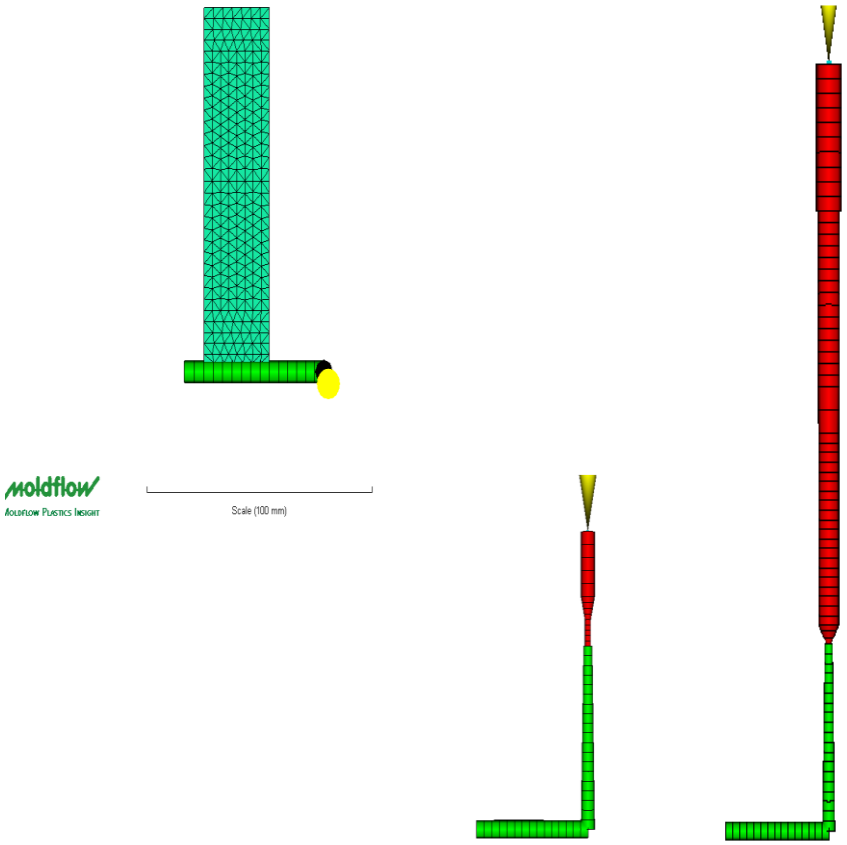

Fig. 31 Schematic drawing of cavity, and Nozzle .

Each test was simulated by setting the injection and mould temperature, the filling time and the experimental packing pressure profile at the nozzle node location. The filling time used in the simulation was determined directly by experimental pressure curves. It was taken as the amount of time that the polymer required to reach the P4 transducer position, starting from the instant in which the pressure transducer signal in P0 began to go up.

IV.2 Moldflow© simulations: pressure curves

The pressure evolutions obtained by simulation, were compared with the experimental data in some conditions, for all transducers position P_i, and for all the series (in **Table 9**). In the upper diagrams in the top right hand side of the plot area in **Fig. 32**, the filling stage is also highlighted, in order to allow

a comparison with the experimental pressure profile, over the entire operative cycle.

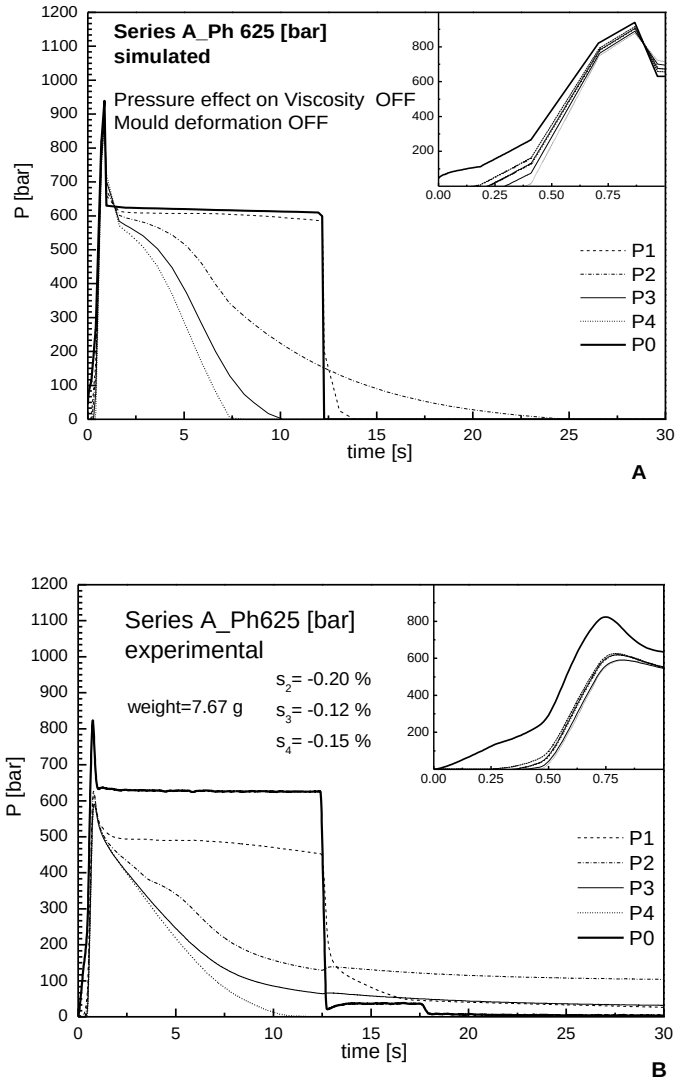

Fig. 32 Simulated (A) and Experimental (B) pressure evolutions of PS 678E recorded in P0 (injection chamber), P1 just before the gate, and P2, P3 and P4 inside the cavity, for tests belonging to, A series (**Table 9**). The predicted pressure curves, refer to simulation performed by setting the default database parameters for Cross WLF equation in rheological description, and Tait equation for PVT properties. (Continued).

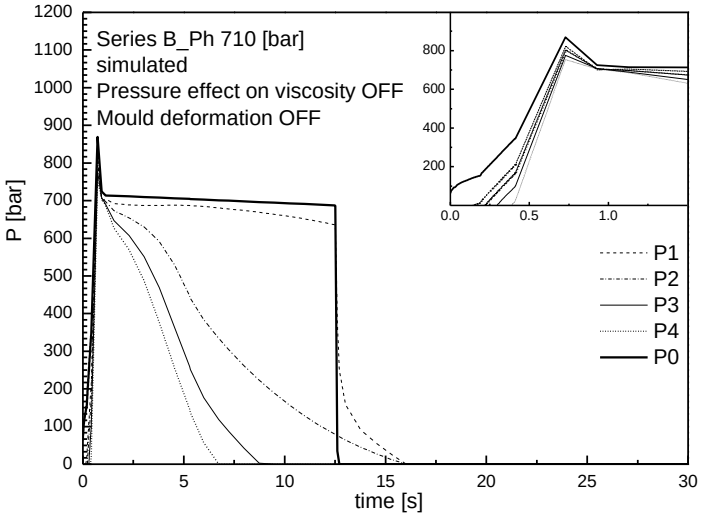

C

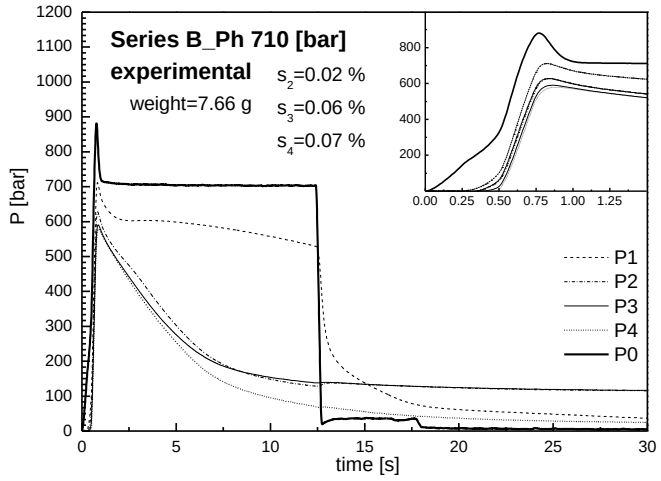

D

Fig. 32 Simulated (C) and Experimental (D) pressure evolutions of PS 678E recorded in P0 (injection chamber), P1 just before the gate, and P2, P3 and P4 inside the cavity, for tests belonging to, B series (**Table 9**). The predicted pressure curves, refer to simulation performed by setting the default database parameters for Cross WLF equation in rheological description, and Tait equation for PVT properties. (Continued).

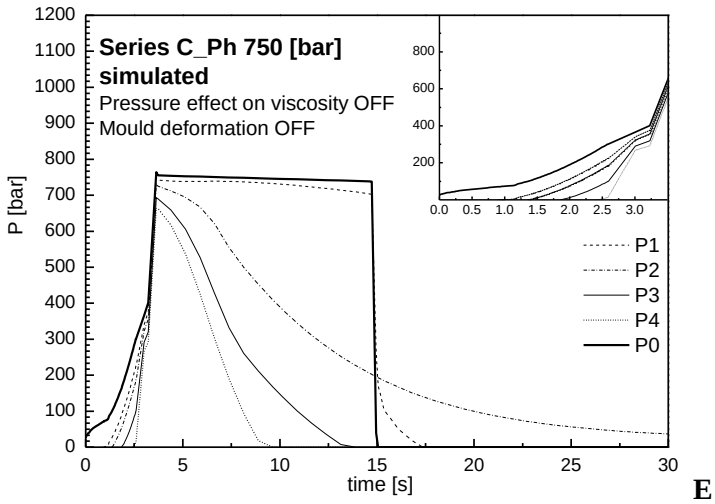

E

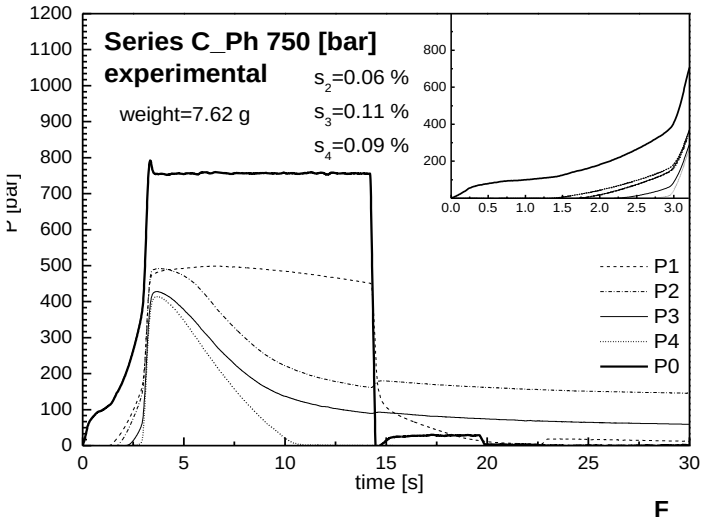

F

Fig. 32 Simulated (E) and Experimental (F) pressure evolutions of PS 678E recorded in P0 (injection chamber), P1 just before the gate, and P2, P3 and P4 inside the cavity, for tests belonging to, C series (**Table 9**). The predicted pressure curves, refer to simulation performed by setting the default database parameters for Cross WLF equation in rheological description, and Tait equation for PVT properties. (Continued).

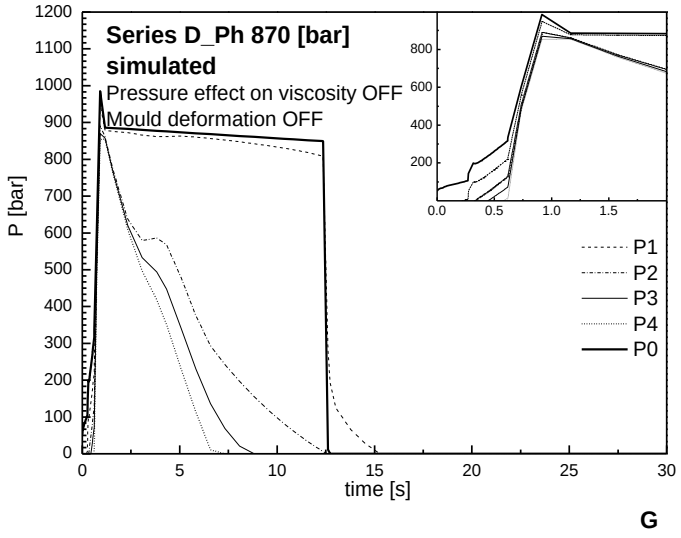

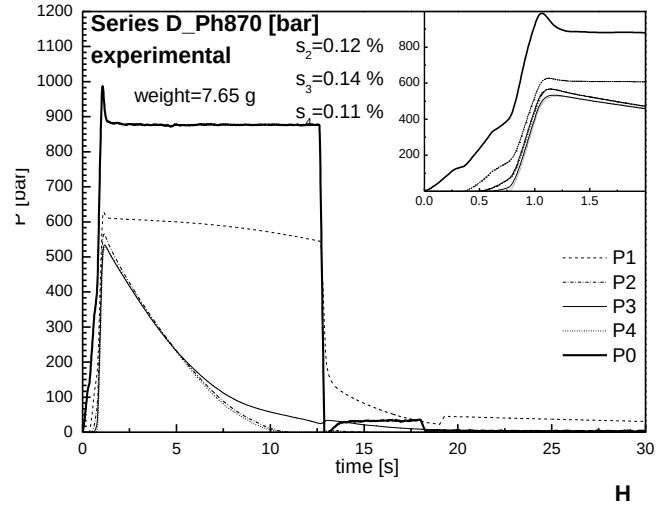

Fig. 32 simulated (G) and Experimental (H) pressure evolutions of PS 678E recorded in P0 (injection chamber), P1 just before the gate, and P2, P3 and P4 inside the cavity, for tests belonging to, D series (**Table 9**). The predicted pressure curves, refer to simulation performed by setting the default database parameters for Cross WLF equation in rheological description, and Tait equation for PVT properties. (Continued).

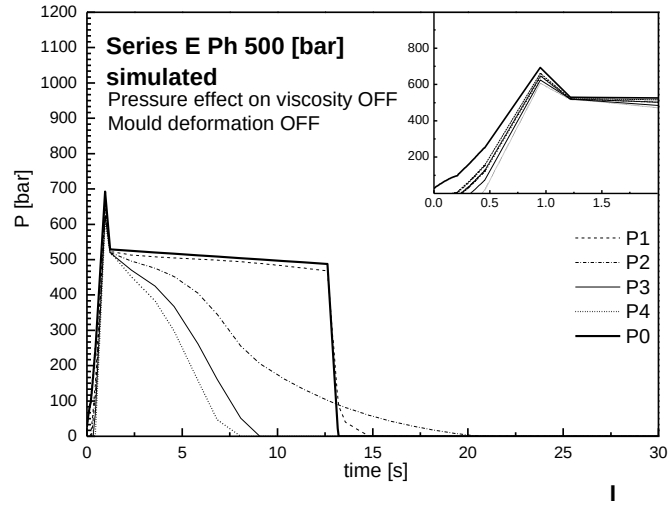

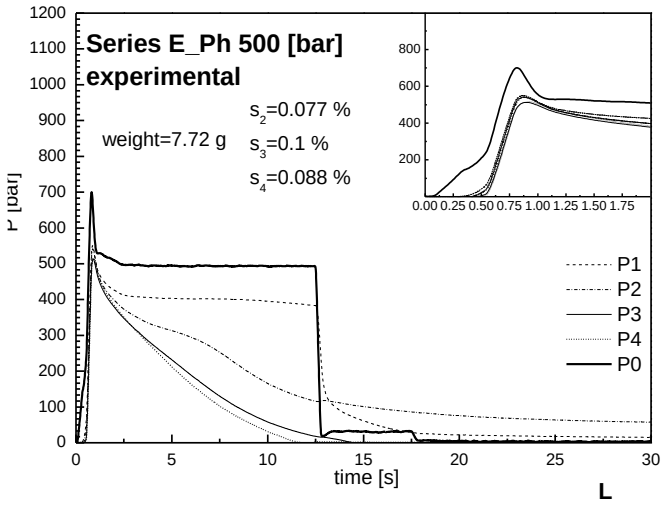

Fig. 32 simulated (I) and Experimental (L) pressure evolutions of PS 678E recorded in P0 (injection chamber), P1 just before the gate, and P2, P3 and P4 inside the cavity, for tests belonging to, E series (**Table 9**). The predicted pressure curves, refer to simulation performed by setting the default database parameters for Cross WLF equation in rheological description, and Tait equation for PVT properties. (Continued).

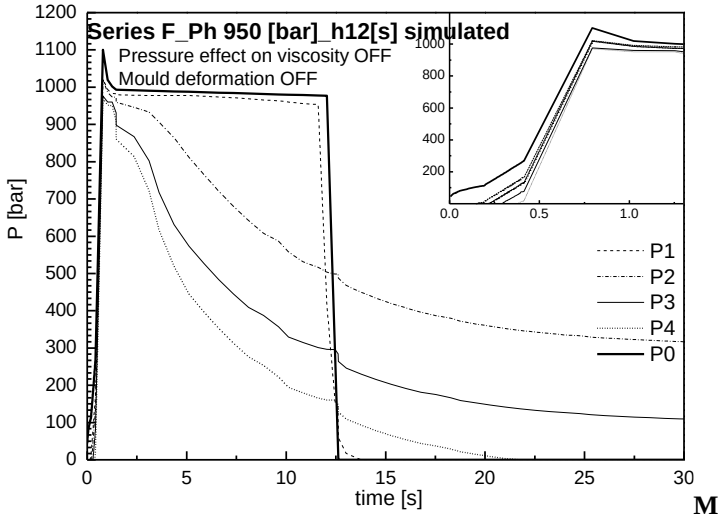

M

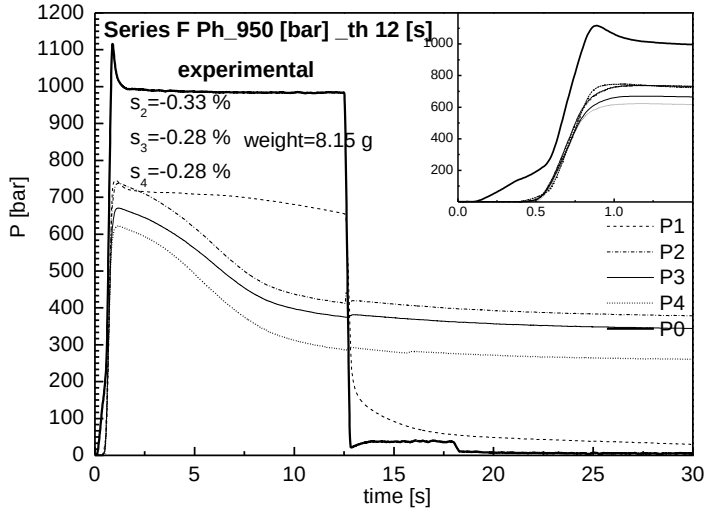

N

Fig. 32 simulated (M) and Experimental (N) pressure evolutions of PS 678E recorded in P0 (injection chamber), P1 just before the gate, and P2, P3 and P4 inside the cavity, for tests belonging to, F series (**Table 9**). The predicted pressure curves, refer to simulation performed by setting the default database parameters for Cross WLF equation in rheological description, and Tait equation for PVT properties. (Continued).

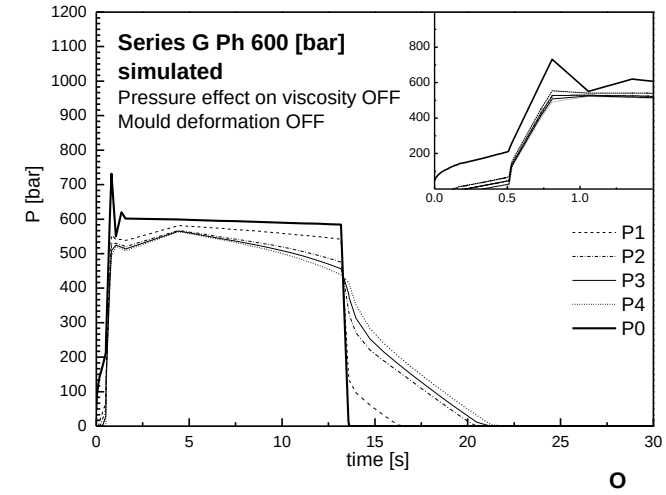

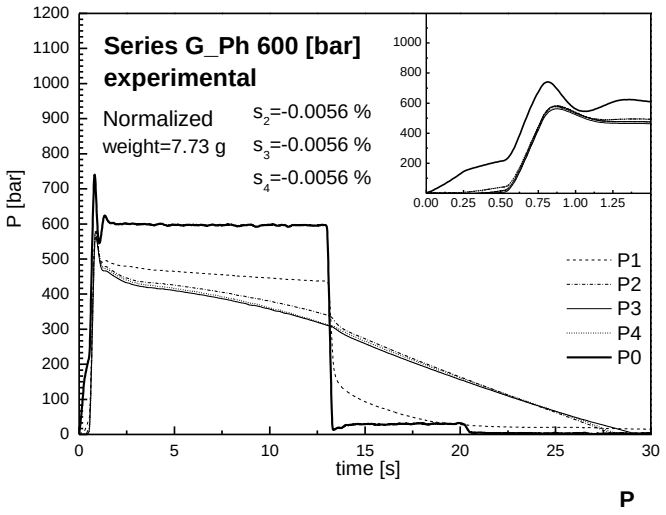

Fig. 32 simulated (O) and Experimental (P) pressure evolutions of PS 678E recorded in P0 (injection chamber), P1 just before the gate, and P2, P3 and P4 inside the cavity, for tests belonging to, G series (**Table 9**). The predicted pressure curves, refer to simulation performed by setting the default database parameters for Cross WLF equation in rheological description, and Tait equation for PVT properties. (Continued).

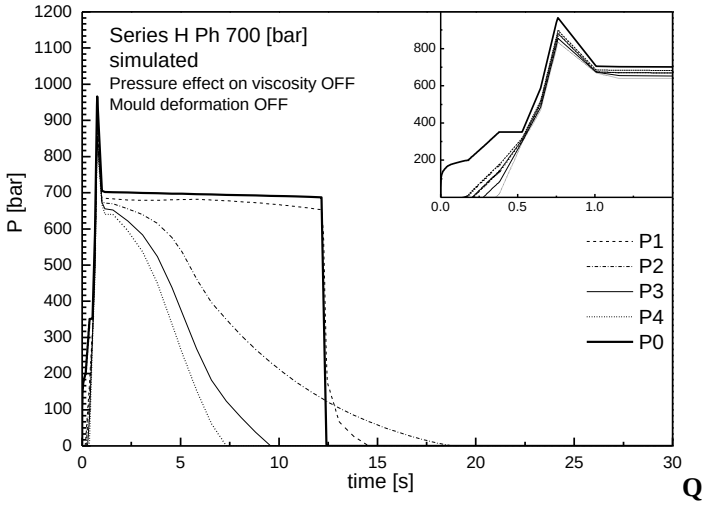

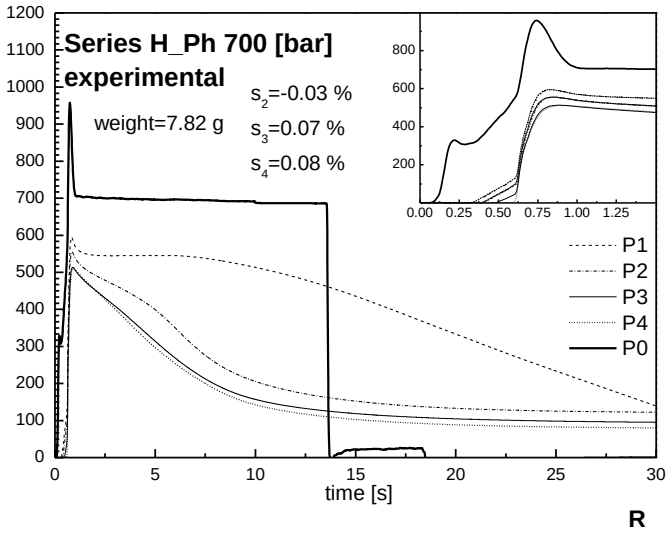

Fig. 32 Simulated (Q) and Experimental (R) pressure evolutions of PS 678E recorded in P0 (injection chamber), P1 just before the gate, and P2, P3 and P4 inside the cavity, for tests belonging to, H series (**Table 9**). The predicted pressure curves, refer to simulation performed by setting the default database parameters for Cross WLF equation in rheological description, and Tait equation for PVT properties.

The comparison for the filling stage is qualitatively good for all the tests performed. However, the predicted pressures at each transducer position are higher than the experimental ones, and this leads to higher pressures in all positions at the end of filling. This effect is also present during the packing stage, in which the simulated pressure drop between the first two transducer positions (P0, inside the injection chamber, and P1, just before the gate) is always lower than the experimental one. Furthermore during the last packing and cooling stage (after about 5 s) the simulated pressure decay at all positions was faster than the experimental ones. This is more evident for higher cavity pressures. The first feature might be ascribed to pressure influence on viscosity which is not considered when referring to standard parameters of the material Moldflow database. Regarding the second aspect, it can be explained by considering that Moldflow assumes a perfectly rigid mould, whereas, it is quite well recognized, however by (Carpenter et al 2006), (Cheng-H. W., Yu-Jen H 2007) (Delaunay et al. 2000), (Leo, Cuvelliez 1996), that mould bends with the effect of pressure and this deformation has a significant effect on both pressure profiles and dimensional accuracy. A mould is a mechanically complex system and this makes the exact description of the mould deformation a rather difficult task, also because pressure distribution inside the whole cavity determines the deformation, which, as mentioned above, in turn influences pressure distribution.

IV.2.2 Improving the accuracy of injection moulding simulation

It was shown that the accuracy of the description of pressure curves inside the cavity can be significantly improved by introducing the effect of pressure on viscosity and the effect of cavity deformation during molding. The former effect is taken into account by estimating the corresponding parameter in the equation which describes material rheology. This parameter is often set to zero but can be estimated on the basis of other material properties. The latter effect can be introduced by modifying the material compressibility.

IV.2.2.1 Effect of pressure on viscosity

The pressure influence on viscosity is not considered when referring to standard parameters of the material Moldflow database. In order to take in account this feature, some parameters in the Cross model WLF should be changed; (Zoetelief 1995) and (Van Krevelen 1997), also suggested non zero values for D_3 parameter (**Table 5**), which permit the improvement of the simulation result. A simple expression can be found in (Van Krevelen 1997) relating the effect of temperature and pressure on viscosity to the volumetric properties. This equation can be written as:

$$\beta \approx -\alpha_T \frac{\beta_V}{\alpha_V} \tag{4.1}$$

in which α_T is the temperature dependence of viscosity, β_V and α_V are the compressibility and the thermal expansion coefficient polymer.

Using the WLF equation (2.2) reported in § II.3, it is possible to obtain α_T, and β as a function of D3, respectively by partial derivative with respect to pressure and temperature:

$$\alpha_T = \frac{1}{\eta_0}\left(\frac{\partial \eta_0}{\partial T}\right)_P = -\frac{A_1 \cdot (A_2 + D_3 P)}{(A_2 - T + D_2)^2} \tag{4.2}$$

$$\beta = \frac{1}{\eta_0}\left(\frac{\partial \eta_0}{\partial P}\right)_T = \frac{A_1 \cdot D_3}{A_2 - T + D_2} \tag{4.3}$$

If Tait equation (2.4) is adopted, the parameters β_V and α_V are expressed by the following equations:

$$\beta_V(T,P) = -\frac{1}{v_0(T)}\left(\frac{\partial v}{\partial P}\right)_T = \frac{C}{B(T)+P} \tag{4.4}$$

$$\alpha_V(T,P) = \frac{1}{v_0(T)}\left(\frac{\partial v}{\partial T}\right)_P = \frac{B_2}{v_0}\left(1 - C\ln\left(1 + \frac{P}{B(T)}\right)\right) - \frac{C\,B_4 P}{B(T)+P} \tag{4.5}$$

Equation (4.1), although very simple, was found to be a good approximation of the experimental data on the effect of pressure on viscosity (Sorrentino, Pantani 2009). The right hand side of eq.(4.1) can be calculated as a function of temperature by adopting eq.(4.4) and (4.5), whose parameters are known for both materials. The value of β_V was expressed in eq.(4.3) as depending on the parameter D_3

A suitable choice for the value of the parameter D_3 can be made in order to obtain the best possible description of the RHS of eq.(4.1) by means of eq. (4.3), as shown in **Fig. 33**. The best result was obtained by setting D_3=0.051 [K bar^{-1}], consistently to the D_3 value found by (Zoetelief 1995) for PS 678E (see **Table 5**).

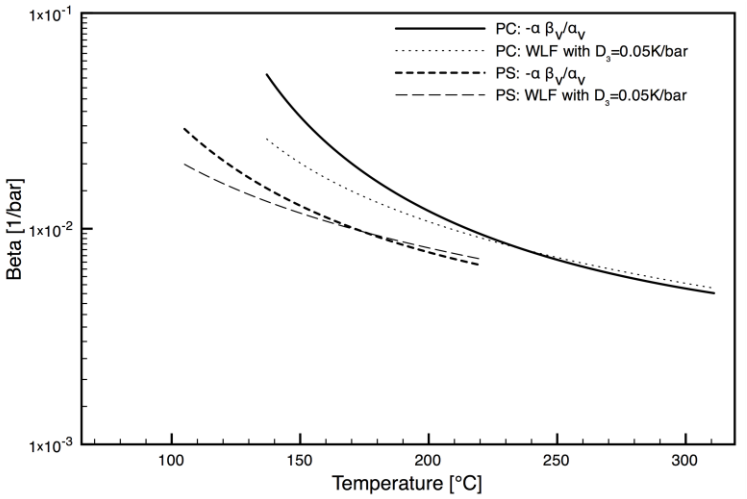

Fig. 33 Research for the best D_3 parameter to take into account the effect of pressure on viscosity in injection moulding simulation.

IV.2.2.2 Effect of mold deformation

As already stated, mould deformation is not considered when referring to the standard parameters of the material Moldflow database. The relevance of mould deformation in the simulation of the injection moulding process, is a pivotal feature in the correct prediction of the pressure evolution. Mould deformation, implies an enlargement of the cavity impression (L-L_0) in thickness/width which can be related to the total pressure distribution acting against the mould walls. An injection mould, which is a mechanically complex system, makes the exact description of the mould deformation a rather difficult task, also because pressure distribution inside the whole cavity determines mould deformation, which, as mentioned above, in turn influences pressure distribution. A somewhat simplified calculation scheme can be followed by relating the local cavity enlargement in thickness/width direction to the total pressure distribution acting against the mold walls (eq. 4.6) (Pantani, Speranza and Titomanlio 2001a).

$$S(x,t) = S_0(x)\left(1 + C_M P(x,t)\right) \tag{4.6}$$

where C_M, depending on the mould material, has dimensions of compliance, and it can be assumed that the relative cavity enlargement is due to deformation caused by pressure. C_M, typically assumes values in the range of magnitude included in $10^{-4} \div 10^{-3}$ [MPa^{-1}]. Starting from this definition, the (Pontes 2002) indicated a model which permits us to take into account the effect of the mould deformability on the simulation, and in particular on the

pressure profile prediction, considering as a corrective factor for the material compressibility, the mould compliance C_M.

$$C_M = \frac{k_M}{S} \tag{4.7}$$

In particular, for a steel rectangular mold of length l (distance between mold tie bars), containing a cavity of half thickness S/2 and width W, loaded by an uniform pressure P, k_M can be estimated as:

$$k_M = \frac{l^3 W}{4\ E\ s^3} + \frac{1.2\ (1+\nu)\ l\ W}{2\ E\ s} \tag{4.8}$$

where s is the plate thickness, E and ν are steel modulus and Poisson ratio.

Depending on mold geometry and material, k_M typically assumes values in the range $10^{-5} \div 10^{-4}$ [mm/bar]. For this work it was found, by analyzing the geometry of the mold, that k_M was about 10^{-4}[mm/bar]. The term E is the elastic modulus of the mould material (typically 210 [GPa] for steel), The k_M constant is calculated on the basis of the mould geometry considerations. In order to introduce the effect of cavity deformation in software simulation, it is necessary to convert it into a parameter which is present in the software. To do this, we will consider the cooling step, namely the stage of injection molding which starts from the gate sealing time, and represents the longest part of the molding cycle. During the cooling stage, although the cavity volume decreases because of mold deformation release, the mass per unit cavity length remains essentially constant with time; thus:

$$\int_0^{S(x,t)} v(x,y,z)dz = const \tag{4.9}$$

Differentiating both terms of (eq.4.9) and making use of (eq.4.6), one simply obtains:

$$\int_0^{S(x,t)} \left(\frac{dv(x,z,t)}{dt} \right) dz + v(x,S(x,t),z) C_M S_0 \frac{\partial P(x,t)}{\partial t} = 0 \tag{4.10}$$

which can easily be rearranged assuming that pressure does not depend on z.

$$\int_0^{S(x,t)} v_0\alpha_v \frac{\partial T(x,z,t)}{\partial t} - v_0\left(\beta_v + \frac{v(x,L(x,t),t)}{v_0} C_M \frac{S_0}{S(x,t)}\right)\frac{\partial P(x,t)}{\partial t} dz = 0 \tag{4.11}$$

which can be written as:

$$\int_0^{S(x,t)} v_0\alpha_v \frac{\partial T(x,z,t)}{\partial t} - v_0\beta_{v,a} \frac{\partial P(x,t)}{\partial t} dz = 0 \tag{4.12}$$

in which $\beta_{v,a}$ is an apparent material compressibility given by;

$$\beta_{v,a} = \left(\beta_v + \frac{v(x,L(x,t),t)}{v_0} C_M \frac{S_0}{S(x,t)}\right) \approx \left(\beta_v + C_M\right) \tag{4.13}$$

It is clear that mold deformation can be taken into account by increasing material compressibility, and thus it can be described by changing the material volumetric parameters in such a way as to keep the values of α_V unchanged and increase the values of β_V. We assume that this method to describe mold deformation, obtained by considering just the cooling stage, can be adopted during the whole molding cycle.

If the Tait equation is adopted for the description of material properties, it is possible to change α_V and β_V nearly independently acting on the parameters B3 and B4. In this work, we changed these two parameters for the solid and the melt, as reported in **Table 7**.

In the following **Fig. 34** some plots for simulating the test belonging to the A series are reported, resulting from an appropriate change in both the rheological parameter model and volumetric parameter one.

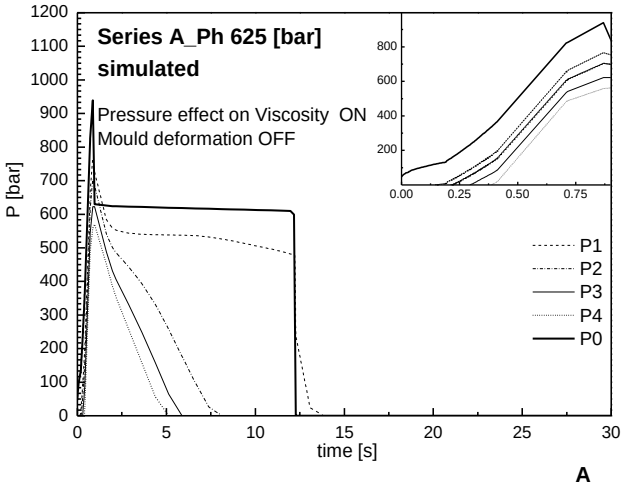

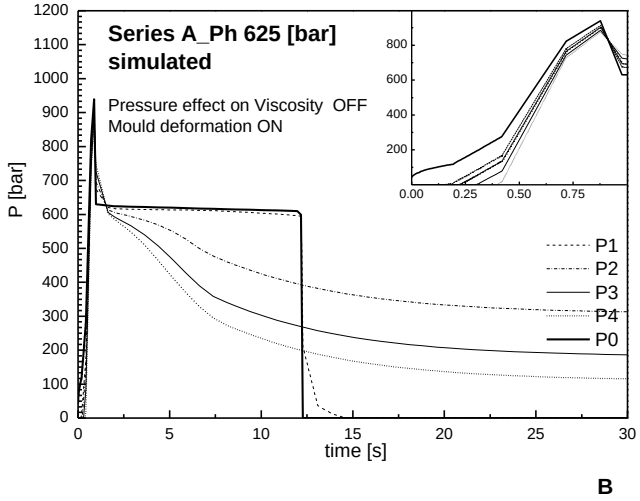

Fig. 34 Simulations for A series carried out with (A) the modification of rheology parameters to take into account only the effect of pressure on viscosity; (B) the modification of PVT parameters to take into account only the mould deformation; (Continued).

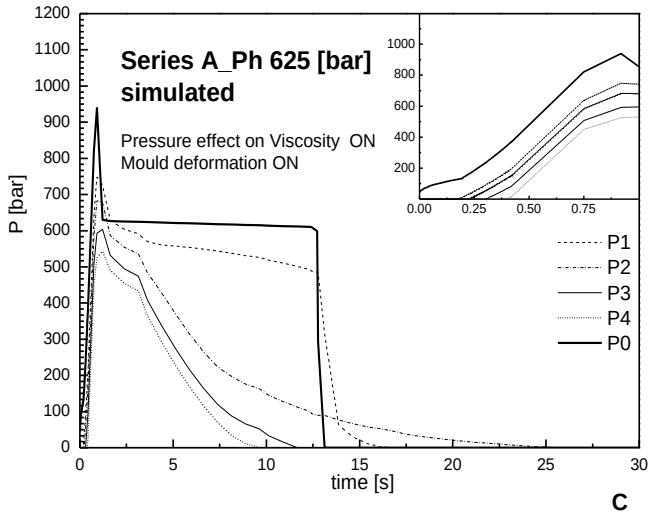

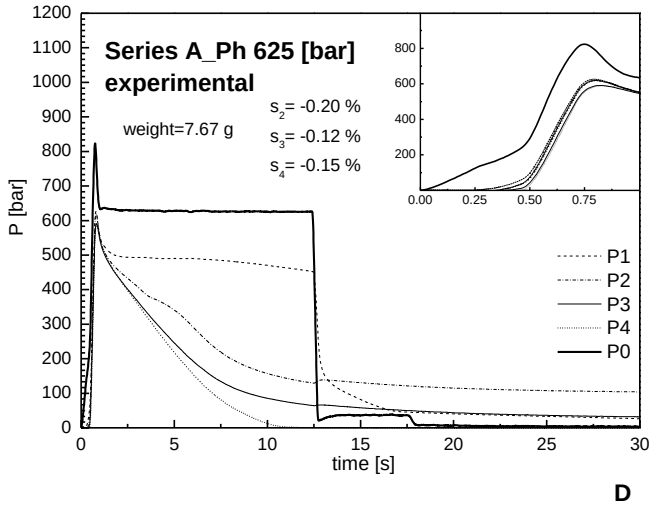

Fig.34 Simulations for A series carried out with (C) the modification of rheology parameters to take into account only the effect of pressure on viscosity; and the modification of PVT parameters to take into account only the mould deformation; (D) corresponding experimental pressure curves.

The plots **Fig. 34 C** and **D**, highlight the fact that a notable improvement in predicting the experimental pressure profile by simulation, has been achieved. In fact the effect produced by setting a non zero value for D3, in simulating the injection molding tests, leads to a satisfactorily pressure drop prediction (between P0 and P1) in comparison with the experimental cases. Also the fact that the pressure drop increases on increasing the holding pressure is captured. A remarkable improvement, was also noted in the pressure profiles' evolution during the cooling stage. The correction of the material compressibility in simulation obtained by modifying the values of the parameters B3 and B4 of the Tait equation, slows down the pressure decrease and allows us to describe the residual pressure for PS 678E.

The improvement of the simulated pressure evolution also occurs also in other investigated cases. In **Fig. 35** the correct simulated pressure evolution, regarding all the operative conditions investigated, is reported. In these plots the sample weight output by Moldflow is also reported.

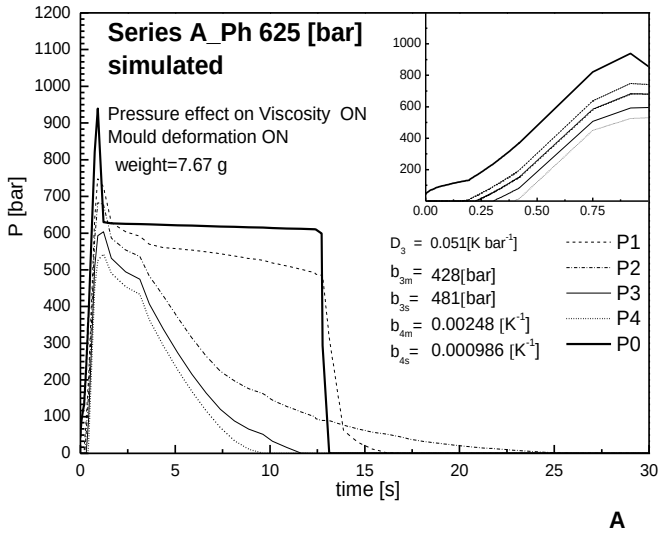

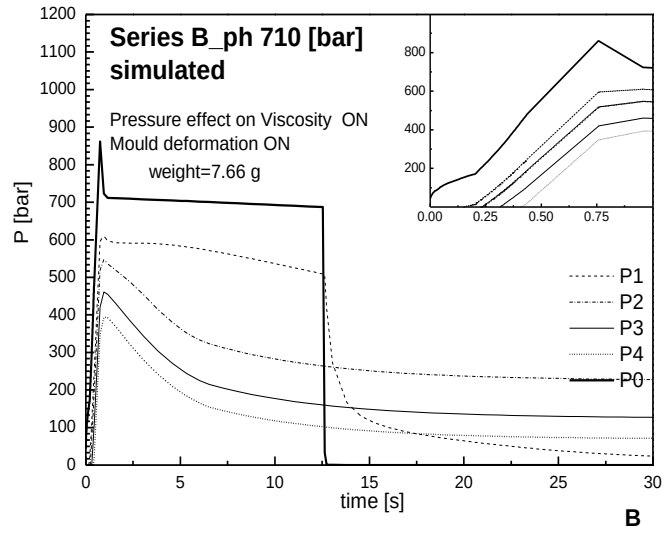

Fig. 35 Simulated pressure profiles for tests belonging to, A series (A) and B series (B). These predicted pressure profiles refer to simulations performed by setting the corrected D_3 parameter in Cross WLF equation, and setting the corrected B_3 in Tait equation, obtained by a best fitting procedure of the corresponding experimental pressure curve. (Continued).

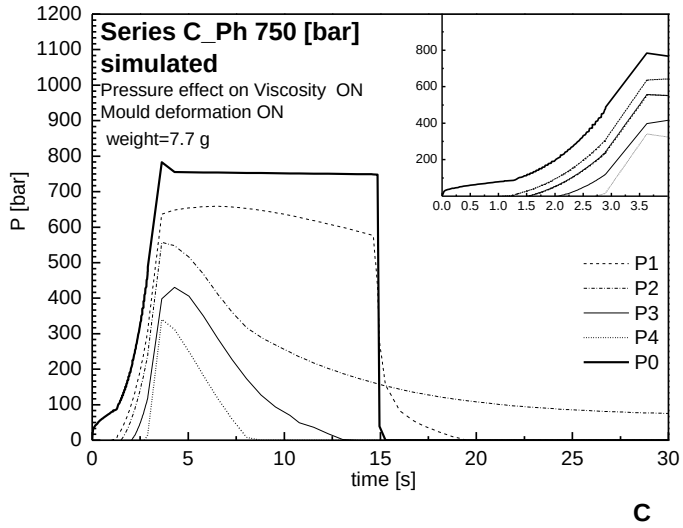

C

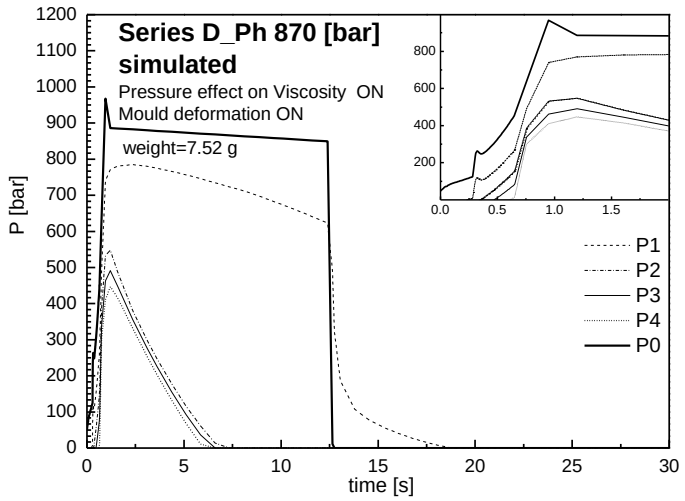

D

Fig. 35 Simulated pressure profiles for tests belonging to, C series (C) and D series (D). These predicted pressure profiles refer to simulations performed by setting the corrected D_3 parameter in Cross WLF equation, and setting the corrected B_3 in Tait equation, obtained by a best fitting procedure of the corresponding experimental pressure curve. (Continued).

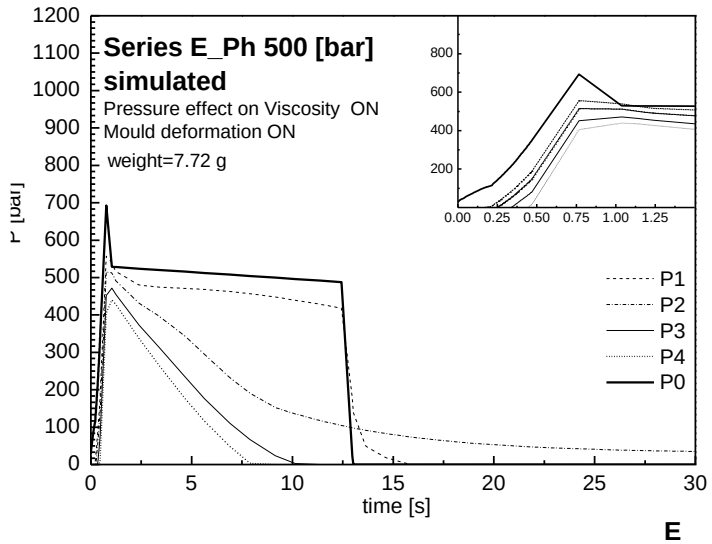

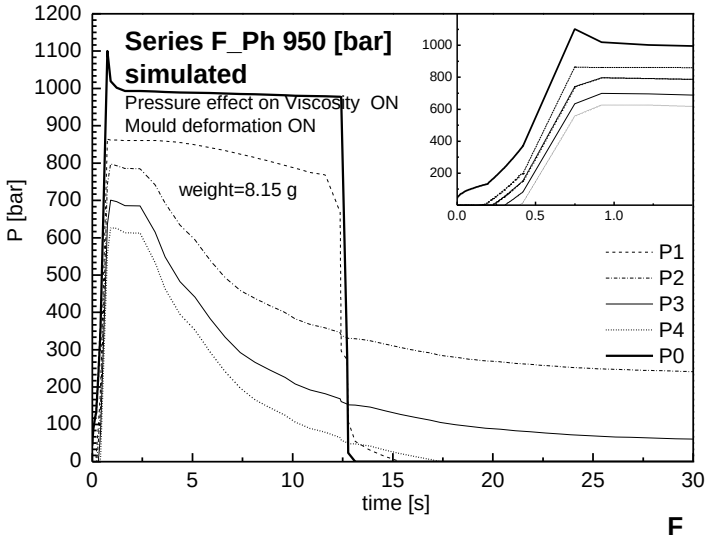

Fig. 35 Simulated pressure profiles for tests belonging to, E series (E) and F series (F). These predicted pressure profiles refer to simulations performed by setting the corrected D_3 parameter in Cross WLF equation, and setting the corrected B_3 in Tait equation, obtained by a best fitting procedure of the corresponding experimental pressure curve. (Continued).

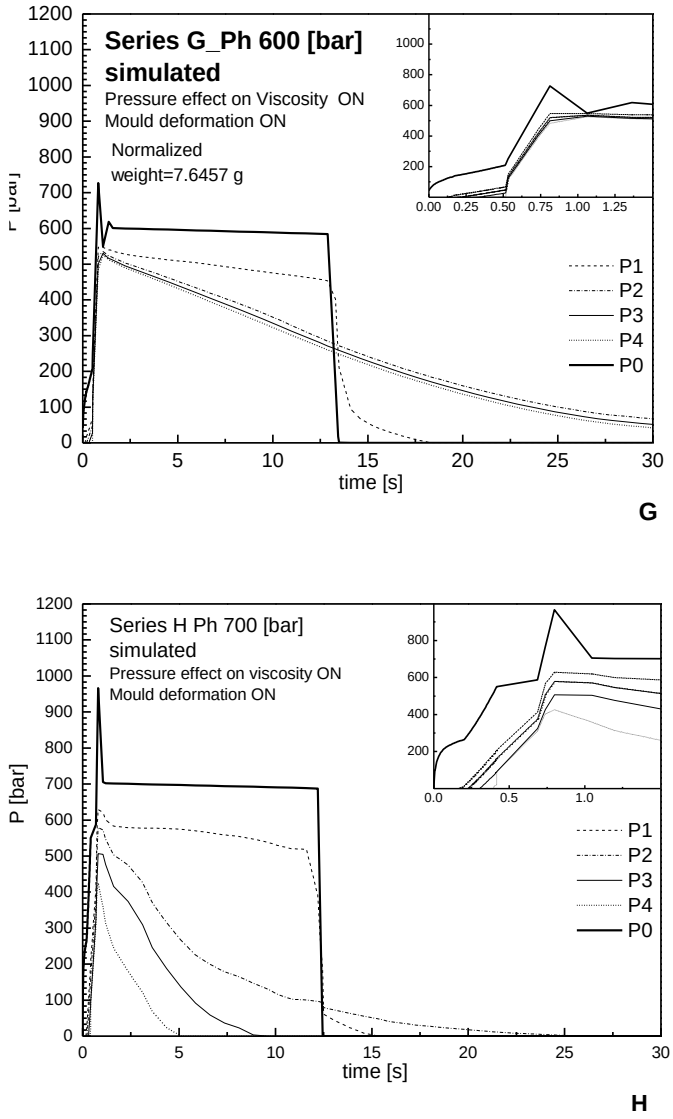

Fig. 35 Simulated pressure profiles for tests belonging to, G series (G) and H series (H). These predicted pressure profiles refer to simulations performed by setting the corrected D_3 parameter in Cross WLF equation, and setting the corrected B_3 in Tait equation, obtained by a best fitting procedure of the corresponding experimental pressure curve.

IV.3 Moldflow© simulations: solidification layer profiles

The simulation software calculates the solidification profile at each position by considering the time at which the polymer is solid (i.e. the time required for each layer to reach the ejection temperature, specified in the database for each material considered: for PS 678E this value was set to 90°C the solidification obviously starts at sample surface, and goes through the sample thickness till the centre of the sample is reached (this instant determines local solidification time). It is clear that both injection and mould temperature, and injection time, contribute mainly to determining the solidification history profile within the cavity thickness. In the following plots **Fig. 36** either local simulated solidification profile z_{sol} vs time for all the position inside to the cavity P2, P3, P4, or solidification pressure vs z_{sol} (upper diagrams in the top left hand side of plot area) are reported, for all the representative series above-mentioned for PS 678E.

As appears, in any case, the frozen layer profiles' shape show an up down concavity initially, whereas they are concave up for a long time. The solidification time depends slightly on the cavity position, and usually it is faster for the position nearest the gate. Furthermore the mould temperature does not significantly affect the amount of time required for local solidification, whereas, in the simulated moulding tests, with a thicker cavity, the highest solidification time was output, regardless of the operative conditions.

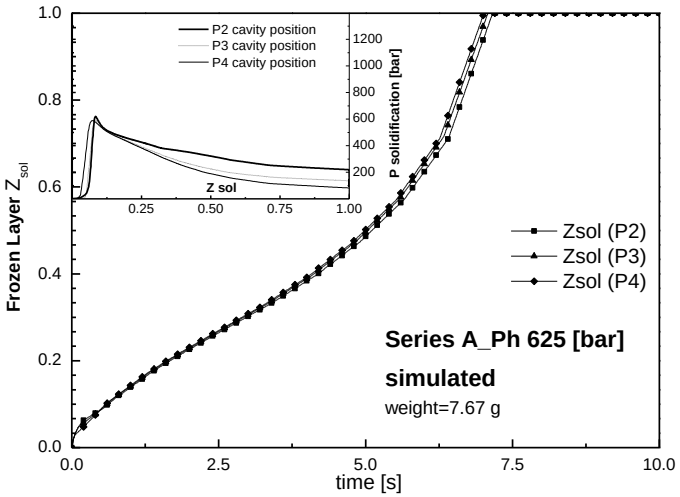

A

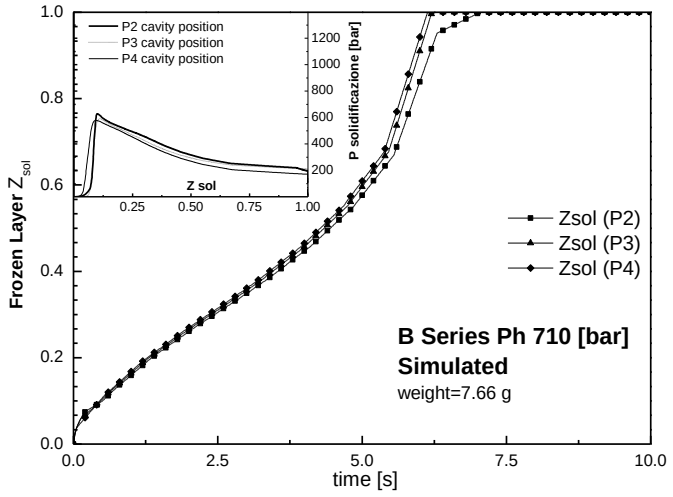

B

Fig. 36 Moldflow description of solidification history for PS 678E simulated tests belonging respectively to A series (A) and B series (B) These results refer to simulations performed by setting the corrected D_3 parameter in Cross WLF equation, and setting the corrected B_3 in Tait equation, obtained by a best fitting procedure of the corresponding experimental pressure curve. (Continued)

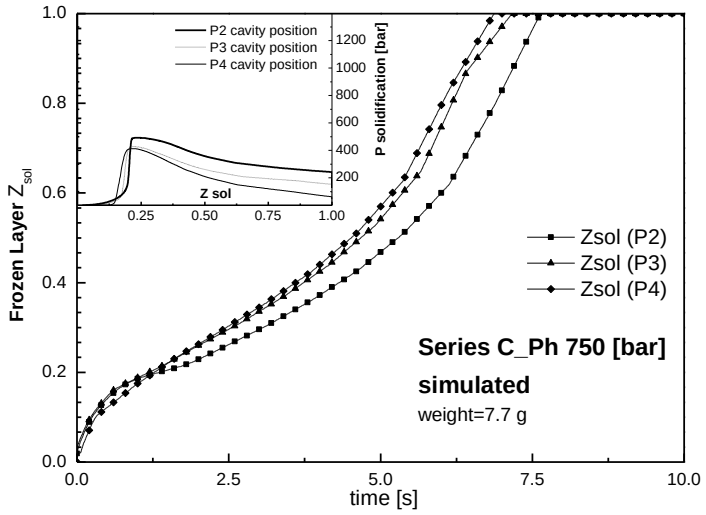

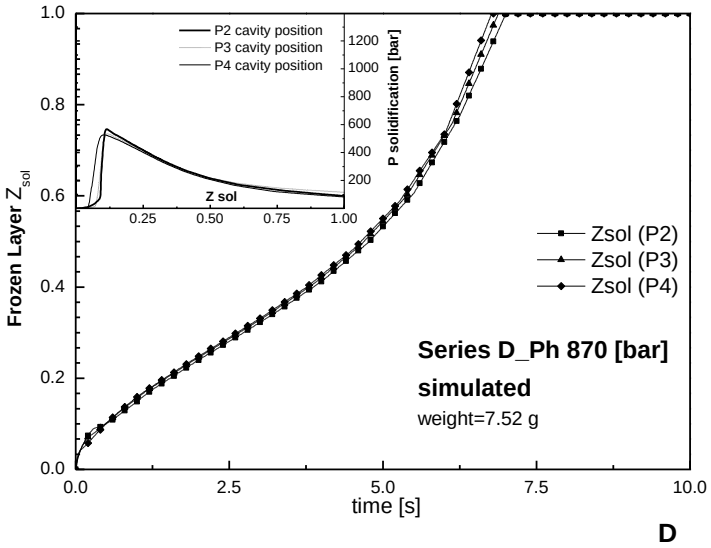

Fig. 36 Moldflow description of solidification history for PS 678E simulated tests belonging respectively to C series (C) and D series (D) These results refer to simulations performed by setting the corrected D_3 parameter in Cross WLF equation, and setting the corrected B_3 in Tait equation, obtained by a best fitting procedure of the corresponding experimental pressure curve. (Continued)

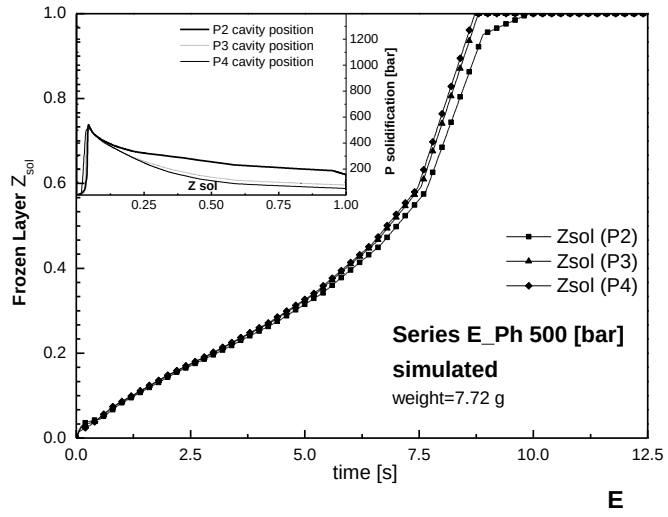

E

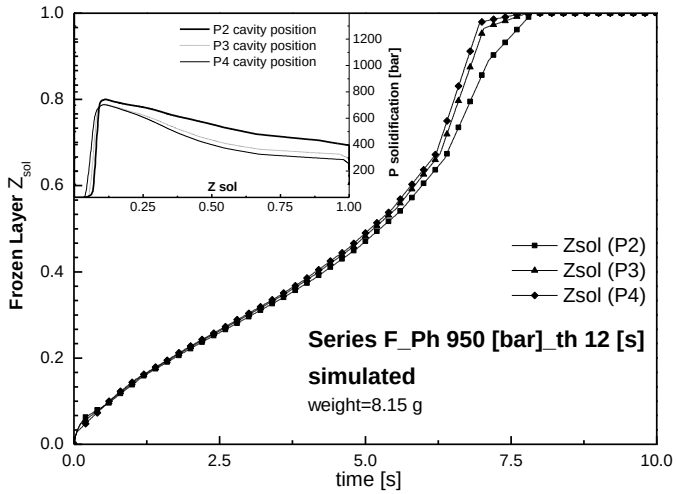

F

Fig. 36 Moldflow description of solidification history for PS 678E simulated tests belonging respectively to E series (E) and F series (F) These results refer to simulations performed by setting the corrected D_3 parameter in Cross WLF equation, and setting the corrected B_3 in Tait equation, obtained by a best fitting procedure of the corresponding experimental pressure curve. (Continued)

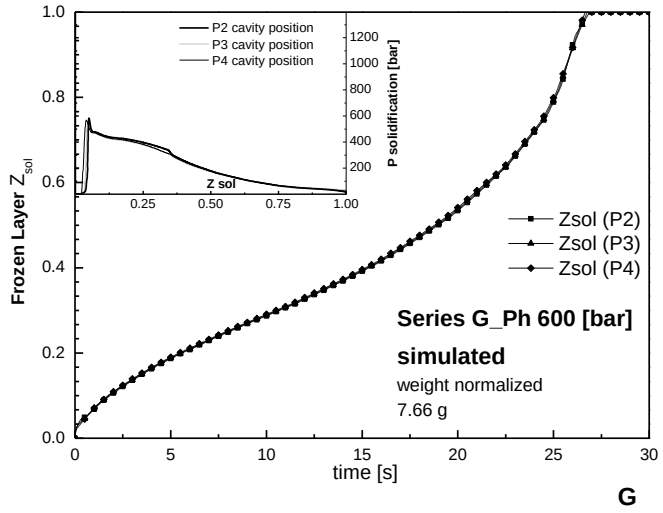

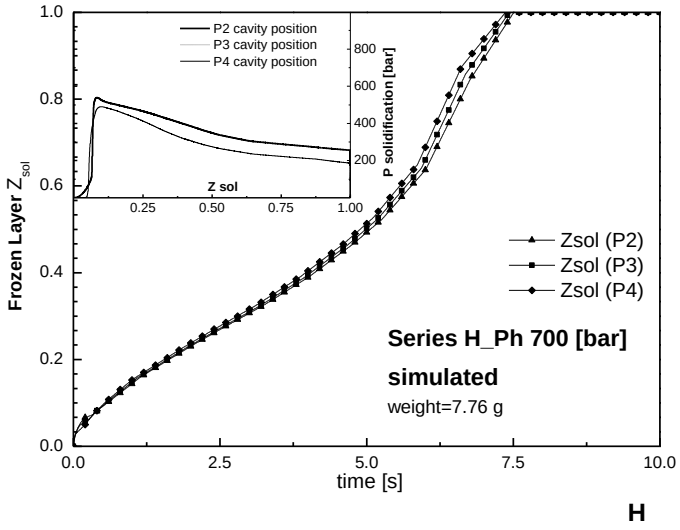

Fig. 36 Moldflow description of solidification history for PS 678E simulated tests belonging respectively to G series (G) and H series (H) These results refer to simulations performed by setting the corrected D_3 parameter in Cross WLF equation, and setting the corrected B_3 in Tait equation, obtained by a best fitting procedure of the corresponding experimental pressure curve.

Moldflow results will be used in the next section in order to validate the approach proposed in this work, by comparing the simulated solidification history output by software, to the one resulting from the application of the approach which does not require simulation. However it should be mentioned that Moldflow simulations, although probably the best reference available, do not perfectly reproduce the real profiles: the pressure profiles are only reasonably reproduced, and show what is expected to happen with solidification profiles.

Chapter Five

The Average Solidification Pressure.

In this chapter the definition of average solidification pressure is given. For its calculation, it is necessary to know both experimental pressure and solidification history. The determination of the latter has required the development of a procedure which allows to calculate the local solidification history from the experimental pressure curves, without requiring the simulation of the whole injection moulding test. Finally, the results of the procedure are compared to the simulated ones in order to evaluate the reliability of the approach proposed.

.

V.1 Definition of the Average solidification Pressure.

Cavity pressure is often considered the dominant factor determining the quality of the product in injection moulding. A lot of software for quality control in the injection moulding field, are based on the statistical approach which involves a comparison, cycle to cycle, between several pressure profile features, with respect to a reference.

Since the resulting quality of an injection moulding product is a complex function of the whole thermo-mechanical history experienced by the polymer during the moulding cycle, and not dependent only on the pressure one, these systems are not able to correctly predict failure conditions.

In the previous section, several difficulties have been encountered in an attempt to identify an adequate single parameter for describing the effect of processing conditions on product quality, taking into account only the pressure histories. Indeed, the fact that different pressure profiles gave rise to the same width shrinkage (§ III.2), confirmed that the whole pressure curve alone, cannot be used as a valid feature for describing or predicting local width shrinkage, hence, a criterion based on the reproducibility of the pressure profiles can cause the rejection of parts which are consistent with quality parameters. Nor did a single value of pressure (i.e. hydraulic pressure) lead to a satisfactory result for our purpose (§ III.3).

As suggested in the literature (Jansen Pantani Titomanlio 1998) a different approach might be considered based on knowledge of the solidification mechanism which the polymer experienced inside the cavity. A clear indication of this feature, is given by a particular value of pressure at which each layer along the thickness direction solidifies. Assuming that the polymer melt turns into an elastic solid as soon as it solidifies, a special case of a more general thermo-mechanical model for shrinkage can be considered. Since solidification proceeds from the mould surfaces, solidification pressure is different for each layer, thus each layer has a different stress-free configuration (larger dimensions for layers solidified under high pressure) as also reported by (Pantani 1999). At the end, each layer will experience a different stress so as to bring all of them to the same final length. On the basis of these considerations, the average values over the thickness of the pressures at which each layer solidifies, Ps_av, was introduced to keep into account the effect of pressure on shrinkage and residual stresses.

$$Ps\_av = \frac{1}{L}\int_{z_{SOL}=0}^{z_{sol}=L} P(t)dz_{SOL}(t) = \int_{\frac{zsol}{L}=0}^{\frac{zsol}{L}=1} P(t)\frac{d}{dt}\left(\frac{z_{SOL}(t)}{L}\right)dt = \int_{t=0}^{t=tsol=\infty} P(t)\,\dot{z}_{sol}(t)dt$$

(5.1)

in which L is the local half-thickness of the cavity and z_{sol} is the layer which is solidifying at time t (z_{sol}=0 at the mould surface); it depends on time only up to complete solidification of the sample. The definition of the average solidification pressure requires the knowledge of the temperature histories inside the polymer, in order to define z_{sol}. This piece of information not being available experimentally could be reached only by simulation.

The research for a new approach into monitoring the injection moulding process, led to the development of an innovative method which permits us to recognize the solidification history of polymer by using the experimental pressure profile alone. For this purpose an automatic procedure based on Labview© platform, was also developed. It allows us to perform a simplified analysis to obtain an estimate of the solidification history and thus of the average solidification pressure without being compelled to simulate the whole process, and at the same time, being dependent on the availability of a software licence for simulation. In the following we will explain the procedure for calculating Ps_av, and the relating results will be compared with those ones obtained by means of Moldflow (for calculating thermal history), which represent probably the best reference available in the field.

V.2 Description of solidification layer profile

Consistently with the observations stated above, the calculation of the average solidification pressure, requires not only the local pressure and temperature time profile, but also the knowledge of the local solidified layer thickness z_{sol}, on the basis of some assumptions which allow us to get simply to the problem task. The solidification of the polymer in the mould, can be described as the solidification of a slab, ignoring the property changes taking place with temperature, pressure and (above all) change of phase (Jansen 1994). After gate solidification, the mass inside the cavity remains constant, and pressure evolution is thus determined only by volumetric properties (Speranza, Titomanlio, 2004). In particular, after gate complete solidification, average material density holds a constant value since both the mass of material present inside the cavity and the volume of the cavity itself are constant. The time derivative of average material density can be written as:

$$\frac{dV}{V}(T,P) = -\alpha_V dT + \beta_V dP \qquad (5.2)$$

where V is specific volume, α_V and β_V are material thermal expansion and compressibility coefficients. Since, after gate sealing time, and as long as, after that the solidification of the local section is reached, the time derivative of the cavity average density is zero, then, the following relationship can be written.

$$\frac{dP}{d\bar{T}}\left(x, t > t_{sol}(x)\right) = \frac{\alpha_V}{\beta_V} \qquad (5.3)$$

The superimposed bar indicates averaging over the cavity thickness, and the volumetric parameters, refer to average too. According to equation (5.3), after local solidification being α_V/β_V a weak function of temperature and pressure, the pressure evolution follows the temperature profile on the basis of the relationship reported below.

$$P(x,t) = P^*(x) + \frac{\alpha_V}{\beta_V}\left[\bar{T}(x,t) - \bar{T}^*(x)\right] \qquad (5.4)$$

The star indicates values corresponding to the instant of local complete solidification.

Let T_{inj}, T_{mould}, L, y and t denote the initial temperature of molten polymer (injection temperature), mould temperature half slab thickness, thickness coordinate, and time respectively. For simplicity, convection and dissipation effects are not taken into account and thermal properties are assumed constant. The Biot number will be assumed to be infinite, that is, the temperature will be fixed at mould wall. Furthermore, the initial temperature profile at each position along the flow-path, will be assumed to be flat and equal to T_{inj}. Under these conditions, the evolution of average temperature over cavity thickness is reported below (Carslaw and Jaeger 1978)

$$\frac{\bar{T}(x,t) - T_{mould}}{T_{inj} - T_{mould}} = 2\left(\frac{2}{\pi}\right)^2 \sum_{n=0}^{\infty} \frac{1}{(2n+1)^2} \exp\left(-(2n+1)^2\left(\frac{\pi}{2}\right)^2 \frac{\alpha t}{L^2}\right) \qquad (5.5)$$

Where x denotes the distance of the generic section of the slab from gate one

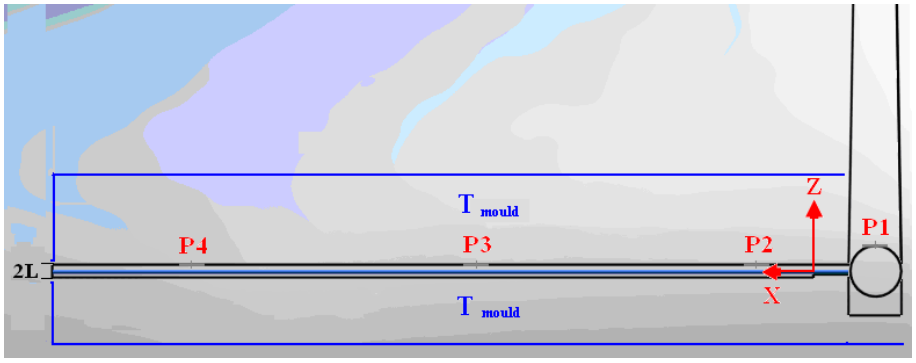

Fig. 37 Section of mould cavity

If Fo>0.1, eq. (5.5) can be approximated as:

$$\frac{\bar{T}(x,t)-T_{mould}}{T_{inj}-T_{mould}} \cong \frac{8}{\pi^2}\exp\left(-\frac{\alpha\pi^2 t}{4L^2}\right) \qquad (5.6)$$

in which α is the thermal diffusivity of the polymer.

Matching eq. (5.6) and eq.(5.4), the relationship for local pressure profile is obtained (valid for $t > t_{sol}(x)$ and Fo>0.1).

$$P(x,t)=P^*(x)+\frac{\alpha_V}{\beta_V}\left[T_{mould}-\bar{T}^*(x)\right]+\frac{\alpha_V}{\beta_V}\left(T_{inj}-T_{mould}\right)2\left(\frac{2}{\pi}\right)^2\exp\left(-\frac{\alpha\pi^2 t}{4L^2}\right) \qquad (5.7)$$

Considering the constant terms, the equation can be rearranged as in the following

$$P(x,t)=P_\infty+A\exp\left(-\left(\frac{\pi}{2}\right)^2\frac{\alpha\left(t-t_{Sol}(x)\right)}{L^2}\right) \qquad (5.8)$$

Here, it is important to remark on the meaning of $t_{sol}(x)$ and P_∞ terms. The term t_{sol} is local solidification time, namely the amount of time required so that thermal and mechanical equilibrium reach the centre of the sample. When solidification is completed locally, that is for $t > t_{sol}(x)$, the cavity pressure drops to a residual pressure value P_∞ which can also be negative.

A characteristic time for cooling can be defined as:

$$\tau = \left(\frac{2}{\pi}\right)^2 \frac{L^2}{\alpha} \qquad (5.9)$$

in which α is the thermal diffusivity of the polymer. This time constant takes into account the rate at which heat flows through the sample thickness, toward the mould wall during the cooling stage , and represents how quickly the cavity pressure decays/drops.

Equation 5.8 can be written as:

$$P(x,t) = P_{\infty} + A\exp\left(-\frac{\left(t - t_{Sol}(x)\right)}{\tau}\right) \qquad (5.10)$$

The Fourier number is related to τby the following equation:

$$Fo = \frac{\alpha t}{L^2} = \left(\frac{2}{\pi}\right)^2 \frac{t}{\tau} \qquad (5.11)$$

The temperature as a function of time t and position y (as distance from cavity midplane) is reported below (Carslaw and Jaeger 1978);

$$\frac{T(t,y) - T_{mould}}{T_{inj} - T_{mould}} = \frac{4}{\pi}\sum_{n=0}^{\infty}\frac{(-1)^n}{(2n+1)}\exp\left(-(2n+1)^2\frac{t}{\tau}\right)\cos\left((2n+1)\frac{\pi y}{2L}\right) \qquad (5.12)$$

For Fo>0.1 (eq. 5.12) becomes (valid for long time)

$$\frac{T(t,y) - T_{mould}}{T_{inj} - T_{mould}} \approx \frac{4}{\pi}\exp\left(-\frac{t}{\tau}\right)\cos\left(\frac{\pi y}{2L}\right) \qquad (5.13)$$

In this relationship, for y=0 (that is when the solidification has reached the midplane of the slab), the local solidification time is reached t= t_{sol}, and thus local solidification temperature $T(t_{sol}, y=0) = T_{Sol}$ is determined:

$$\frac{T_{sol} - T_{mould}}{T_{inj} - T_{mould}} = \frac{4}{\pi}\exp\left(-\frac{t_{sol}}{\tau}\right) \qquad (5.14)$$

Similarly, each point reaching the solidification temperature, defines the solidified layer growth along the thickness.

$$\frac{T_{sol}-T_{mould}}{T_{inj}-T_{mould}}=\frac{4}{\pi}\exp\left(-\frac{t_{sol}}{\tau}\cos\left(\frac{\pi}{2}\frac{y_{sol}(t)}{L}\right)\right) \qquad (5.15)$$

By combining eq.(5.14) and eq.(5.15) the solidified layer profile is obtained, and reported in the equation (5.16):

$$\frac{4}{\pi}\exp\left(-\frac{t_{sol}}{\tau}\right)=\frac{4}{\pi}\exp\left(-\frac{t_{sol}}{\tau}\cos\left(\frac{\pi}{2}\frac{y_{sol}(t)}{L}\right)\right) \qquad (5.16)$$

That is it was implicitly supposed that all layers along the slab thickness, solidify at the same temperature of midplane. In the following section (§ VI.1.1.1), it will take into account the effects of both, solidification pressure, and cooling rate on the solidification temperature, and therefore, it will be considered dependent on the y position coordinate). Rearranging eq (5.16):

$$\frac{1}{\exp\left(\frac{(t-t_{sol})}{\tau}\right)}=\cos\left(\frac{\pi}{2}\frac{y_{sol}(t)}{L}\right) \qquad (5.17)$$

It is possible to define a complementary variable $z=L-y$ and thus $z_{sol}=L-y_{sol}$ which describes the solidified layer growth starting from the mould wall till midplane of the slab.

The boundary conditions are written as:

$$\begin{cases}\dfrac{z_{SOL}(t=0)}{L}=0 & @\ \text{initial instant } t=0\cdot\\ \dfrac{z_{SOL}(t=t_{sol})}{L}=1 & @\ \text{complete solidification instant } t=t_{sol}\end{cases}$$

Using the eq.(5.17), and indicating with 1/f the term on the left in eq. (5.17):

$$\frac{1}{f(t)}=\cos\left(\frac{\pi}{2}\frac{(L-z_{SOL}(t))}{L}\right) \qquad (5.18)$$

Hence by using eq.(5.13) it is possible to obtain $z_{sol}(t)$ solution for long times;

$$\frac{z_{SOL}(t)}{L} = 1 - \frac{2}{\pi}\arccos\left(\frac{1}{f(t)}\right) \qquad (5.19)$$

Differentiating the eq.(5.19) with respect to time:

$$\frac{d}{dt}\left(\frac{z_{SOL}(t)}{L}\right) = \left(\frac{2}{\pi}\right)\left(\frac{1}{\tau}\right)\left(\frac{1}{\sqrt{f^2(t)-1}}\right) \qquad (5.20)$$

On the basis of the average solidification pressure definition eq.(5.1), it is possible to write;

$$Ps\_av = \int_{t=0}^{t=tsol=\infty} P(t)\frac{d}{dt}\left(\frac{z_{SOL}(t)}{L}\right)dt = \left(\frac{2}{\pi}\right)\left(\frac{1}{\tau}\right)\int_{t=0}^{t=tsol=\infty} P(t)\frac{1}{\sqrt{f^2(t)-1}}dt \qquad (5.21)$$

As the eq. (5.13) defined the temperature as a function of time t and position y, for long time, the corresponding solution for short time is obtained by the penetration theory as reported in equation (5.22):

$$\frac{T(z,t)-T_{mould}}{T_{inj}-T_{mould}} = erf(\eta) \qquad (5.22)$$

Where z is the thickness coordinate starting from the mould wall, whereas η is the normalized coordinate for thickness defined in equation (5.23):

$$\eta = \frac{z}{\sqrt{4\alpha t}} = \frac{z/L}{\sqrt{4\alpha t/L^2}} = \frac{z/L}{2\sqrt{Fo}} = \frac{z/L}{\sqrt{4\left(\frac{2}{\pi}\right)^2\frac{t}{\tau}}} \qquad (5.23)$$

Furthermore , it can be possible to write the solidification layer evolution by means of the following equation (5.24):

$$\frac{T_{sol}-T_{mould}}{T_{inj}-T_{mould}} = erf\left(\frac{z_{SOL}/L}{\sqrt{4\alpha\left(t_{sol}/L^2\right)}}\right) = erf\left(\frac{z_{SOL}/L}{\sqrt{4F_0}}\right) \qquad (5.24)$$

Considering the eq. (5.14) it follows:

$$: \frac{z_{SOL}(t)/L}{\sqrt{4\alpha t/L^2}} = erf^{-1}\left(\frac{T_{sol}-T_{mould}}{T_{inj}-T_{mould}}\right) = erf^{-1}\left(\frac{4}{\pi}\exp\left(-\frac{t_{sol}}{\tau}\right)\right) \quad (5.25)$$

It is possible to obtain $z_{sol}(t)$ solution for short times:

$$\frac{z_{SOL}(t)}{L} = erf^{-1}\left(\frac{4}{\pi}\exp\left(-\frac{t_{sol}}{\tau}\right)\right)\sqrt{4\alpha t/L^2} \quad (5.26)$$

By differentiating with respect to time the eq (5.26), one can write:

$$\frac{d}{dt}\left(\frac{z_{SOL}(t)}{L}\right) = erf^{-1}\left(\frac{4}{\pi}\exp\left(-\frac{t_{sol}}{\tau}\right)\right)\sqrt{4\alpha/L^2}\,\frac{1}{2\sqrt{t}} = \frac{\dot{z}_{sol}(t)}{L} \quad (5.27)$$

Therefore, it was possible to obtain a double solution for the local solidification layer evolution:

$$\frac{z_{sol}^{s,t}}{L} = \tilde{\tilde{T}}_{sol}\sqrt{\pi\frac{t}{\tau}} \quad (5.28a) \qquad for Fo < 0.1 \; shot\ times$$

$$\frac{z_{sol}^{l,t}}{L} = 1 - \frac{2}{\pi}a\cos\left(\frac{\pi}{4}\tilde{\tilde{T}}_{sol}\exp\left(\frac{\pi^2}{4}\frac{t}{\tau}\right)\right) \quad (5.28b) \qquad for Fo > 0.1 \; long\ times$$

Where $\overline{T_{sol}}$ is a dimensionless solidification temperature, which in the case of slab solidification should be defined as following;

$$\tilde{T}_{sol} = \frac{T_{sol}-T_{mold}}{T_{inj}-T_{mold}} \quad (5.29)$$

However, in the investigated cases, for each test and position one cannot be sure about the temperatures. In fact it can happen that T_{mould} changes slightly from case to case. T_{inj}, on the other hand, holds less uncertainties for the value of τ and thus it's more suitable to adopt the following relationship for T_{sol}.

$$\tilde{T}_{sol} = \frac{4}{\pi}\exp\left(-\frac{\pi^2}{4}\frac{t_{sol}}{\tau}\right) \quad (5.30)$$

Consistently with this statement, a relationship which allows us to describe the solidification layer profile is given:

$$\frac{z_{sol}}{L} = \frac{z_{sol}^{s,t}}{L} + \xi(t)\left(\frac{z_{sol}^{l,t}}{L} - \frac{z_{sol}^{s,t}}{L}\right) \qquad (5.31)$$

in which

$$\xi(t) = \frac{1}{1+\exp(10(t-t_C))} \qquad (5.32)$$

whereas

$$t_C = \frac{\tau}{10}$$

$$\begin{cases} \xi(t) = 0 & for \cdot t << t_C \\ \xi(t) = 1 & for \cdot t >> t_C \end{cases}$$

Finally, eq (5.31) permits us to describe the whole local solidification layer profile, **Fig. 38**.

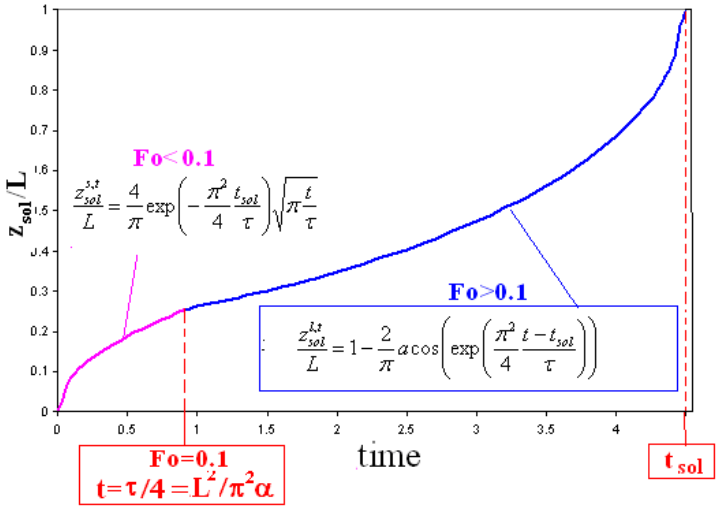

Fig. 38 Qualitative local solidification layer profile along the moulded part thickness

V.3 Determination of the solidification history by experimental pressure curves.

To be consistent with what is stated above, in order to calculate the local solidification layer profile it is necessary to know two parameters τ and t_{sol}. If the experimental local pressure profile is available, it is possible to obtain both these parameters. In a generic section, when the solidification is completed, the local pressure evolution should follow an exponentially decay law, on the basis of the relationship (5.10) already stated.

$$P(x,t) = P_{\infty} + A\exp\left(-\frac{(t - t_{Sol}(x))}{\tau}\right) \qquad (5.10)$$

Therefore, by an exponential model fitting of experimental pressure curves, τ and t_{sol} could be obtained in each condition. Indeed on the basis of this approach the local solidification time can be defined as the instant after which the pressure profile moves away from the exponential model fitting (within an error tolerance range), with an appropriate τ value too (**Fig. 39**).

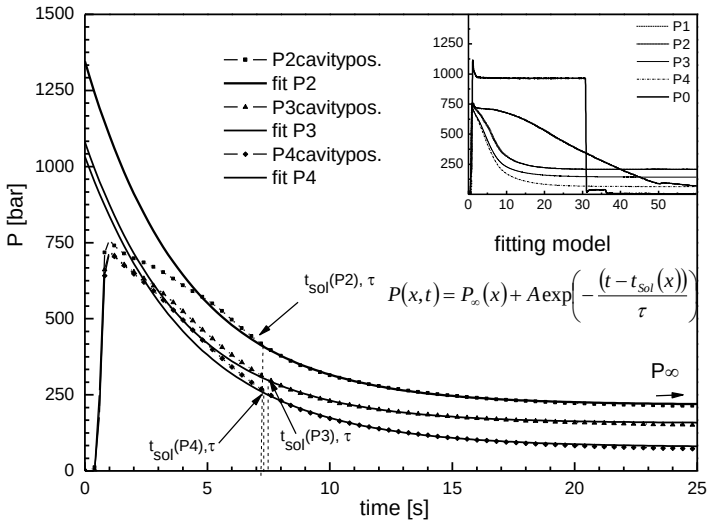

Fig. 39 Qualitative exponential fit model for experimental pressure curves.

Both P_{∞} and t_{sol} depend on either polymeric physical properties, or process conditions, and on flow direction in the mould's cavity too. In addition the time constant τ depending on mould cavity geometry (as defined

by eq.5.9). It should be noted that P_∞ is a positive value which is attained when the moulded part gets to the thermal and mechanical equilibrium within the mould. Notwithstanding, if the pressure into the mould goes to zero before thermal equilibrium has occurred, no residual pressure is involved, and P_∞ is a negative value. Carrying out the injection moulding tests with higher holding pressure values, over a sufficiently long time, guarantees a positive residual pressure value P_∞,, which obviously helps the procedure to find a more reliable value for the parameters. For this reason, some tests were carried out imposing high holding pressure and keeping it for 30 [s] at least (see **Table 9**).

V.4 Labview© procedure for determining of the Ps_av

A calculus procedure based on this approach, has been implemented, by means of Labview© platform; it works on a text file of data input, containing a column for time, and some columns for cavity pressure data points.

First of all it is necessary to establish a time interval for iterative calculation on the basis of pressure data files. The first time value t_{onset} is detected as the instant at which a certain number of pressure data points begin to rise, guaranteeing that polymer has just reached the position in the cavity. Also the instant t_{fin} corresponding to zero pressure cavity is detected by reversal of text data files. In this manner the time interval for calculating is set (t_{onset} -t_{fin}). After that a value for time is required in input, $t_i = t_{in}$ (where i=1…n) which belongs within the time interval above defined.

In order to run the calculus procedure, it is necessary to set a value for Pressure, P_∞ (j)= $-P_{min}$ (where j=1…m) which will determine the pressure interval $-P_{min} \div P_{min}$ within which the procedure runs for searching for the correct value for P∞. An external routine works starting from $-P_{min}$ as a hypothetical residual pressure, and updating it (by increasing in 5 bar) for each cycle, till the real residual pressure is found exactly at $t= t_{fin}$.

For each P_∞ (j) value, an internal subroutine starts for calculating the interval time abovementioned, as explained in the following.

The procedure consists in a nested loop sequence of calculus which involves an internal cycle and external one, and it will be explained below.

On the basis of P_∞ value, the internal cycle, runs the calculus routine starting from $t_{i=1} = t_{in}$, and updating it (by increasing in 1/5 of second) till it reaches $t_{i=n} = t_{fin}$. Setting the P_∞(j), for each t_i, the procedure compares the fitting results relating to the linear best fit model (which is eq.(5.10) linearized) with the experimental data point, calculating both $\ln(P- P_\infty)$ and $(t- t_{in})$. each update for the time, the number of points for calculation decrease, the procedure reduces to 20 points both the $(t- t_{in})$ and $\ln(P-P_{fin})$ arrays in order to work on the basis of the same point number.

For each step of the calculus routine, the procedure carries out the intercept A, and slope (which is $-1/\tau$) of the best fit model linearized, the latest updated value of t_{in} (which is t_{sol}), and the maximum discrepancy between linearized fitting and experimental pressure data.

It is possible to operate also setting a value for τ_i. In this case the procedure works on the basis of a linear fitting of experimental data, characterised by an imposed slope ($-1/\tau_i$). Apart from the slope results, the outputs of the procedure are the same. This is particularly helpful in the case in which the local pressure profile does not present residual pressure.

Another routine operates on the basis of a matrix which groups all the results recorded for each calculus routine. After an allowable margin of error has been imposed, it considers only the results which are included within the imposed tolerance, and it detects the least absolute error value, outputting τ and as small as possible value for t_{sol} as a result of best fit. In the case in which τ is imposed, the procedure detects, the least absolute error value, carrying out a value, as small as possible, for t_{sol} as a result of imposed fit.

The flow chart describing the main steps involved in the computation of τ and t_{sol} is reported in **Fig. 40**

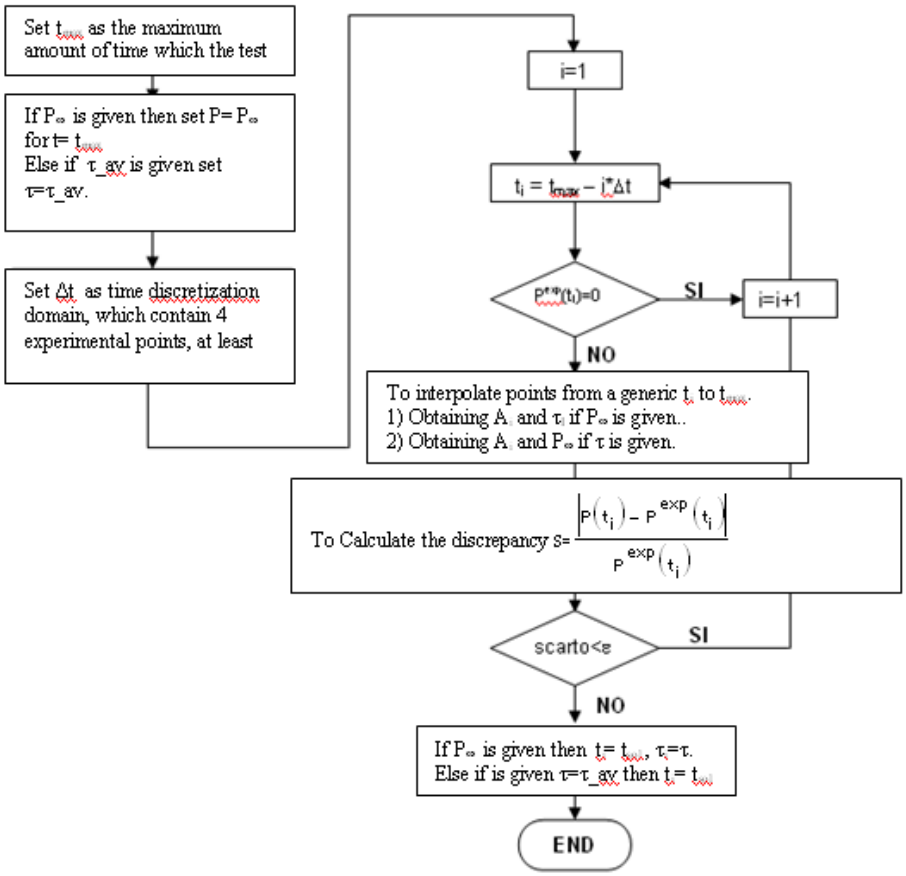

Fig. 40 Schematic flow chart refers to calculus algorithm procedure.

V.4.1 Relevance of the results of the procedure for PS678E: τ constant results

The calculus procedure was used for estimating both τ and t_{sol} parameters for all the investigated series. In the following **Fig. 41**, the same plots refer to longer holding time tests condition (Hydraulic Pressure 45÷65 [bar], holding time 30 [s], except for H series holding time 20 [s]). These plots highlight the best exponential fit of the experimental pressure curves in cavity positions performed by the calculus procedure approach, and for each case also τ and t_{sol} calculated values are reported.

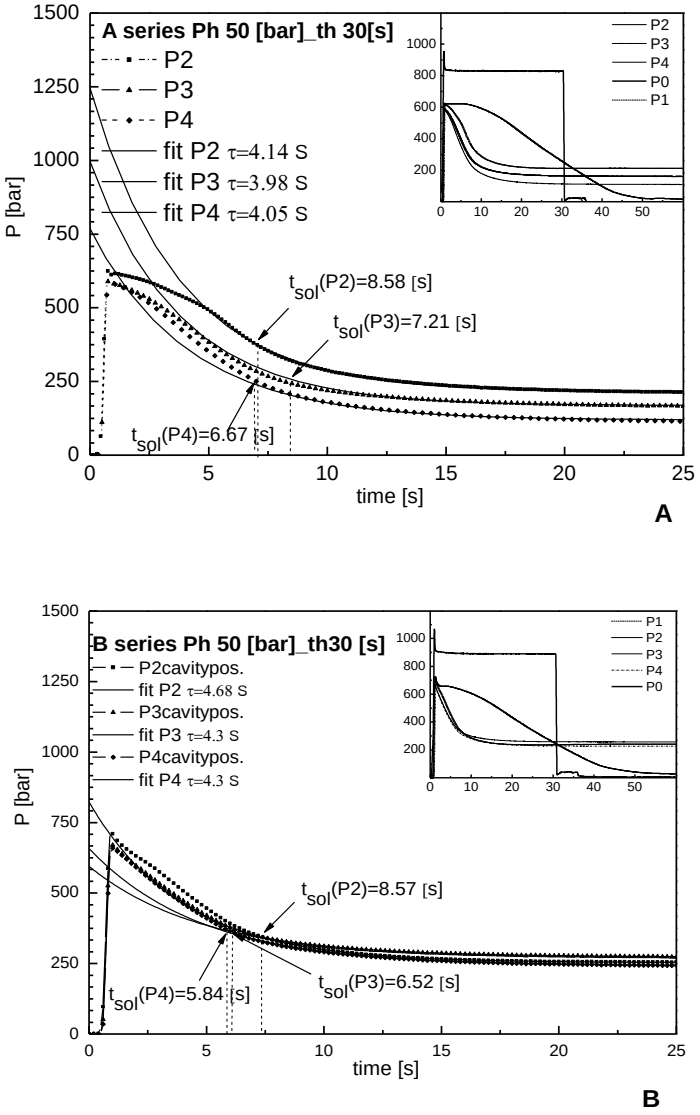

Fig. 41 Exponential best fit of PS 678E pressure data referred to longer holding test conditions; respectively for A series (A) and B series (B).(Continued).

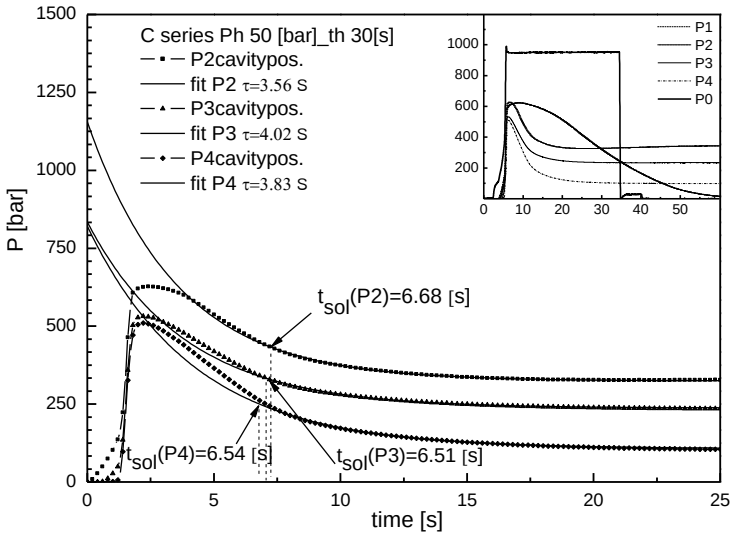

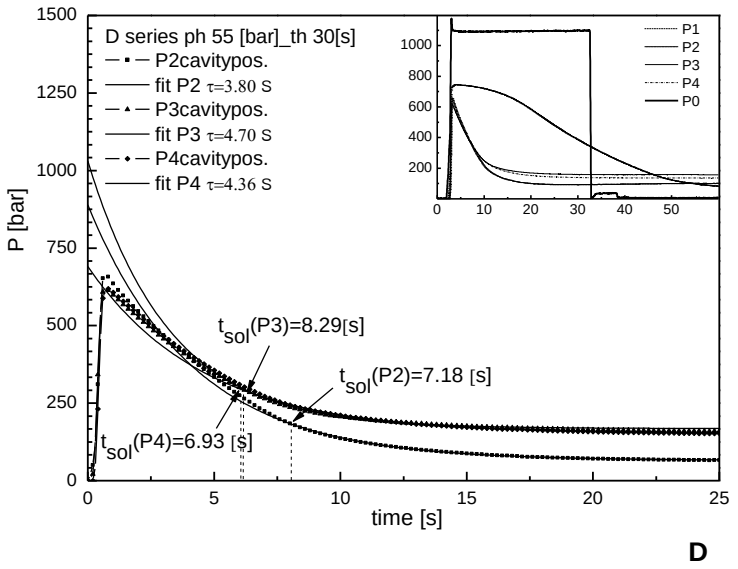

Fig. 41 Exponential best fit of PS 678E pressure data refer to longer holding test conditions; respectively for C series (C) and D series (D).(Continued).

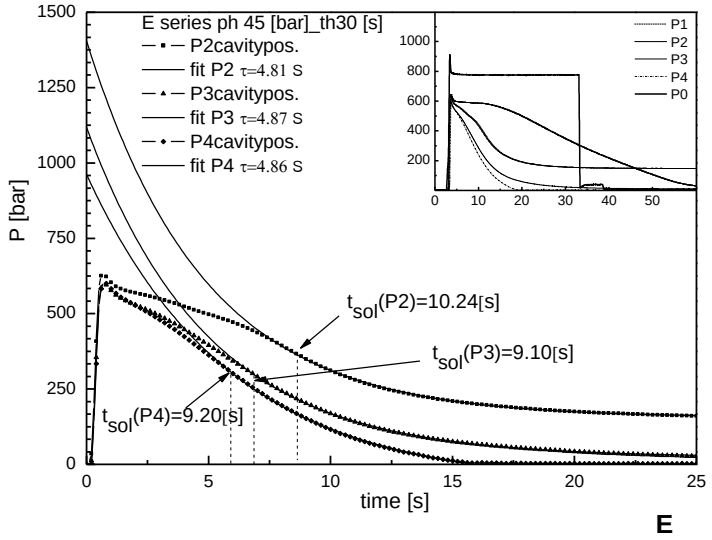

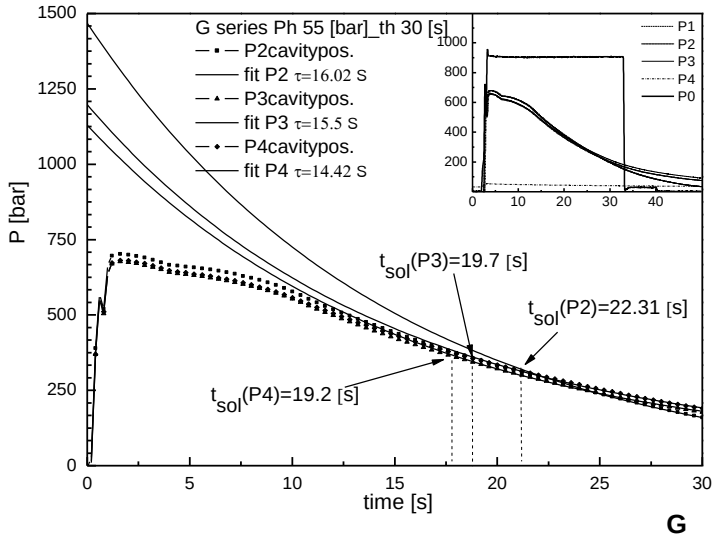

Fig. 41 Exponential best fit of PS 678E pressure data refer to longer holding test conditions; respectively for E series (E) and G series (G). (Continued).

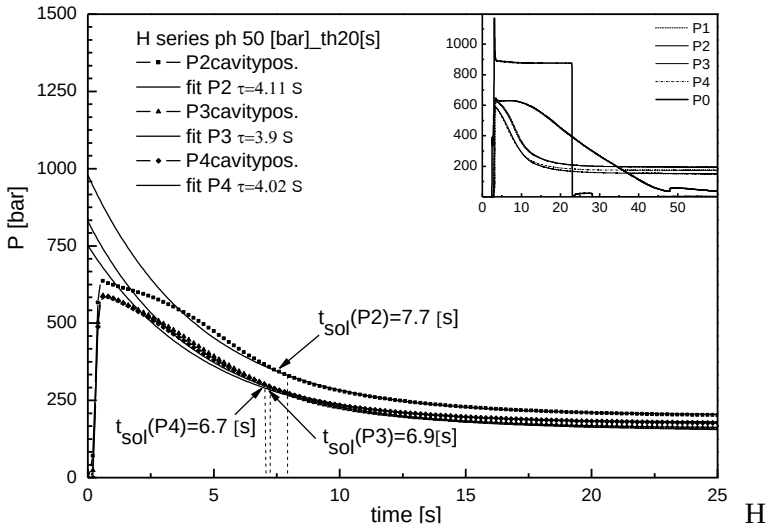

Fig. 41 Exponential best fit of PS 678E pressure data refer to longer holding test conditions; respectively for H series (H).

In **Fig. 42** the values of τ refer to best fit mode calculation for all experimental tests above mentioned. The relevancy on data pointed out by the plot, is consistent with the eq.(5.9) for τ definition, since a proportionality factor (≅ 4) exists relating to the τ values for the different cavity thickness.

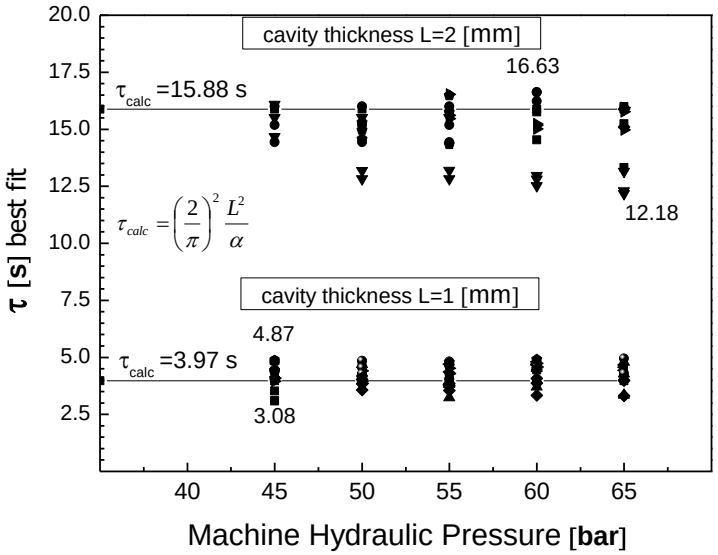

Fig. 42 Relevance of comparison between τ results referring to use of the procedure for PS 678E

Furthermore it can be observed that τ results referring to use of the procedure, are in agreement with the τ_{calc} calculated values with eq.(5.9) on the basis of the physical properties reported in **Table 2** [§ II.2.1] (Pantani 1999). All these occurrences, suggest the reliability of the method from the determination of τ point of view; in order to validate the method, it is necessary to also support the results regarding t_{sol}. This aspect will be discussed in the following section dedicated to the solidification layer results.

V.4.2 Relevance of the results of the procedure for PS 678E: Z_{sol} results

Once both the local solidification time t_{sol} and τ are determined, the whole solidification history can be described by means of eq.(5.19) and eq.(5.26). As regards relevance, it is necessary to remark on some aspects of this operative approach. The definitions of τ eq.(5.9) and z_{sol} eq.(5.19) and (5.26), implied only a dependence on thermal condition (i.e. both injection and mould temperature, and injection time too which contribute to define the

thermal diffusivity α), and by cavity thickness 2L. This suggested that, in determining the solidification description, τ and t_{sol} values referring to a particular operative condition on the pressure, can be extended to other ones (i.e. to short holding time and smaller pressure values) but referring to the same thermal condition. These observations were consistent with the experimental results. The results of the solidification layer profiles, obtained by using the procedure, from experimental pressure curves belonging to the tests listed in **Table 9** [§ II.4.3], are reported in **Fig. 43**. It can be noticed how the local solidification layer profile reaches the unitary value in correspondence with local solidification t_{sol}.

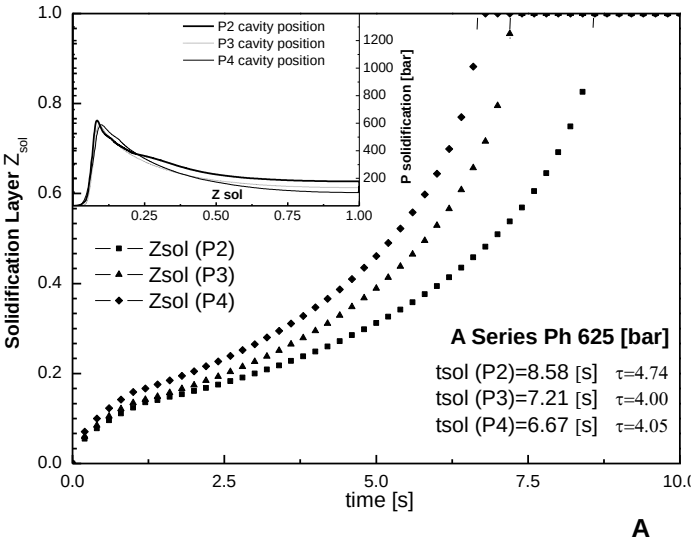

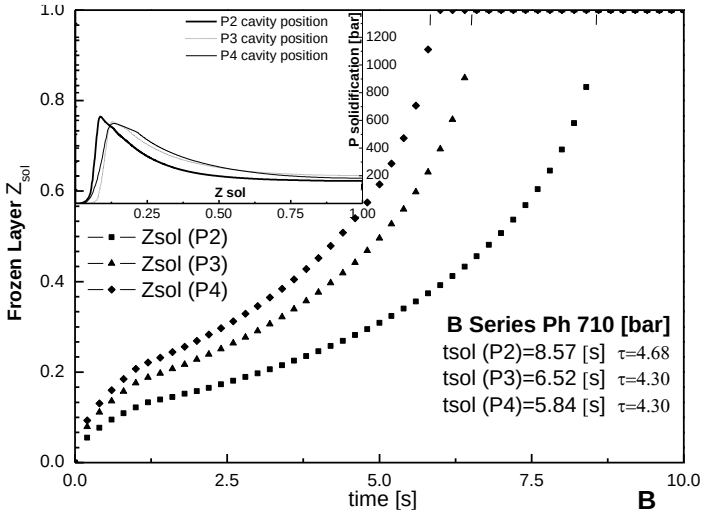

Fig. 43 Solidification layer profile obtained by using the procedure for PS 678E experimental pressure curves belonging to A series tests (A) and B series tests (B), indicated in [§ II.4.3]. (Continued).

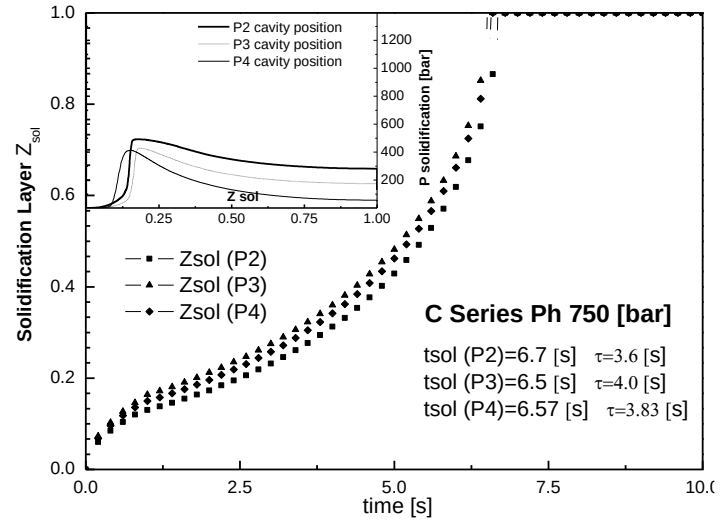

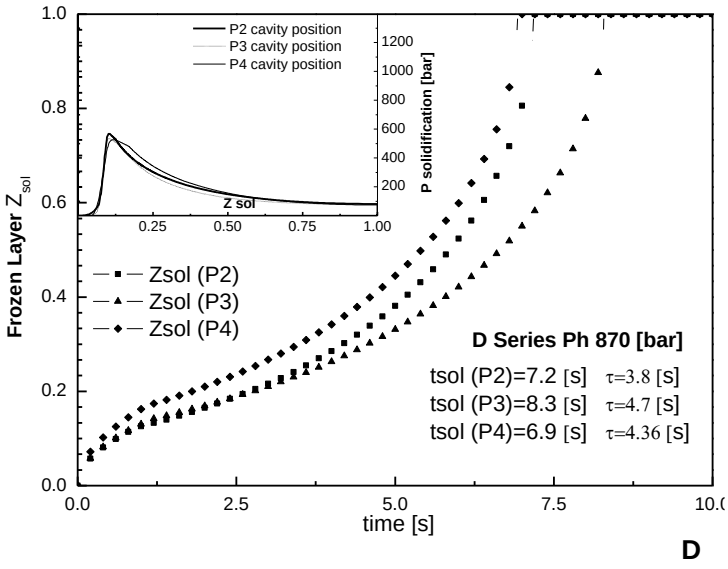

Fig. 43 Solidification layer profile obtained by using the procedure for PS 678E experimental pressure curves belonging to C series tests (C) and D series tests (D), indicated in [§ II.4.3]. (Continued).

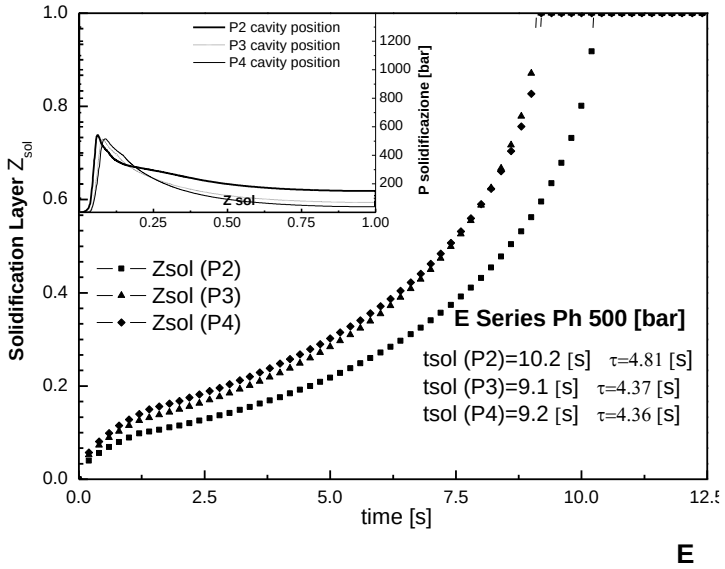

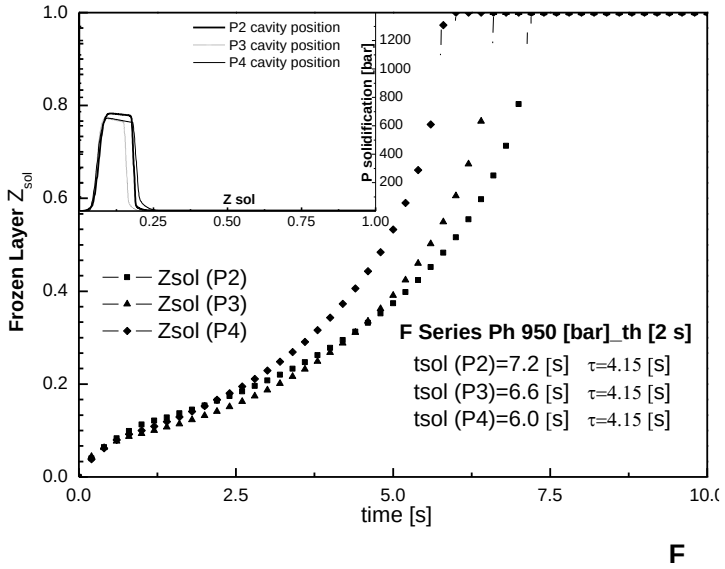

Fig. 43 Solidification layer profile obtained by using the procedure for PS 678E experimental pressure curves belonging to E series tests (E) and F series tests (F), indicated in [§ II.4.3]. (Continued).

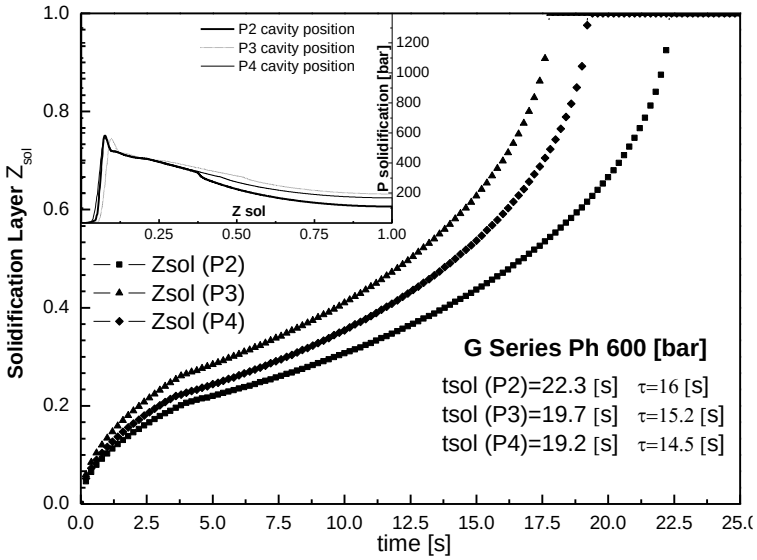

G

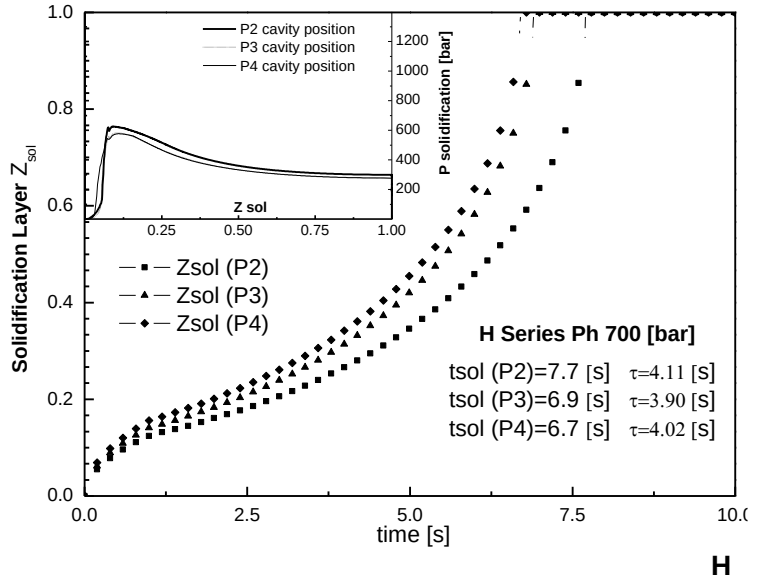

H

Fig. 43 Solidification layer profile obtained by using the procedure for PS 678E experimental pressure curves belonging to G series tests (G) and H series tests (H), indicated in [§ II.4.3].

V.4.3 Comparison on Z_{sol} results between experimental procedure and simulation

A comparison with Moldflow description of solidification history at the same operative condition reported in [§.IV.3] was carried out, for all positions in the mould cavity in **Fig. 44**.

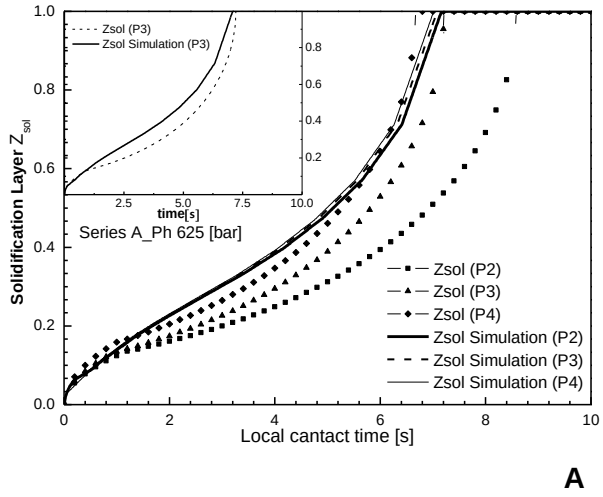

A

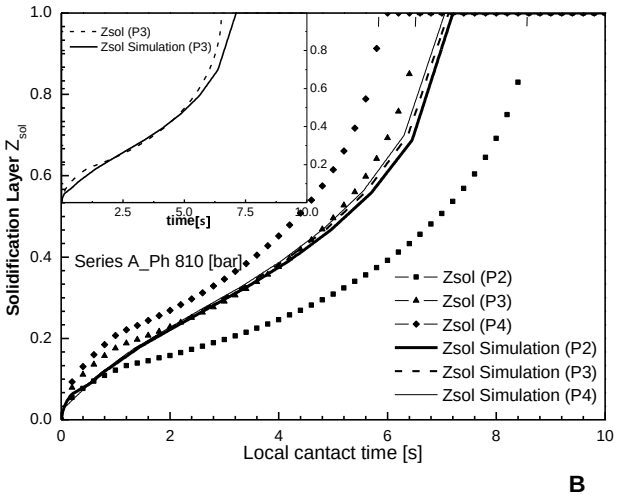

B

Fig. 44 Comparison between Moldflow description of solidification history and the solidification layer growth obtained by using the procedure from experimental pressure curves for several tests belonging to A series; Ph625 [bar] (A) and Ph 810 [bar] (B). (Continued).

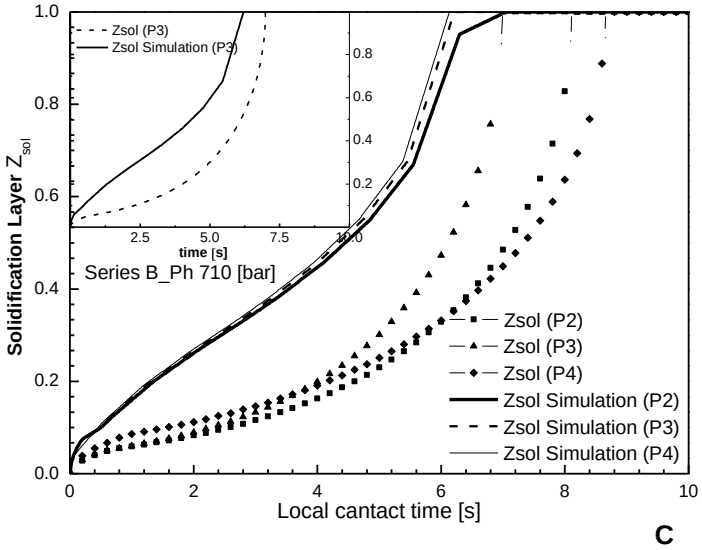

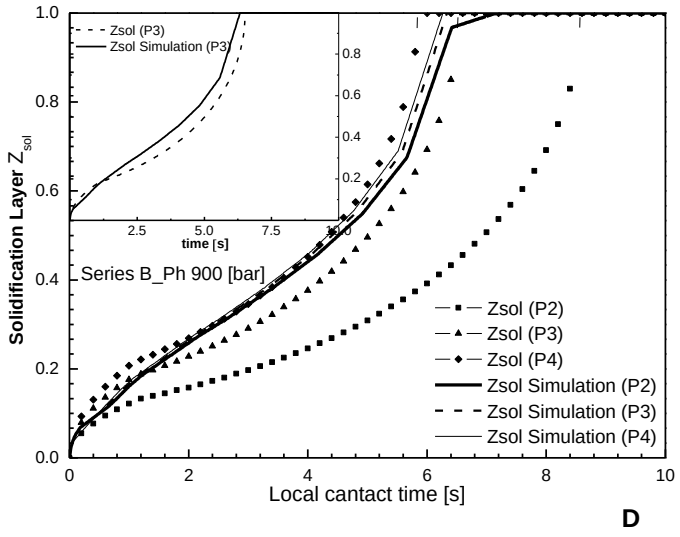

Fig. 44 Comparison between Moldflow description of solidification history and the solidification layer growth obtained by using the procedure from experimental pressure curves for several tests belonging to B series; Ph 710 [bar] (C) and Ph 900 [bar] (D). (Continued).

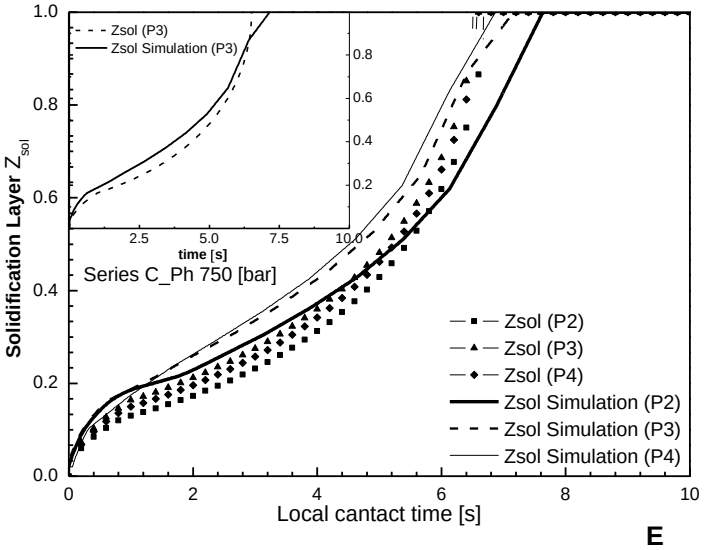

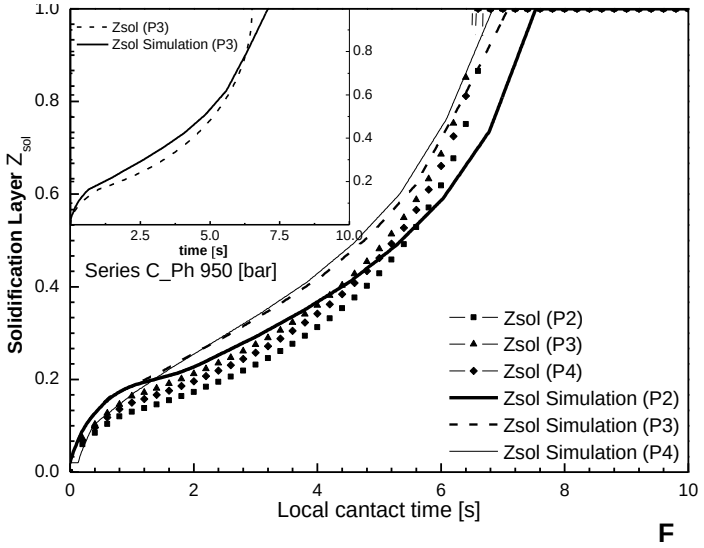

Fig. 44 Comparison between Moldflow description of solidification history and the solidification layer growth obtained by using the procedure from experimental pressure curves for several tests belonging to C series; Ph 750 [bar] (E) and Ph 950 [bar] (F). (Continued).

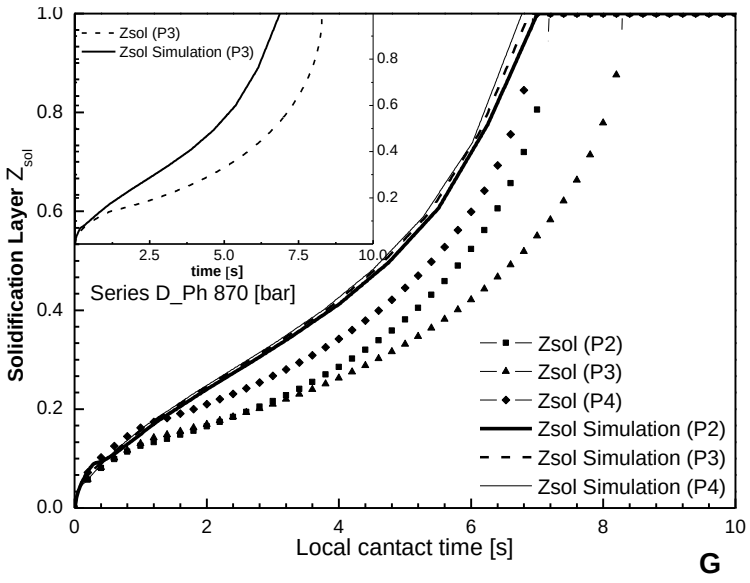

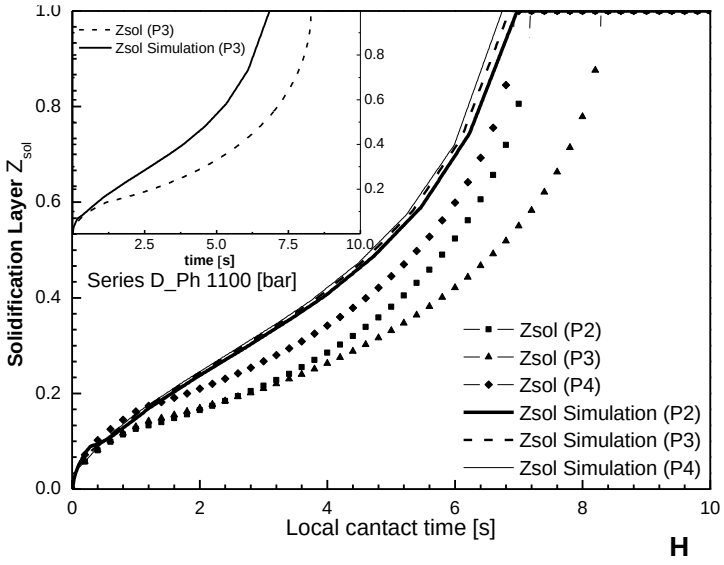

Fig. 44 Comparison between Moldflow description of solidification history and the solidification layer growth obtained by using the procedure from experimental pressure curves for several tests belonging to D series; Ph 870 [bar] (G) and Ph 1100 [bar] (H). (Continued).

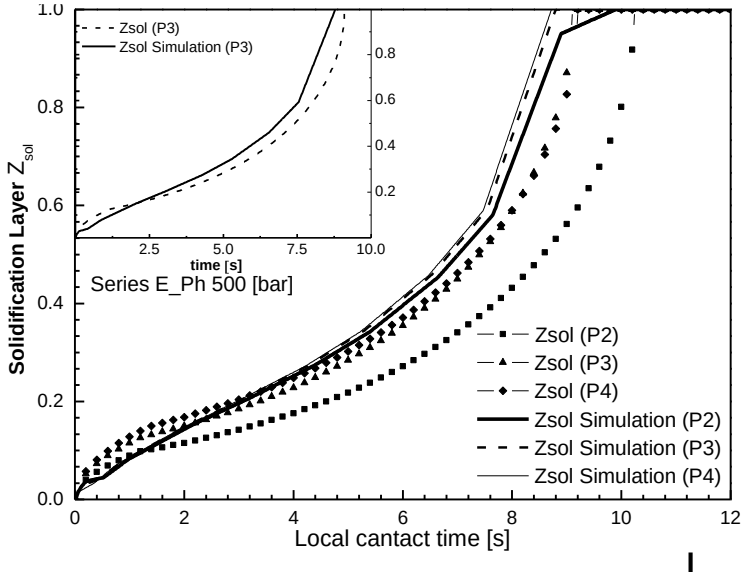

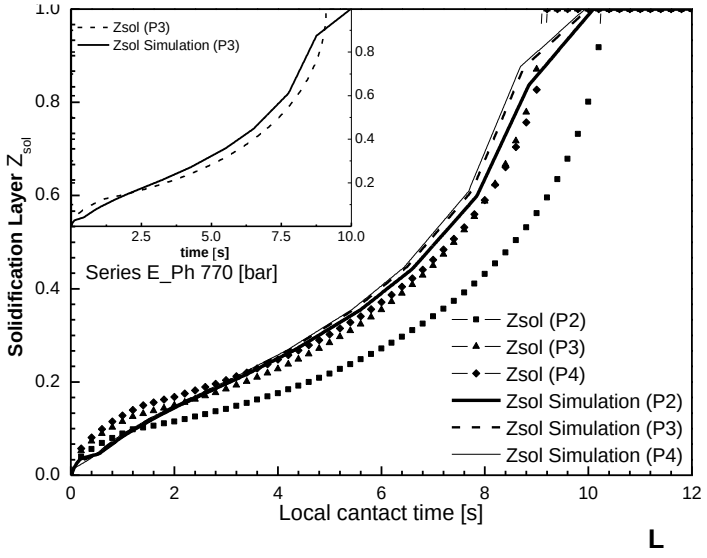

Fig. 44 Comparison between Moldflow description of solidification history and the solidification layer growth obtained by using the procedure from experimental pressure curves for several tests belonging to E series; Ph 500 [bar] (I) and Ph 770 [bar] (L). (Continued).

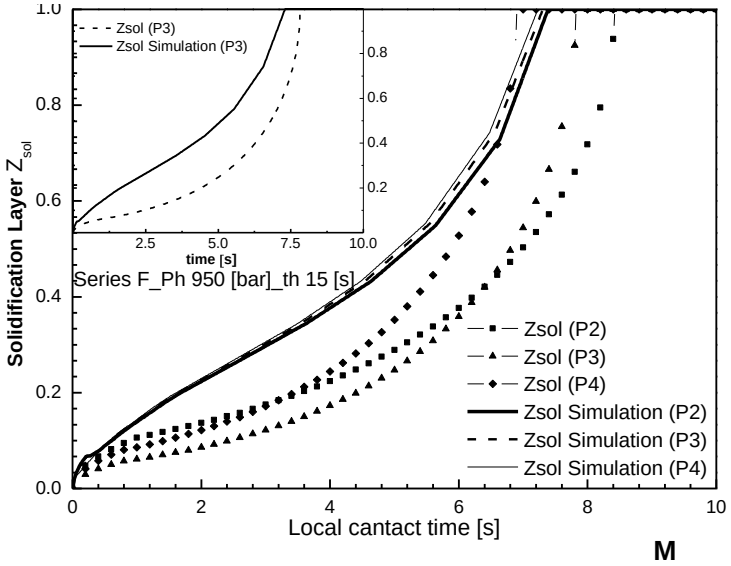

M

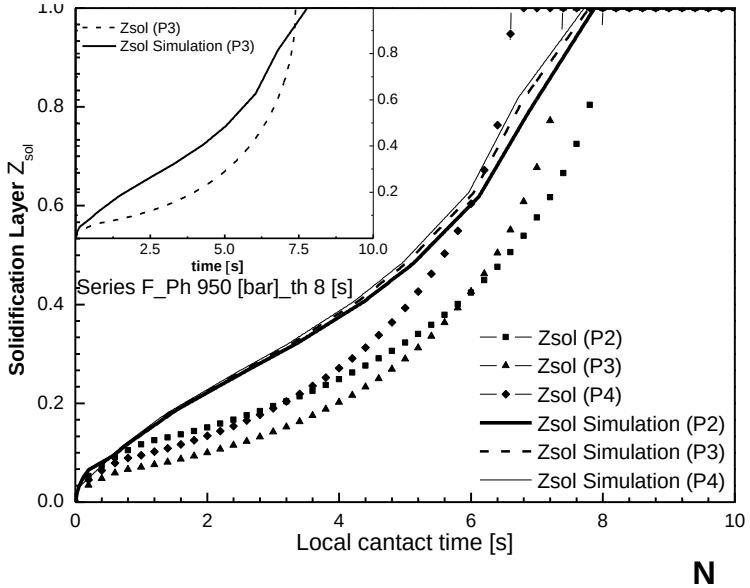

N

Fig. 44 Comparison between Moldflow description of solidification history and the solidification layer growth obtained by using the procedure from experimental pressure curves for several tests belonging to F series; Ph 950 [bar] th 15 [s](M) and Ph 950 [bar] th 8 [s] (N). (Continued).

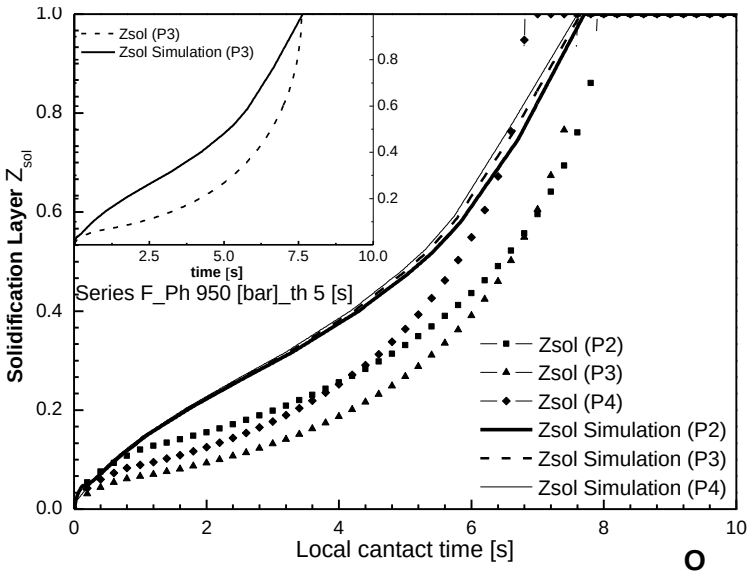

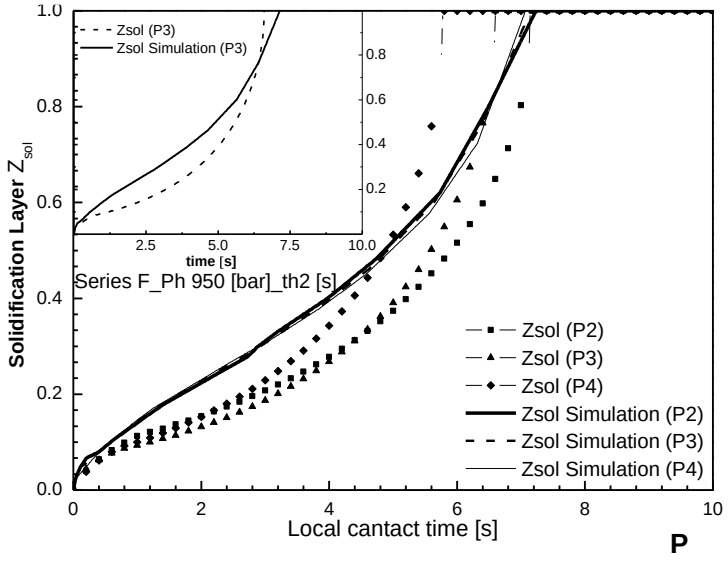

Fig. 44 Comparison between Moldflow description of solidification history and the solidification layer growth obtained by using the procedure from experimental pressure curves for several tests belonging to F series; Ph 950 [bar] th 5 [s](O) and Ph 950 [bar] th 2 [s] (P). (Continued).

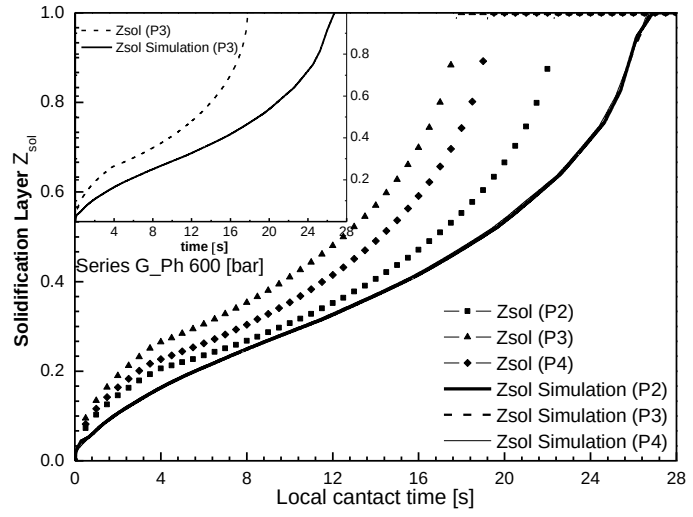

Q

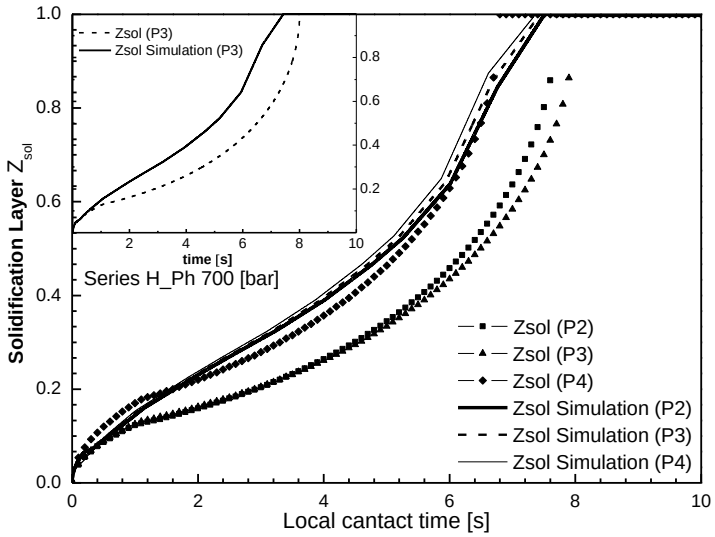

R

Fig. 44 Comparison between Moldflow description of solidification history and the solidification layer growth obtained by using the procedure from experimental pressure curves for several tests belonging to G series; Ph 600 [bar] (Q) and H series Ph 700 [bar] (R).

Although not perfectly superposed, the plots highlighted the same shape, and the difference between the amount of time required by each layer for solidifying was within 20%, except for Z_{sol} profile referred to G series (thicker cavity) **Fig. 44Q**. Furthermore, the results obtained by the procedure described in this work also detected differences in solidification times at different positions; however, it was found that, in most cases, the solidification took place in pos P2 (closer to the injection point) at delayed times with respect to positions P3 and P4, which in turn seemed to solidify almost at the same time. The Moldflow solution, however , didn't predict any relevant differences in solidification times among the cavity positions. For the position P4, the furthest from the gate, it can be supposed that the flow stopped immediately just after the flow passed by. This suggests that both, convection and dissipative effects can be neglected, leading to the approach of numerical prediction for layer solidification. On the other hand, as regards the P2 position, the nearest to the gate, further upstream, the convective and dissipative effects slow down the solidification process, which implies a deviation from the simulated solution. Evidently this occurrence also affects the middle of the cavity, leading to deviation e from the Moldflow solution in several cases. With regard to the G series, results referring to thicker cavity, much more time is required for solidification, and this occurrence was emphasized by the numerical approach. However, it should be mentioned that Moldflow simulations, although being probably the best reference available, do not perfectly reproduce the real profiles: the pressure profiles (showed in § III.2) are only reasonably reproduced, and indicate what the same is expected to happen with solidification profiles. Apart from every other issue, the relevant matter as regards our aim is the reliability of the procedure, in describing the solidification history of the polymer, based on knowledge of the local experimental pressure profile alone.

V.4.4 Relevance of the results of the procedure for PC Lexan 141R

The procedure was also applied to the experimental pressure curves of polycarbonate PC Lexan 141R, in order to test the reliability of using calculus procedure for different materials. The plot in **Fig. 45**, highlights the best exponential fit of the experimental pressure curves in cavity positions performed by the calculus procedure, and for each case also τ and t_{sol} values are reported.

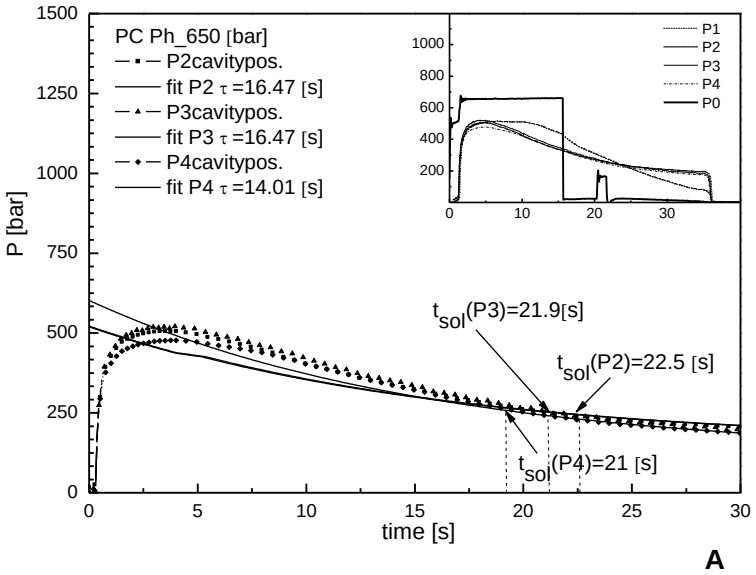

Fig. 45 Exponential best fit of PC Lexan 141R cavity pressure curve (A)

Even with this polymer, the results of τ values carried out using this method, are consistent with the eq.(5.9), on the basis of the values reported in **Table 3** and **Table 4**, for their thermal properties. The results of the solidification history for PC Lexan 141 R, obtained from experimental pressure curves belonging to the tests listed in **Table 10**, are reported in **Fig. 46**

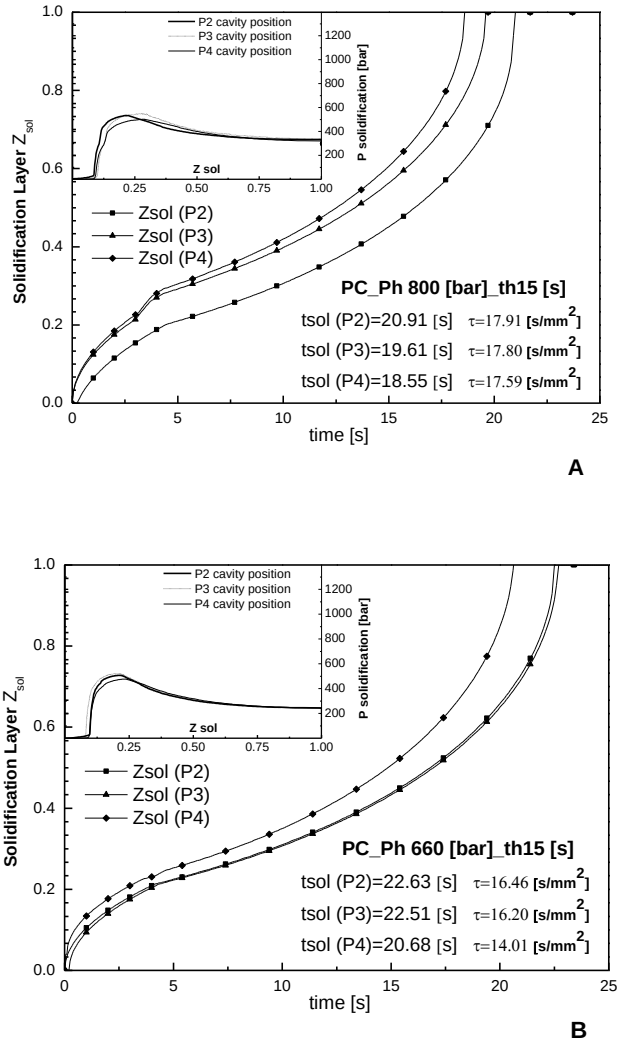

Fig. 46 Solidification layer profile obtained by using the procedure for PC Lexan 141R experimental pressure curves for Ph 800 [bar] (A) and Ph 660 [bar] (B) test conditions indicated in **Table 10** [§ II.4.4] (Continued).

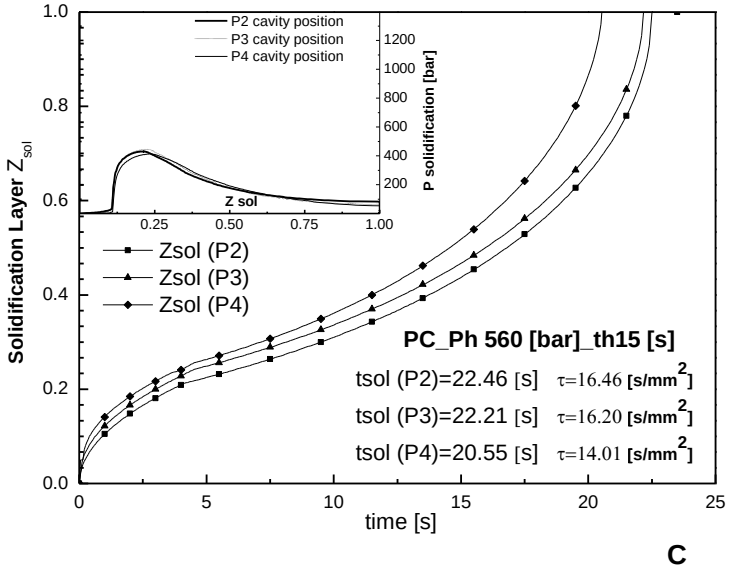

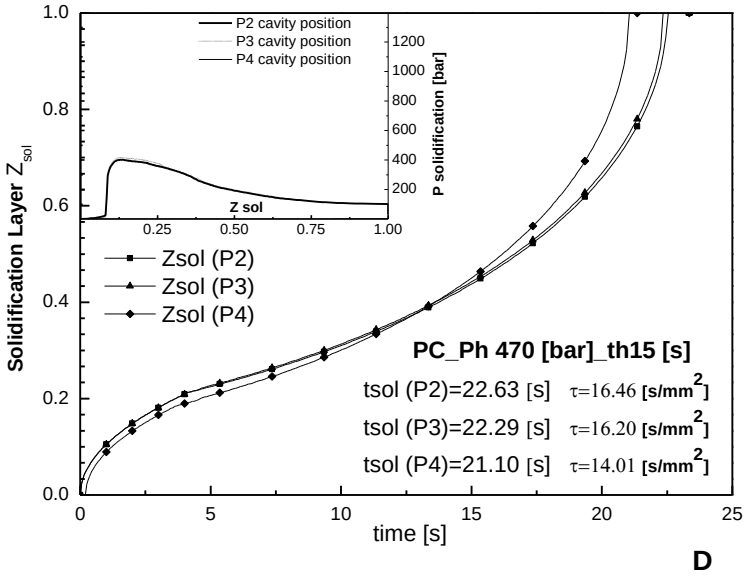

Fig. 46 Solidification layer profile obtained by using the procedure for PC Lexan 141R experimental pressure curves for Ph 560 [bar] (C)and Ph 470 [bar] (D) test conditions indicated in **Table 10** [§ II.4.4]. (Continued).

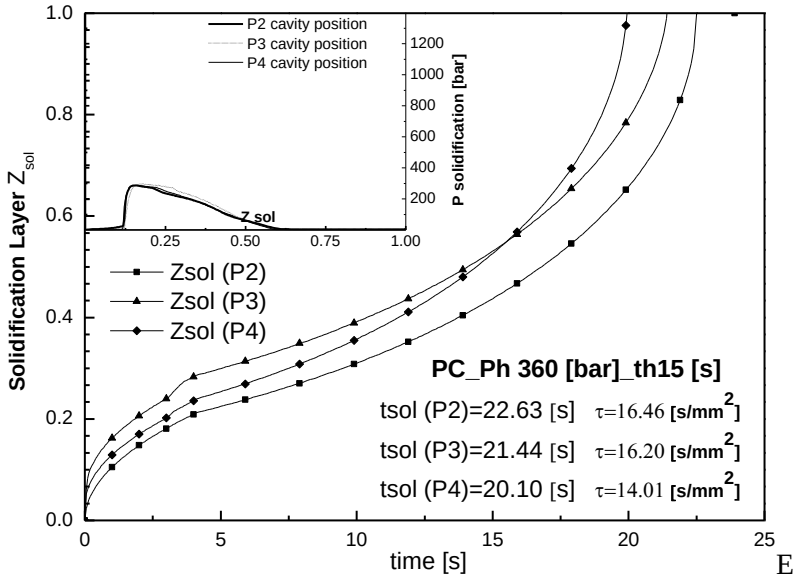

Fig. 46 Solidification layer profile obtained by using the procedure for PC Lexan 141R experimental pressure curves for Ph 360 [bar] (E) test conditions indicated in **Table 10** [§ II.4.4].

V.4.5 Relevance of the results of the procedure for PP BA238GE

Similarly, the results of the Exponential best fit applied to HIFAX BA 238 GE pressure curves, and the solidification history for PP HIFAX BA 238 GE obtained from experimental pressure curves referring to tests listed in **Table 11**, are respectively, reported in the following **Fig 47** and **Fig 48**

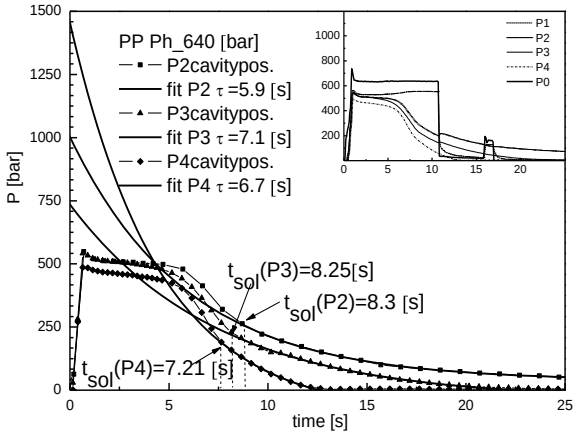

Fig. 47 Exponential best fit of HIFAX BA 238 GE cavity pressure curves

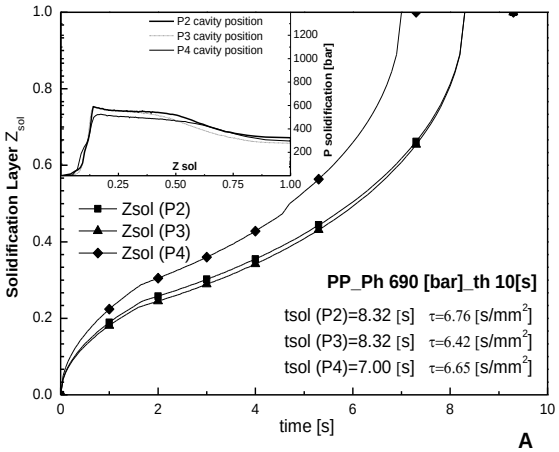

Fig. 48 A Solidification layer profile obtained by using the procedure for PP HIFAX BA 238 GE from experimental pressure curves for Ph 690 [bar].

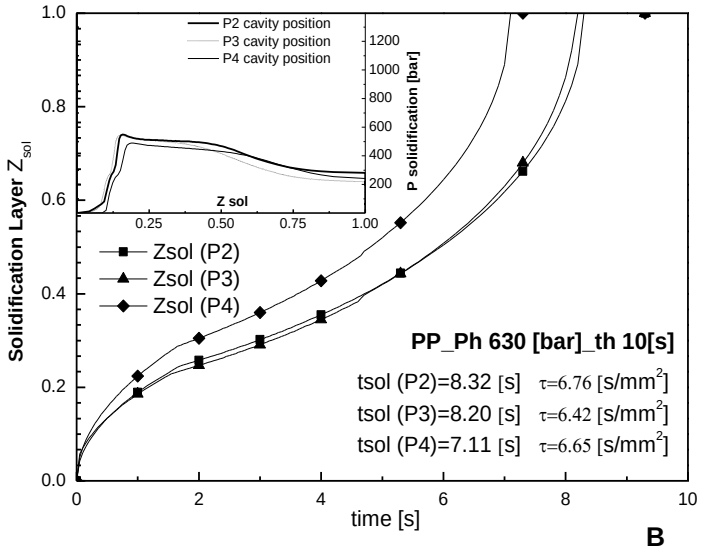

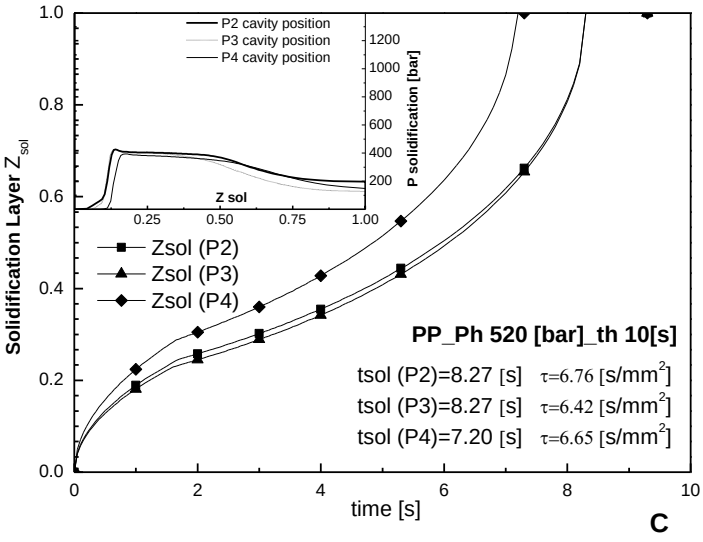

Fig. 48 Solidification layer profile obtained by using the procedure for PP HIFAX BA 238 GE from experimental pressure curves for Ph 630 [bar] (B) and for Ph 520 [bar] (C) tests conditions indicated in **Table 11** [§ II.4.5]. (Continued).

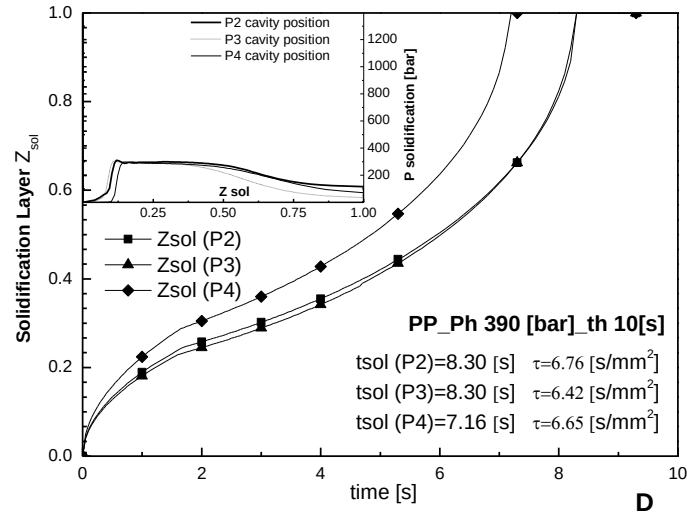

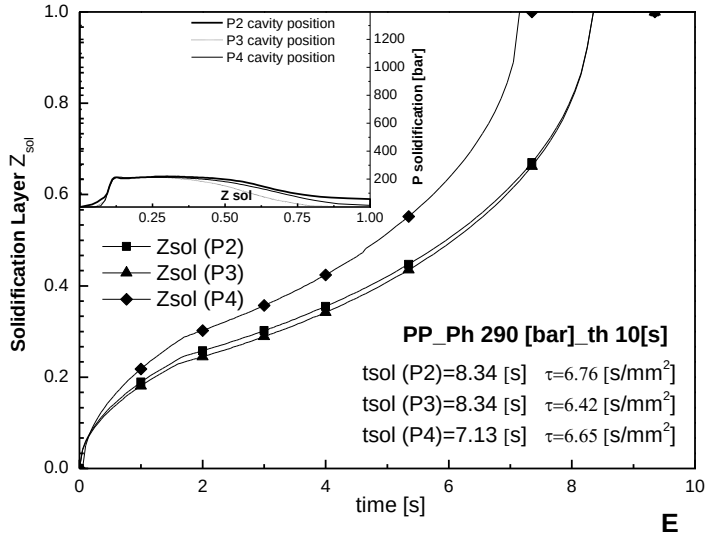

Fig. 48 Solidification layer profile obtained by using the procedure for PP HIFAX BA 238 GE from experimental pressure curves for Ph 390 [bar] (D) and for Ph 290 [bar] (E) test conditions indicated in **Table 11** [§ II.4.5]. (Continued).

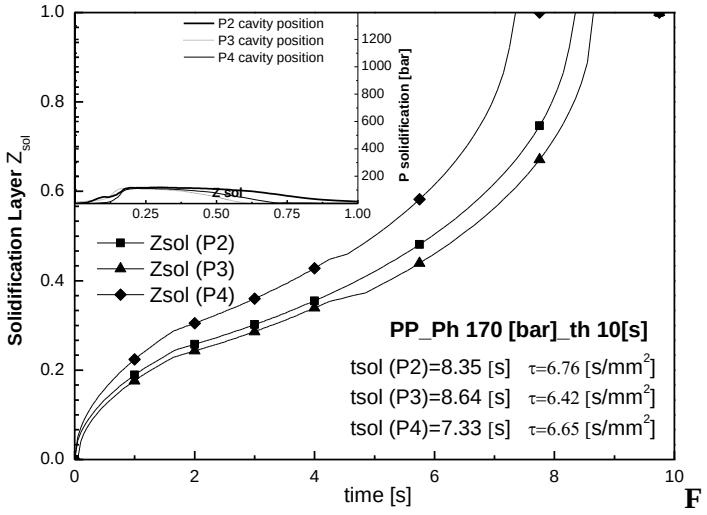

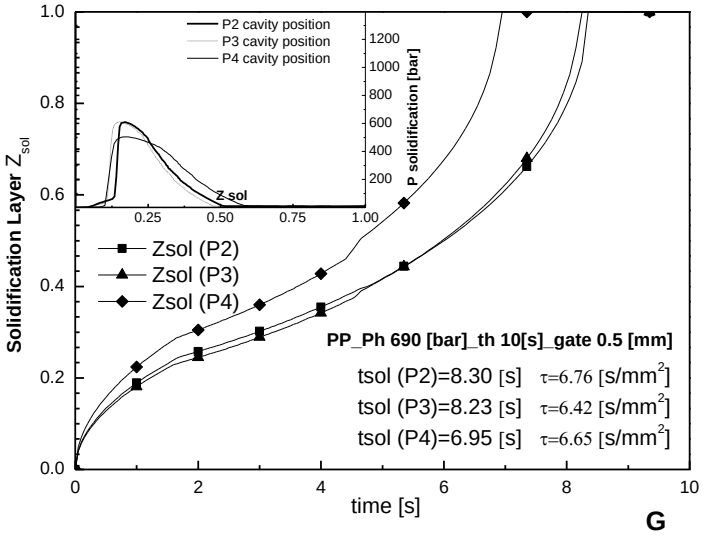

Fig. 48 Solidification layer profile obtained by using the procedure for PP HIFAX BA 238 GE from experimental pressure curves for Ph 170 [bar] (F) and for Ph 690 [bar] (gate thickness 0.5 [mm], indicated in **Table 11** [§ II.4.5] (G). (Continued).

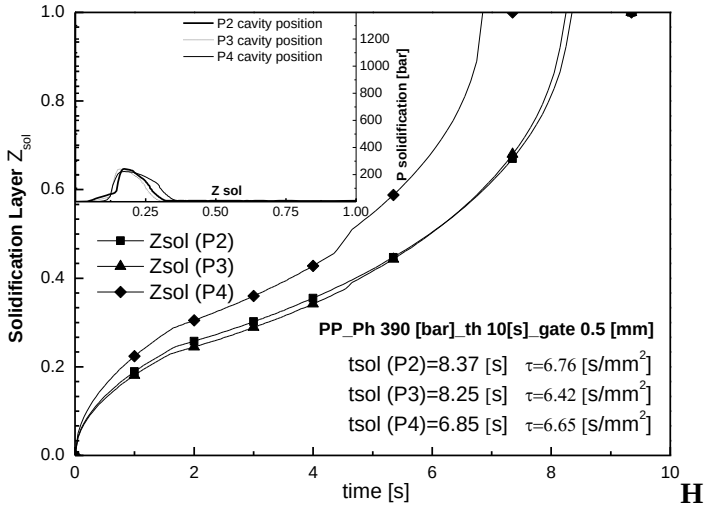

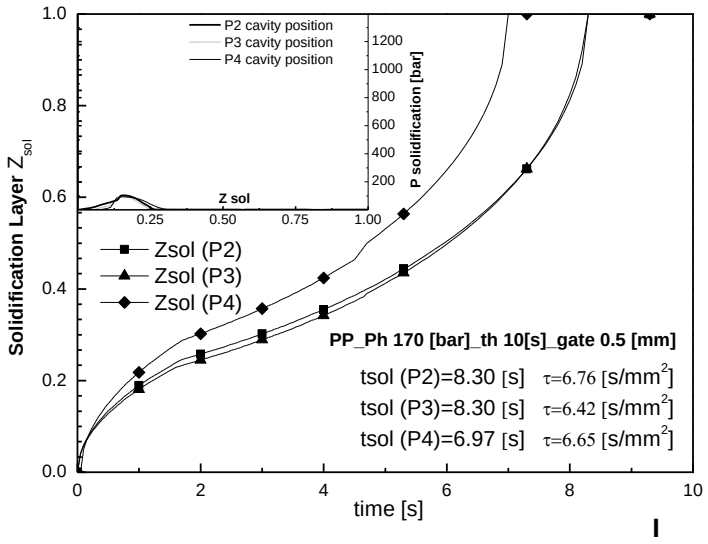

Fig. 48 Solidification layer profile obtained by using the procedure for PP HIFAX BA 238 GE from experimental pressure curves for Ph 390 [bar] (H) and for Ph 170 [bar] (I) test conditions (gate thickness 0.5 [mm], indicated in **Table 11** [§ II.4.5]. (Continued).

As can be observed in **Fig. 46** and **Fig. 48** the procedure also detected differences in solidification times at the different positions as well as in the case of PS678E. In particular, solidification in position P4 takes place at earlier times. This suggests that near the gate, the solidification process slows down due to the convective phenomena which affect this cavity section, whereas they weakly influence the furthest cavity positions. Therefore, local solidification in P2 took place later with respect to pos. P3 and P4 which, in turn, required less time to solidify. Finally in **Fig. 49** the values of τ refer to best fit mode calculation applied to all the experimental pressure profile (for PC Lexan 141R and PP Hifax BA238GE. It can be observed that for both polymers, the τ values obtained by applying the best fit procedure are in agreement with the τ_{calc} calculated values with eq.(5.9) on the basis of the physical properties reported in **Table 4** [§ II.2.3].

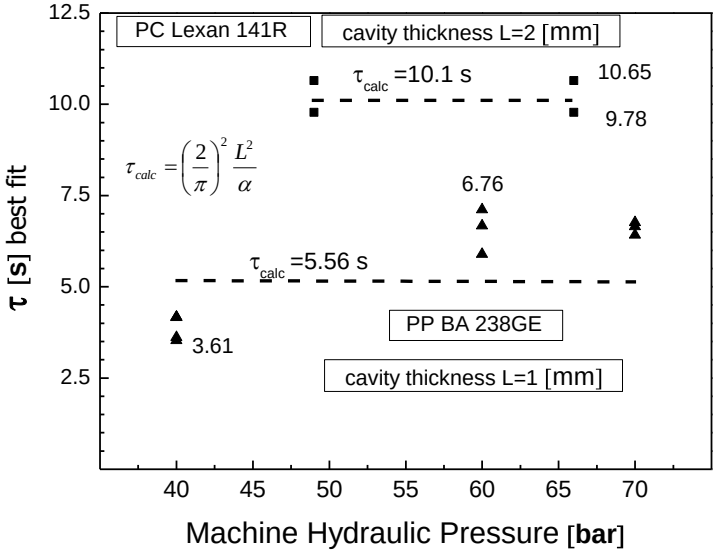

Fig. 49 Relevance of comparison between τ results refer to use of the procedure for PC Lexan 141R and PP Hifax BA 238 GE.

Chapter Six

Shrinkage data vs Average solidification pressure

In this chapter ,both the width shrinkage and normalized part weight data, vs the average solidification pressure calculated using the procedure illustrated earlier, are plotted.

It will be shown that Ps_av is an adequate parameter to correlate with width shrinkage, regardless of both the operative condition and polymer used. On the contrary, as regards concerning the part weight data, the correlation appears very poor, and this suggested the necessity of a separate analysis to achieve our aim. Also a further analysis regarding the effects of pressure on layer solidification temperature was introduced in order to provide as general as possible study of the phenomena.

VI.1 Ps_av vs as descriptive parameter for part quality in the injection moulding process: results and discussion

On the basis of the definition (eq.5.1), reported in [§. V.1] both the knowledge of local pressure and solidification history, permit us to calculate the Ps_av for each moulding condition. The main purpose is to prove that Ps_av is the best operative parameter to correlate with chosen quality parameters (width shrinkage and normalized part weight which in its turn is directly proportional to the volumetric shrinkage) for on-line part quality control in the injection moulded process. To calculate the Ps_av values, a twofold approach was adopted. Initially, the simulated solidification history of Moldflow was imposed, jointly to experimental pressure curves, to integrate the eq.(5.1) for obtaining Ps_av. After that, the same calculus was done using the solidification history resulting from the experimental pressure curve, obtained by applying the approach proposed. In both cases, the width shrinkage measurements, and normalized part weight data, have been plotted versus the Ps_av values.

VI.1.1 Width shrinkage data vs Ps_av for PS 678E.

In **Fig. 50** width shrinkage data are reported vs. Ps_av calculated by imposing the solidification history of Moldflow.

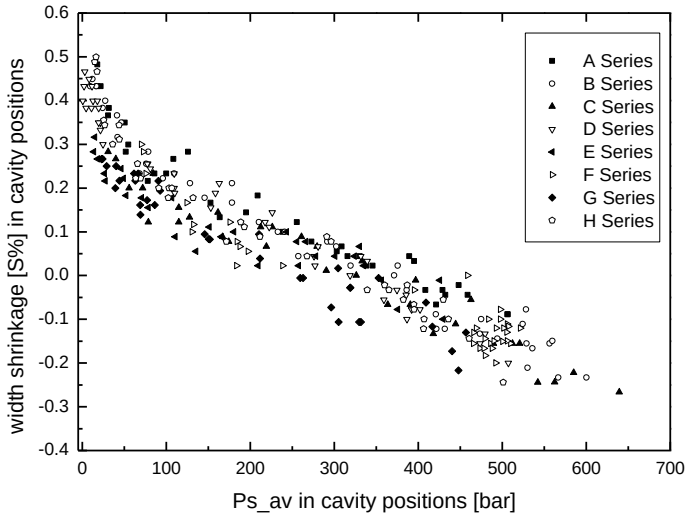

Fig. 50 In plane width shrinkage data vs average solidification pressure obtained by Moldflow© simulation of solidification history for PS 678E in each cavity position.

In **Fig. 51** the same width shrinkage measurement data, are reported vs Ps_av calculated by means of the Labview® procedure, (which uses the solidification history obtained from experimental pressure curves).

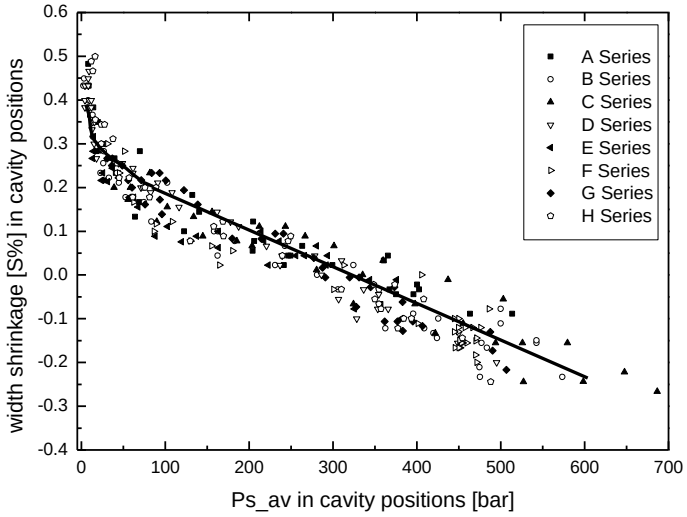

Fig. 51 In plane width shrinkage data vs average solidification pressure values are calculated by means of procedure introduced in this work, for PS678E in each cavity position.

A twofold consideration can be made. By the comparison to Fig.49 and Fig.50, it can be observed that the approach based on experimental solidification history description for calculating Ps_av , is in agreement with the result obtained imposing the simulated solidification history. Regarding data description, higher level pressures in the cavity position, resulting mainly, from higher holding pressure and time applied, lead to lower (negative) width shrinkage values. Clearly, as the holding pressure increases, much more extra material is forced into the mould after the injection stage, which compensates for the shrinkage caused by polymer/mould surface contact. As shown most of width shrinkage data reported in **Fig. 50** and **Fig. 51** lie on a single plot, identifying a master curve for describing the width shrinkage of Polystyrene moulded samples. For the same average solidification pressure values, width shrinkage data present a scatter which is smaller than 0.2% (it is worth recalling that the accuracy of measurement is about 0.01 mm for the caliper used, which results in about ± 0.025% of systematic error). These confirm the suitability of the procedure described in this work for obtaining a single parameter correlated to width shrinkage regardless of the moulding conditions. This means that, measuring the pressure evolution during an injection moulding test carried out with the polystyrene chosen for this work, we are now able to calculate the average

solidification pressure and thus to evaluate its shrinkage. Furthermore, by removing the data point, belonging to the tests, in which the shrinkage started before complete solidification, it is possible to assume a model for describing in plane constrained shrinkage, for isotropic amorphous materials like PS 678E, which takes into account average solidification temperature $\overline{T_S}$ and P_{S_Av} pressure and average temperature at the instant of complete solidification (Jansen, K. M.B., R. Pantani, and G. Titomanlio 1998).

$$[S\%] = \alpha_S \left(\overline{T_S} - \overline{T}\right) - \beta_S P_{S\_Av} \tag{6.0}$$

On the basis of this assumption, some physical considerations can be carried out by considering the slope and the intercept of the master curve which accounts, respectively, for the coefficient of linear thermal expansion α_S (which was estimated α_S=5 10^{-5} [K^{-1}]) and for the coefficient of linear compressibility β_S (which was estimated β_S=0.82 10^{-4} [MPa^{-1}]), and these values are also consistent to the ones set out in the literature (Pantani 1999) **Fig. 52**.

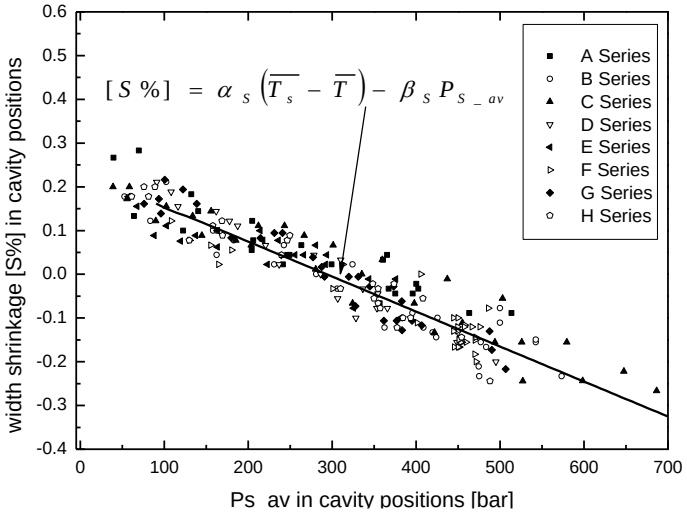

Fig. 52 Reduced in plane width shrinkage data vs average solidification pressure values calculated by means of the procedure introduced in this work, for PS678E in each cavity position.

VI.1.1.1Effect of pressure on the solidification temperature.

In order to attain a model which is as general as possible for describing the local polymer solidification history by experimental pressure profile, in the present paragraph, the local solidification layer solution for long time,

eq. (5.28 b) presented in § V.II, will be recognized removing the hypothesis cited earlier , and taking into account pressure effect, and cooling rate on solidification temperature. As already reported in eq. (5.13) for Fo>0.1;

$$\frac{T(t,y)-T_{mould}}{T_{inj}-T_{mould}} \approx \frac{4}{\pi}\exp\left(-\frac{t}{\tau}\right)\cos\left(\frac{\pi}{2}\left(1-\frac{z}{L}\right)\right) \qquad (6.1)$$

In considering the instant at which the slab midplane solidifies, eq. (6.1) becomes;

$$\frac{T_{sol}^{c}-T_{mould}}{T_{inj}-T_{mould}} \approx \frac{4}{\pi}\exp\left(-\frac{t_{sol}}{\tau}\right) \qquad (6.2)$$

Where the subscript indicates the value of the solidification temperature for slab midplane y=z, at the instant of local complete solidification $t_{sol}(x)$ (obtained as the result of the procedure, with τ time constant from the local experimental pressure).

It is possible to consider the solidification temperature as a function of pressure. In (Pantani 1999) the local glass transition temperature of polymer T_g for a generic position along the thickness direction (which is related to solidification temperature), was related to solidification pressure P_{sol} and cooling rate $\dot{T}_{sol}$. Taking as a reference the conditions of solidification at the midplane, the following equation can be obtained::

$$T_g\left(\dot{T}_{sol},P_{sol}\right)=T_g\left(\dot{T}_{sol},P_{sol}\right)+a\log\left(\frac{\dot{T}_s}{\dot{T}_s^{C}}\right)+b\left(P_{sol}-P_{sol}^{C}\right) \qquad (6.3)$$

where the subscript “C” refers to the midplane solidification conditions. According to eq. 6.2, which describes the solidification in the central part of the sample (far from the surface), all the layers solidify at the same cooling rate. It is possible to ignore the effect of the cooling rate and rearrange eq. (6.3), as;

$$T_{sol}\left(y,t_{sol}(x)\right)=T_{sol}^{c}+b\left(P\left(y,t_{sol}(x)\right)-P_{sol}{}^{C}\right) \qquad (6.4)$$

Therefore eq. (6.4) related the solidification temperature (in a generic y position coordinate along the slab thickness) to the midplane temperature at complete solidification, taking into account the variation of solidification temperature induced by solidification pressure through an a constant b,

which was estimated 0.03 [K/bar] (Pantani 1999). Matching eq.(6.1) and (6.4), the following equation is obtained;

$$\frac{T_{sol}^{C}-T_{mould}}{T_{inj}-T_{mould}}+\frac{b\left(P-P_{sol}^{C}\right)}{T_{inj}-T_{mould}}\approx\frac{4}{\pi}\exp\left(-\frac{t}{\tau}\right)\cos\left(\frac{\pi}{2}\left(1-\frac{z_{sol}}{L}\right)\right) \quad (6.5)$$

It is possible to define another parameter Λ_s as the ratio between the solidification temperature of a generic layer in the y position, and in the midplane.

$$\Lambda_s=\frac{T_{sol}\left(y,t_{sol}(x)\right)}{T_{sol}^{c}}\approx\frac{\frac{T_{sol}\left(y,t_{sol}(x)\right)-T_{mould}}{T_{inj}-T_{mould}}}{\frac{T_{sol}^{c}-T_{mould}}{T_{inj}-T_{mould}}} \quad (6.6)$$

Therefore, taking into account the eq.(6.4) we can obtain ;

$$\Lambda_s=1+\frac{b\left(P-P_{sol}^{C}\right)}{T_{sol}^{C}-T_{mould}} \quad (6.7)$$

And matching it with eq.(6.5) the following relationship is obtained:

$$\Lambda_s=1+\frac{b\left(P-P_{sol}^{C}\right)}{T_{inj}-T_{mould}}\frac{\pi}{4}\exp\left(\frac{t_{sol}}{\tau}\right) \quad (6.8)$$

The parameter Λ_s is equal to 1 for the midplane of the cavity, larger than 1 for most of the layers, and lower than 1 only for the layers close to the wall, which solidify at low pressures. For the layers close to the mould wall, the solidification occurs at low pressure levels, and this causes a lower solidification temperature with respect to the midplane. However those layers solidify under faster cooling rates with respect to the midplane and thus the effect of the cooling rate compensates for the lower pressure (see also **Fig. 53**). It will thus be assumed that the minimum allowed value for Λ_s is 1.

Considering eq.(6.6), and substituting the expressions given in eq.(6.2) and (6.1), the following relationships are obtained:

$$\exp\left(-\frac{t_{sol}}{\tau}\right)\Lambda_s\approx\exp\left(-\frac{t}{\tau}\right)\cos\left(\frac{\pi}{2}\left(1-\frac{z_{sol}}{L}\right)\right) \quad (6.9)$$

$$\cos\left(\frac{\pi}{2}\left(1-\frac{z_{sol}}{L}\right)\right)\approx\exp\left(-\frac{t-t_{sol}}{\tau}\right)\Lambda_s \qquad (6.10)$$

And finally the solidification layer profile solution for long time (Fo>0.1) which takes into account for the pressure effect on solidification, the temperature along the thickness is obtained:

$$\frac{z_{sol}}{L}\approx 1-\frac{2}{\pi}\arccos\left(\exp\left(-\frac{t-t_{sol}}{\tau}\right)\Lambda_s\right) \qquad (6.11)$$

Consequently, also the Labview© procedure introduced in § V.4 for Ps_av calculations, was changed in order to take into account these devices. In fact, for any given time included from $t=0.1\cdot\tau\left(\pi/2\right)^2$ to t_{sol} (x), it is possible to:

- set the time t;
- evaluate the pressure from the experimental evolution;
- calculate Λ_s;
- calculate $z_{sol}(t)$ by eq.(6.11), instead of eq.(5.28b).

In the following an example of the way in which the solidification profile changes is reported, due to the introduction of the effect of pressure on solidification temperature. For our purpose, the local experimental pressure in P3 belonging to the A series for PS 678E, (performed by holding pressure 625 [bar]) was considered. By applying the procedure described above, both the solidification time about 7.2 [s] and τ=3.98 [s/mm^2] were calculated, and the local pressure and solidification layer were obtained. In **Fig. 53 A** the effect of pressure on the solidification temperature layer, is highlighted. It can be noticed that, the solidified layer at each time, increases. In particular, for a generic layer y=0.32, an increase of solidification temperature about 4.5[°C] is noticed . However , if no pressure effect on T_{sol} is considered, the layer at position y=0.32 solidifies at conditions indicated by the "b" point, and at the same midplane temperature. When the abovementioned effect is considered, the layer at position y=0.32, solidifies at conditions indicated by the "a" point, and at a higher temperature than the midplane, as indicated in the upper right plot of **Fig. 53 B**.

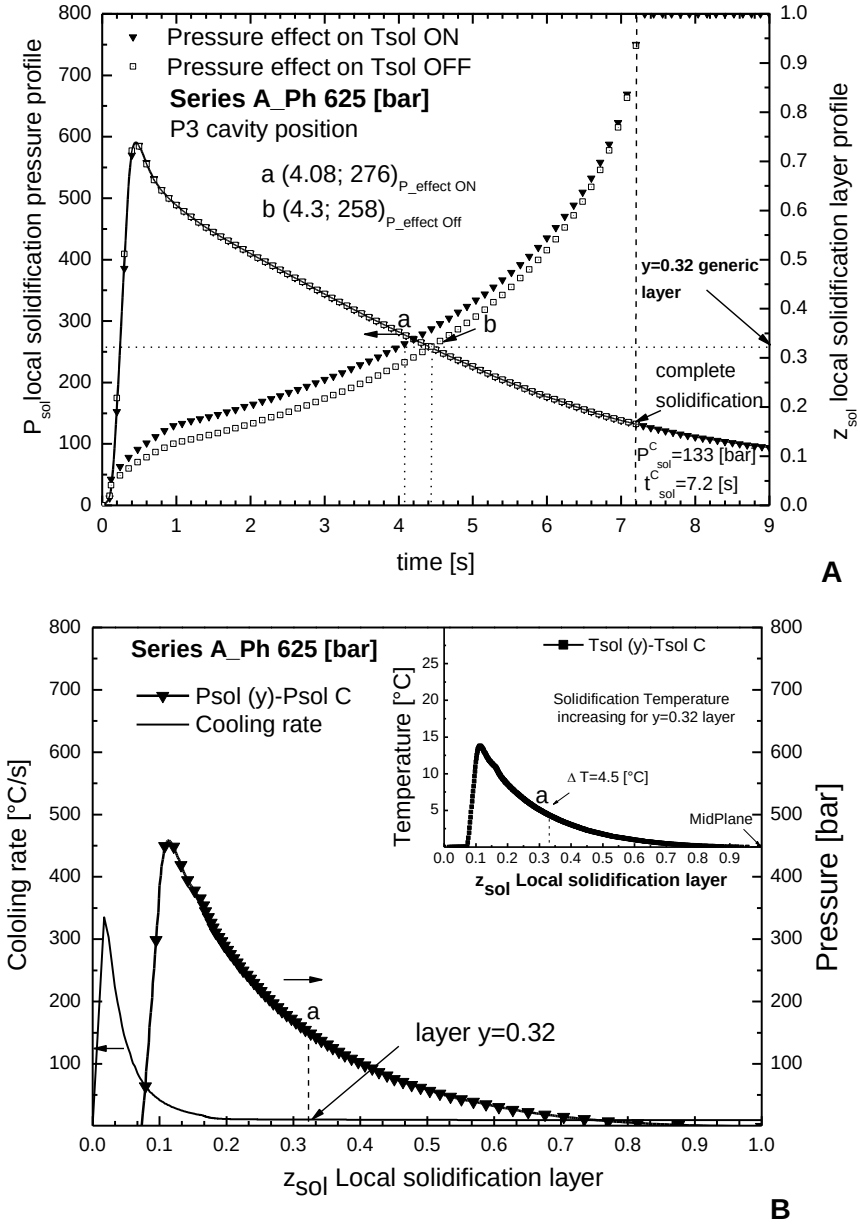

Fig. 53 The effect of pressure on solidification temperature, and on the resulting solidification layer .

Consistently with eq.(5.1), the effect of pressure on the solidification temperature, led to an increase also in the average solidification pressure value. Therefore for each PS 678E series investigated, the Ps_av, were

recalculated by considering eq.(6.11) for local $z_{sol}(x)$ profiles. The results are reported in **Fig. 54**.

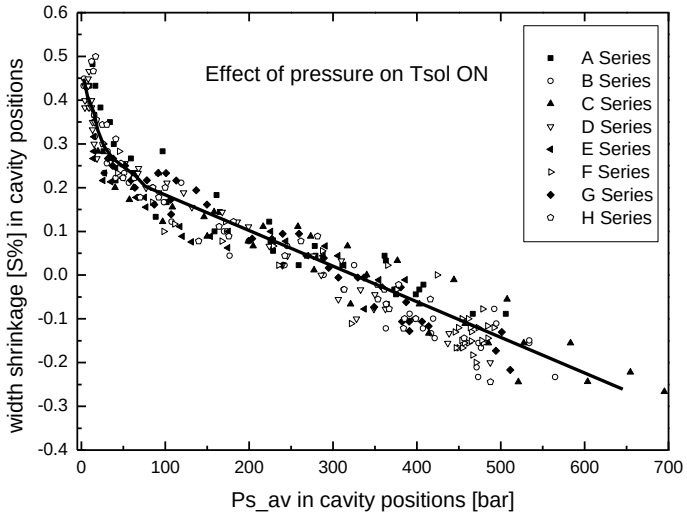

Fig. 54 In plane width shrinkage data vs average solidification pressure values calculated by means of the procedure introduced in this work, for PS678E in each cavity position. (Pressure effect on solidification temperature included).

Notwithstanding the fact that the pressure effect on the solidification temperature was considered, the results reported in **Fig. 54**, showed that no considerable differences, are detectable with regard to the result reported in the previous plot in **Fig. 51**.

VI.1.2Width shrinkage data vs Ps_av for PC Lexan 141R and PP BA238GE

The same analysis was applied to the experimental pressure curves obtained from the injection moulding tests performed using Polycarbonate PC Lexan 141R and Polypropylene HIFAX BA 238 GE. The corresponding width shrinkage data, have been plotted versus Ps_av values referring to experimental solidification history obtained from pressure curves through procedure **Fig. 55 A,B**.

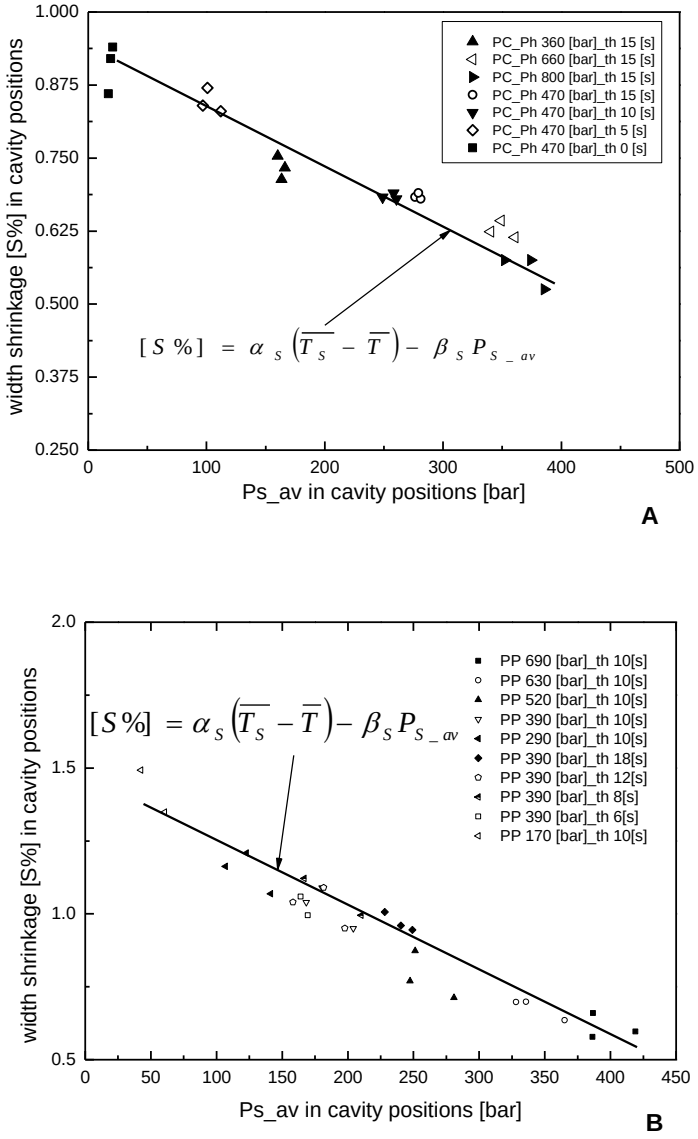

Fig. 55 In plane width shrinkage data vs average solidification pressure values calculated by means of the procedure developed in this work; (A) for PC Lexan 141R and (B) for PP Hifax BA 238 GE in each cavity position.

Despite the lower number of data, **Fig. 55 A**, demonstrates that all data collapse around a single plot, confirming that it is possible to correlate width shrinkage data to Ps_av which is the most adequate parameter for describing this qualitative target. Considering the slope and the intercept of the master curve (eq.6.0) which goes through the experimental data, it was possible to carry out, both the coefficient of linear thermal expansion α_S (which was estimated $\alpha_S=6.5\ 10^{-5}$ [K^{-1}]) and the coefficient of linear compressibility β_S (which was estimated $\beta_S=1\ 10^{-5}$ [MPa^{-1}]), which result in the same order of magnitude as the ones described in the literature (Pantani 1999).

Higher width shrinkage values occurred in Polypropylene samples for low holding process conditions, which caused premature local shrinkage during the post pressure stage. These data points were removed, and as appears in **Fig. 55 B**, an acceptable correlation of the width shrinkage measurements with Ps_av for Polypropylene moulded samples, was obtained. Apart from any other considerations, the relevance of the results in **Fig. 55 B**, demonstrate the reliability of the approach based on Ps_av in also describing the width shrinkage data for a semicrystalline Polypropylene, regardless of the operative conditions. By considering the (eq 6.0) for shrinkage data description valid, it was possible to obtain, both the coefficient of linear thermal expansion α_S (which was estimated $\alpha_S=2.0\ 10^{-4}$ [K^{-1}]) and the coefficient of linear compressibility β_S (which was estimated $\beta_S=2.2\ 10^{-5}$ [MPa^{-1}]), which are in agreement with the order of magnitude of the ones described in the literature (Pontes 2002) (De Santis 2010).

VI.1.2 Normalized part weight data vs Ps_av

In this paragraph, an attempt was made to correlate part weight data with Ps_av values for all the materials considered, using the same approach adopted to analyze the width shrinkage results. For this purpose, normalized part weight percentage (or volumetric shrinkage) was considered (earlier defined in § II.4.7 equation (2.6).

In **Fig. 56** Normalized part weight data (volumetric shrinkage) are reported vs. average values of Ps_av calculated by imposing the solidification history of Moldflow. As shown , the normalized part weight values resulting from samples which have expansion, exhibit high scattering, showing a poor correlation to the Ps_av.

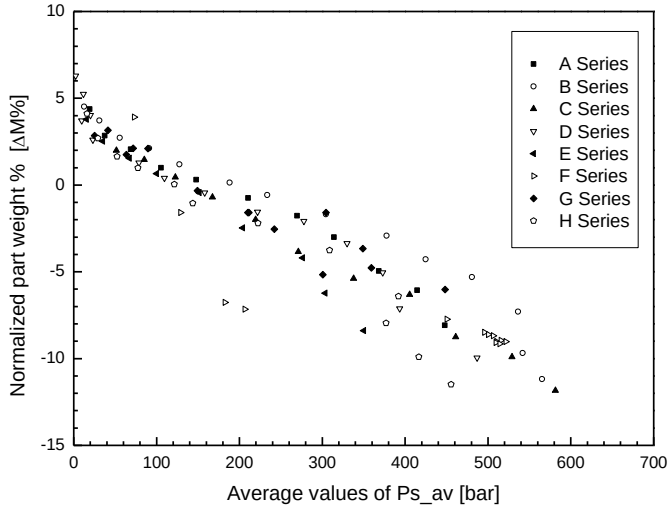

Fig. 56 Normalized part weight percentage vs average values of Ps_av obtained by the Moldflow simulation of solidification history for the PS 678E series

Fig. 57, the same part weight data, are plotted versus the average values of Ps_av, calculated by imposing the thermal history obtained by experimental pressure profiles. As shown, most of the data resulting from samples which have an expansion, turn aside from the single plot, and this fact, suggests that, for describing part weight (volumetric shrinkage), a separate analysis is needed particularly for a higher operative pressure level condition.

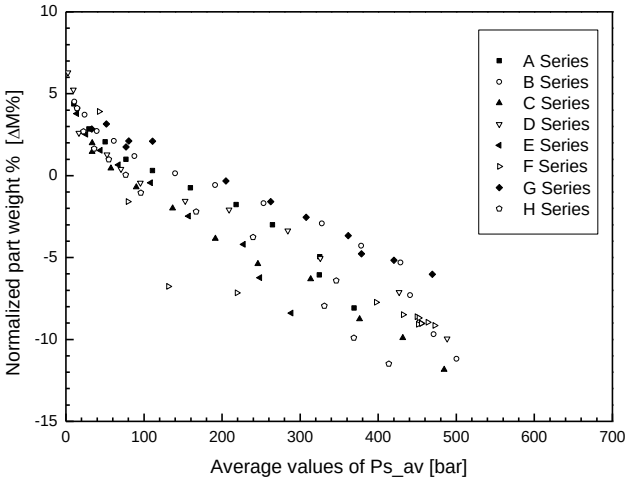

Fig. 57 Normalized part weight percentage vs average values of Ps_av calculated by means of the procedure introduced in this work, for the PS 678E series.

Consistently with the previous approach, the same normalized weight data was reported vs the average values of Ps_av recalculated taking into account the effect of pressure on solidification temperature. As can be noticed, no relevant improvement on data distribution was obtained; in particular for the samples which have an expansion scattering of data remaining still large **Fig. 58**.

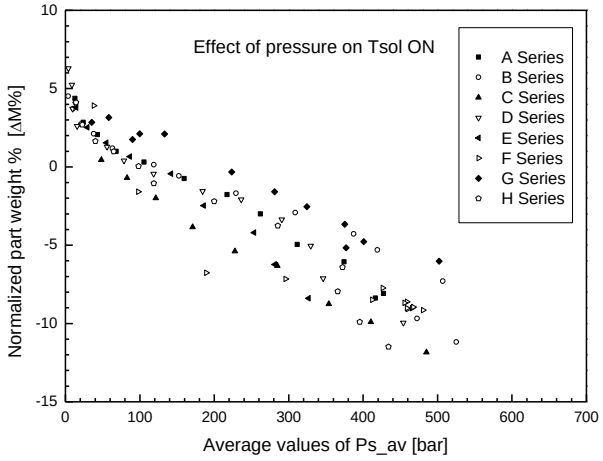

Fig. 58 Normalized part weight percentage vs average values of Ps_av calculated by means of the procedure introduced in this work, for the PS 678E series. (Pressure effect on solidification temperature included).

The same approach for analyzing the normalized part weight data was extended to Polycarbonate and Polypropylene, Fig. 59 show the normalized part weight data (volumetric shrinkage) vs. Ps_av values calculated by using the approach developed in this work, for the Polycarbonate. In this case, weight data appear to be well correlated to Ps_av, regardless of the operative condition. This is probably due to the fact that only a few tests carried out wit Polycarbonate show expansion.

In **Fig. 60** the normalized part weight data (volumetric shrinkage) vs. Ps_av values for Polypropylene are plotted. For low operative pressure conditions, the samples, exhibit very high volumetric shrinkage values due to the premature shrinkage which occur during the post pressure stage. Also in this case, the data showing expansion are just a few, and Ps_av, results as a suitable parameter for the part weight description.

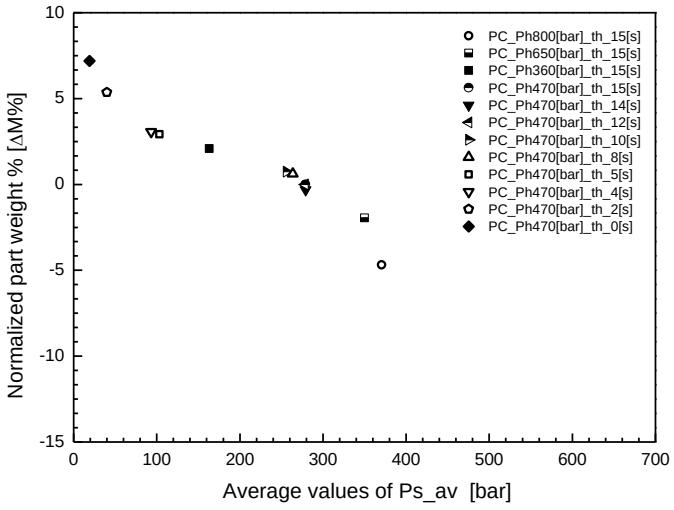

Fig. 59 Normalized part weight percentage vs average values of Ps_av calculated by means of the procedure introduced in this work, for the PC Lexan 141R series.

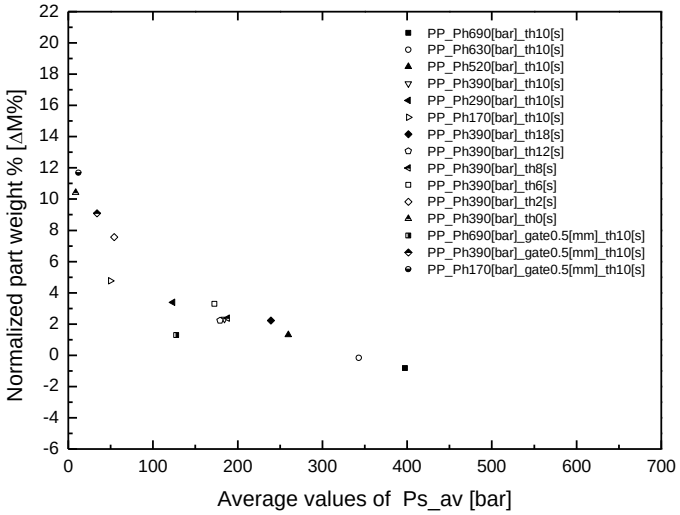

Fig. 60 Normalized part weight percentage vs average values of Ps_av calculated by means of the procedure introduced in this work, for the PP Hifax BA 238GE series.

Chapter Seven

Normalized weight percentage data vs Gate solidification pressure

A further research task was to find a parameter able to describe the weight of the samples Consistently with the literature, the pressure at the gate freeze off instant namely, P_{gf}, represents the most appropriate parameter for the case, as it is recognizable in plotting the normalized part weight data P_{gf} An approach based on measuring the pressure evolution was adopted to calculate P_{gf}

VII.1 Width shrinkage vs normalized part weight percentage: results and discussion

In order to obtain a better description of the part weight of the moulded samples, a different operative parameter, was considered for this aim.

It was shown as in-plane (width) shrinkage (at least for the case in which shrinkage starts after complete solidification) which depends on the average solidification pressure in a very wide range of operating conditions.

However, Ps_av cannot describe part weight (or volumetric shrinkage). This occurrence is confirmed by a further analysis of data which highlighted the fact that no direct proportionality exists between the local in-plane shrinkage, and local expansion in the sample thickness, and vice-versa. In **Fig. 61** normalized part weight percentage (volumetric shrinkage) data were plotted vs the average width shrinkage data for all operative conditions investigated for PS 678E.

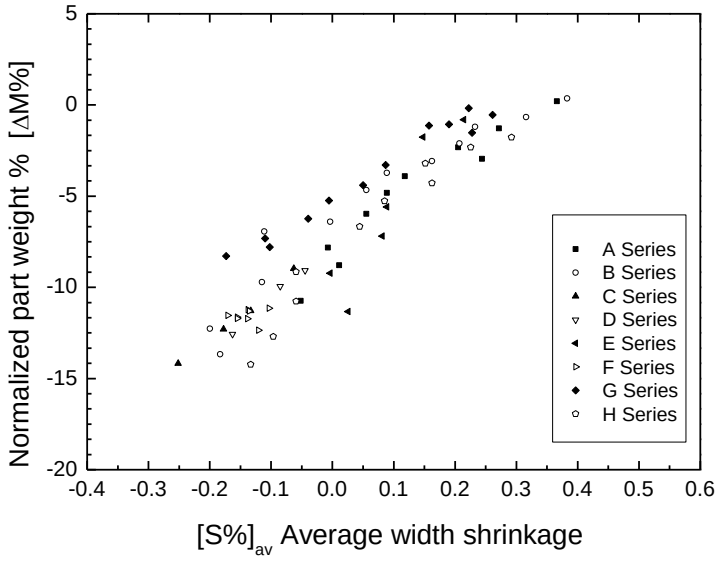

Fig. 61 Normalized part weight percentage (volumetric shrinkage) vs Average width shrinkage data for the PS 678E series.

It immediately appears that the normalized part weight values (volumetric shrinkage) of moulded samples, are much larger (more than one order of magnitude) than the corresponding average width shrinkage values measured. All these considerations are valid assuming that the density of the polymer at room conditions does not depend on processing conditions, and then, sample weight is proportional to volumetric shrinkage, which in turn is

the sum of in-plane (width) and through thickness shrinkage. As already demonstrated, the in-plane (width) depends only on Ps_av, whereas, the latter also depends on the average specific volume of the polymer inside the cavity at the instant of complete solidification. Furthermore, this is already recognized in literature, as cavity deformation phenomena may arise during the injection process (Jansen, Pantani and Titomanlio 1998). The mould deformation, implies an enlargement of the cavity impression ($2L-2L_0$) in the thickness direction which can be related to the total pressure distribution acting against the mould walls. This occurrence could be the main reason why the correlation between weight and width shrinkage reported in **Fig. 61**, is very poor for samples which present expansion, namely, for high operative pressures inside the cavity. In **Fig. 62** normalized part weight % vs average width shrinkage data, are plotted for Polycarbonate PC Lexan 141R. Despite the lack of data, it appears that larger values of the normalized part weight (volumetric shrinkage) occur in comparison to the width shrinkage, particularly for samples which belong to tests performed with high operative pressure.

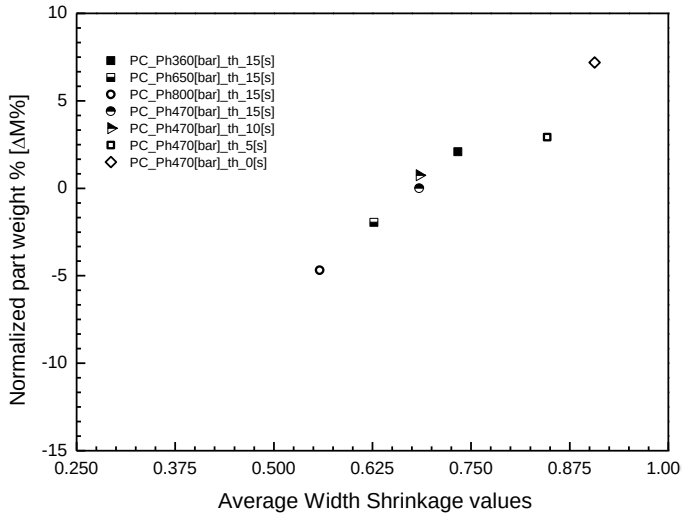

Fig. 62 Normalized part weight percentage data (volumetric shrinkage) vs Average width shrinkage for PC Lexan 141R series.

In **Fig. 63** the normalized part weight % vs average width shrinkage data for PP Hifax BA 238GE are displayed. It confirms that for high values of operative pressure, high normalized part weight (or volumetric shrinkage) occur in Polypropylene samples, in comparison to the in-plane shrinkage measured.

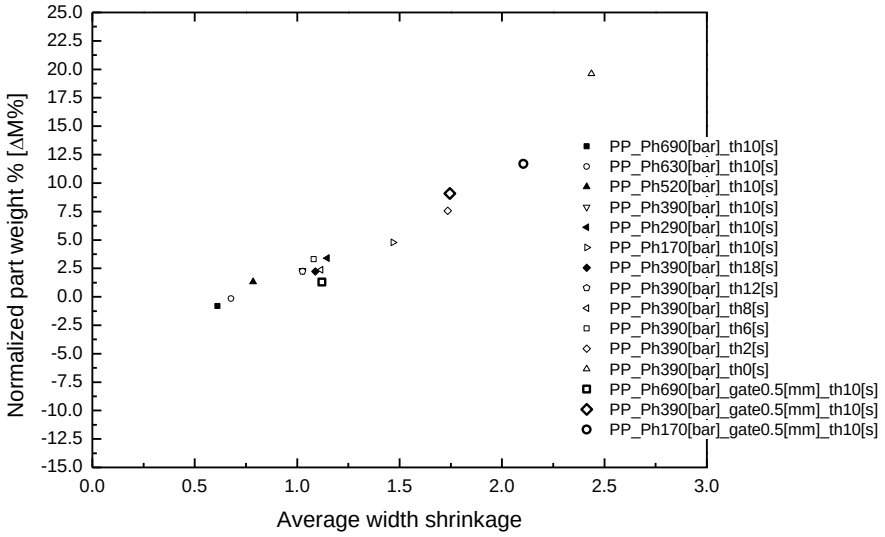

Fig. 63 Normalized part weight percentage (volumetric shrinkage) vs Average width shrinkage data for the PP Hifax BA 238GE series

Finally, as a general result, the sample weight variation % data, need a separate analysis to establish an adequate processing parameter for mass description of the moulded part.

VII.1.1 Normalized part weight (or volumetric shrinkage) of the moulded part: thermo-mechanical model.

Following the suggestions of scientific literature, an attempt was made to correlate the normalized part weight of the moulded part with the pressure at gate freeze off time P_{gf}. The packing phase is effective until the gate solidifies, as mass is not allowed to enter cavity. Thus, the gate freeze off instant, determines the mass of the polymer inside the cavity, and the corresponding cavity pressure distribution which involves cavity deformation determines the thickness of the samples. On the bases of these considerations, a thermo-mechanical model which takes into account these occurences, was already suggested. It was based on the assumption that the polymer melt turned into an elastic solid as soon as it solidified. Further details about the model are given elsewhere (Jansen and Titomanlio 1996). In this respect a special case of a more general model for describing the

solidification of thermo-viscoelastic melt can be considered, which kept account of the effects of processing conditions on volumetric shrinkage proposed by (Bushko and Stokes 1995). Then for constrained, isotropic amorphous materials, if the local shrinkage starts after complete solidification, local in-plane shrinkages reduce respectively to equation (7.1):

$$s_i(x,t) = -\frac{1}{3}\ln\left(\overline{\frac{v(x,z,t)}{v_s(x,z)}}\right) \tag{7.1}$$

In which v_s is the specific volume at the instant of local solidification and v is the specific volume at the generic instant t. The superimposed bar represents the average value over the solidified layer thickness. If a constant parameter model is adopted for describing the material volume, the average volumetric shrinkage is:

$$\overline{\ln\left(\frac{v(x,z,t)}{v_s(x,z)}\right)} \cong \frac{\overline{v(x,z,t) - v_s(x,z)}}{vo} = \alpha^{sol}(\overline{T(x,z,t)} - \overline{T(x,z,t_{sol})}) - \beta^{sol}\left(P(x,t) - \overline{Ps(x,z)}\right)$$

(7.2)

By matching eq. (7.1) and (7.2), the expression for in plane shrinkage is obtained:

$$s_x = s_y = -\frac{1}{3}\ln\left(\overline{\frac{v(x,z,t)}{v_s(x,z)}}\right) \cong \left[\alpha^{sol}(\overline{T(x,z,t_{sol})} - \overline{T(x,z,t)}) - \beta^{sol}(P_{S\_av} - P(x,t))\right]$$

(7.3)

Where, α^{sol} and β^{sol} are respectively, the linear thermal expansion coefficient and the linear compressibility at complete local solidification conditions. ($\overline{T(x,z,t)}$ is the average temperature value for a generic instant along the thickness direction, and $\overline{T(x,z,t_{sol})}$ is the average temperature distribution at the local solidification instant along the thickness direction,. Likewise $P(x,t)$ is the pressure for a generic layer z in a generic instant, and P_{S_av} is the average solidification pressure over the solidified cross section. The shrinkage along the thickness is related to in plane shrinkage by the Hook equation, if the local shrinkage starts after complete solidification:

$$s_z(x,t) = \frac{1+\upsilon}{1-\upsilon}\frac{1}{3}\ln\left(\overline{\frac{v(x,z,t)}{v(x,z,t_{z,shr})}}\right) - \frac{2\upsilon}{1-\upsilon}\frac{1}{3}\ln\left(\overline{\frac{v(x,z,t)}{v_s(x,z)}}\right) + C_M P_{gf} \tag{7.4}$$

In which the first term on the right hand side of the equation, is related to the local shrinkage at the instant of complete solidification conditions, as indicated by index S, (υ is the Poisson's coefficient).

$$\overline{\ln\left(\frac{v(x,z,t)}{v(x,z,t_{z,shr})}\right)} \cong \alpha^S\left(\overline{T(x,z,t)} - \overline{T(x,z,t_S)}\right) - \beta^S\left(P(x,t) - \overline{Ps(x,z)}\right) \qquad (7.5)$$

The second term is the above mentioned local shrinkage at the instant of local solidification conditions. The latter one takes into account the deformation of the mould wall due to pressure distribution inside the cavity at the instant of gate freeze off. (C_M is the mould compliance).

Assuming that the local pressure goes to zero after complete solidification, then, the density of the polymer at room conditions does not depend on the processing condition, thus sample weight is proportional to volumetric shrinkage, which in turn is the sum of in-plane (width) and through thickness shrinkage:

$$\frac{M_0 - M}{M_0} = \frac{V_0 - V}{V_0} \cong 2s_y + s_z \qquad (7.6)$$

In this equation, the actual volume is normalized with respect to the specific volume of polymer evaluated at mould temperature. Taking into account the equations (7.3) and (7.4) it is possible to write a thermo-mechanical model for the description of normalized part weight data:

$$\frac{M_0 - M}{M_0} = \frac{V_0 - V}{V_0} \cong 2s_y + s_z \cong 2\left[-\frac{1}{3}\ln\left(\overline{\frac{v(x,z,t)}{v_s(x,z)}}\right)\right] + \frac{1+\upsilon}{1-\upsilon}\left[\frac{1}{3}\ln\left(\overline{\frac{v(x,z,t)}{v(x,z,t_{z,shr})}}\right)\right] - \frac{2\upsilon}{1-\upsilon}\frac{1}{3}\ln\left[\left(\overline{\frac{v(x,z,t)}{v_s(x,z)}}\right)\right] + -C_M P_{gf} \qquad (7.7)$$

If the local pressure goes to zero after complete solidification, for $t(x)>t_{sol}(x)$, specific volume is constant and thus it is possible to assume that:

$$\frac{1}{3}\overline{\ln\left(\frac{v(x,z,t)}{v(x,z,t_{z,shr})}\right)} = \frac{1}{3}\overline{\ln\left(\frac{v(x,z,t)}{v(x,z)}\right)} \qquad (7.8)$$

The eq.(7.7) can be rearranged:

$$\frac{M_0 - M}{M_0} = \frac{V_0 - V}{V_0} \cong -\frac{2}{3}\ln\left[\overline{\left(\frac{v(x,z,t)}{v_s(x,z)}\right)}\right] - \frac{1}{3}\ln\left[\overline{\left(\frac{v(x,z,t)}{v_s(x,z)}\right)}\right] - C_M P_{gf} \qquad (7.9)$$

$$\frac{M_0 - M}{M_0} = \frac{V_0 - V}{V_0} \cong -\ln\left[\overline{\left(\frac{v(x,z,t)}{v_s(x,z)}\right)}\right] - C_M P_{gf} \qquad (7.10)$$

On the basis of eq (7.1) it can be reduced to a simplified expression for a thermo-mechanical model:

$$\frac{M_0 - M}{M_0} = \frac{V_0 - V}{V_0} \cong 3s_y - C_M P_{gf} \qquad (7.11)$$

VII.1.2 Thermo-mechanical model for Normalized part weight prediction: PS 678E cases, several considerations

By analyzing Fig. 61 it can be observed that the volumetric shrinkage was larger by one order of magnitude with respect to in-plane shrinkage; consequently it can be legitimate to assume that the mould deformation contribution has a pivotal role in determining the volumetric shrinkage of the injected moulded PS 678E samples, as the contribution of the in-plane shrinkage term is not relevant. An excess of Normalized part weight can be defined, as reported in the following:

$$Excess = \frac{M_0 - M}{M_0} - 3s_y = \frac{V_0 - V}{V_0} - 3s_y = -C_M P_{gf} \qquad (7.12)$$

Starting from this approach, the normalized part weight data will be reported in function of the parameter P_{gf}, by using a linear model (7.12), to achieve a better description of data than observed previously. Another part of the activity, concerns the development of an approach for estimating the P_{gf} from experimental pressure curves. (Pantani, De Santis, et al. 2004) stated that a careful analysis of pressure curves both inside the cavity and just upstream from the gate can identify a correlation between the features of pressure evolution curves and gate solidification time. On the bases of these considerations, an automatic procedure on the Labview platform was developed and implemented for the calculation of P_{gf}.

VII.2 Relevance of the results of the excess of normalized part weight vs pressure at the gate freeze off time for PS 678E

In **Fig. 64** the excess of normalized part weight data (referred to M_0 values reported in **Table 13**), are plotted vs the average pressure at gate freeze off time.

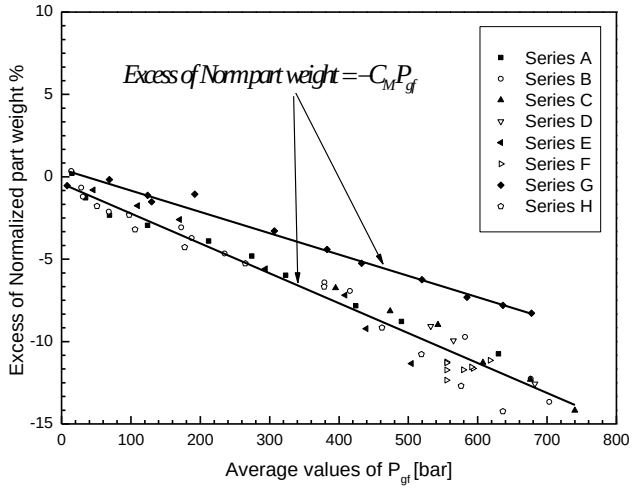

Fig. 64 Excess of Normalized part weight percentage (volumetric shrinkage) vs Average values of Pressure at gate freeze off time, for the PS 678E series.

As shown, most of the data lie around a single line plot, whereas the data point belonging to samples moulded by adopting a cavity which has a double thickness (see **Table 9**), are identified by a different straight line which has nearly the same intercept, but a smaller slope value, which is nearly half. In considering the model (7.12) valid for data description, it can be legitimately assumed that the slope of line plot is the mould compliance. Starting from this, the result in plot **Fig. 64**, was predictable since for the same average pressure distribution inside the cavity at gate sealing instant, the percentage displacement along the thickness, is about half, for the thicker cavity, when compared to the thinner cavity. On the basis of these considerations, it is possible to assume the model (7.12) as a reliable master curve for PS 678E part weight data, and make an estimation of mould compliance for each cavity using slope values. In literature, mould compliance values were estimated by (Pantani 1999) in an order of the magnitude of 10^{-3} [MPa^{-1}], which is consistent with the values estimated by experimental data: 1.2 10^{-3} [MPa^{-1}] and 1.9 10^{-3} [MPa^{-1}] respectively for the thicker and thinner cavities. However, apart from any other consideration, it was demonstrated that the P_{gf} is the best operative parameter for part weight description, regardless of the operative conditions.

VII.3 Relevance of the results of normalized part weight vs pressure at the gate freeze off time for PC Lexan 141R.

The same approach used for analyzing the normalized part weight data, was extended to Polycarbonate and Polypropylene. In **Fig. 65**, the Excess of Normalized part weight data (referred to M_0=16.6 [g]) vs the average values of Pressure at gate freeze off time Pgf are plotted for the PC Lexan 141R samples.

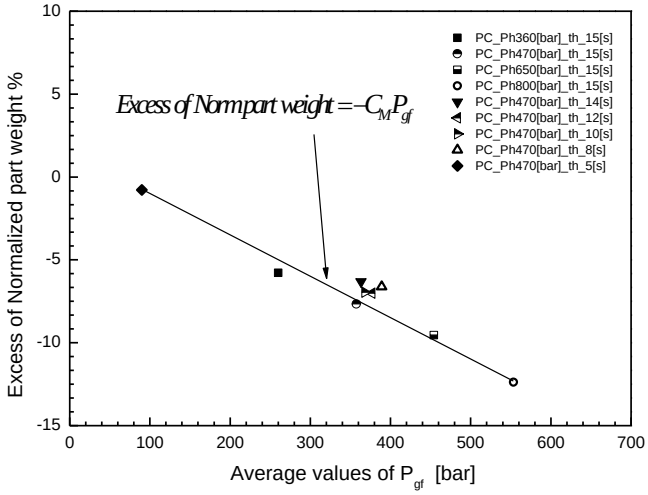

Fig. 65 Normalized part weight percentage (volumetric shrinkage) vs Average values of Pressure at gate freeze off time, for the PC Lexan 141R series

Despite the lack of data points, **Fig. 65** confirms that the approach based on the eq (7.12) for part weight data description, is valid and allows us to identify a master curve for data description, considering P_{gf} as the best parameter for our aim. The line slope for estimating the mould compliance, gives a value of 2.2 10^{-3} [MPa^{-1}].

Further analysis allows us to compare this result with the corresponding line plot for polystyrene (series G) referring to the case in which the same thickness cavity was used **Fig. 66**.

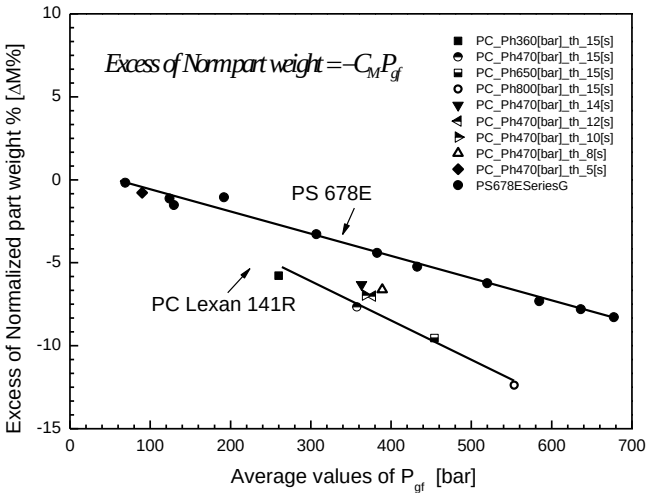

Fig. 66 Comparison of the line plot slopes between PS 678E and PC Lexan 141R data.

Even though the same mould cavity was used for injection moulding tests, it appears that the data point lay around two different plot lines. This event suggests that in the case of tests performed using PC Lexan 141R, the contribution of mould deformation in determining the samples weight, is larger than the PS 678E cases, since a higher value of mould compliance was estimated. This event can be explained by observing that due to the higher average mould temperature used for Polycarbonate, a different mechanism in mould deformation occurred. Furthermore, higher average pressure distribution inside the cavity, is required to inject the Polycarbonate, due to its higher viscosity in comparison with the Polystyrene. This occurrence also led to larger thickness displacement. However, in attempting to improving the accuracy of simulation in the injection moulding tests, for the Polycarbonate, taking into account mould deformation, the same approach adopted in § IV.2.2, has shown that a higher correction of the compressibility factor (eq.4.13) of the Polycarbonate was expected to obtain a reliable reproduction of experimental pressure curves. In the following **Fig.67** , a comparison between the experimental pressure curve (A) for PC Lexan 141R (for the middle cavity position) and simulated ones, are reported. **Fig. 67 B** shows the simulated pressure profile which was obtained by adopting (eq 4.13) the same mould compliance used for the simulation of the PS 678E tests, for the Polycarbonate compressibility correction. In **Fig. 68 C**, the simulated pressure curve was obtained by adopting a mould compliance estimated by the experimental approach based on the line plot slope in **Fig. 66** for the correction of Polycarbonate compressibility factor.

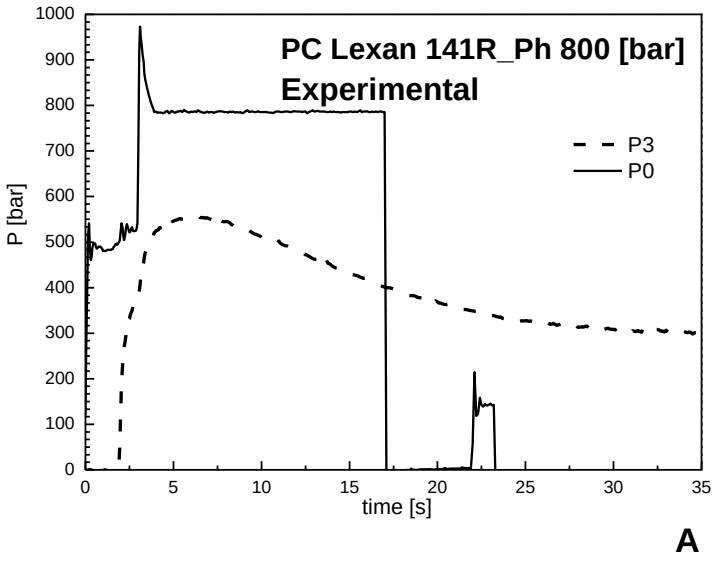

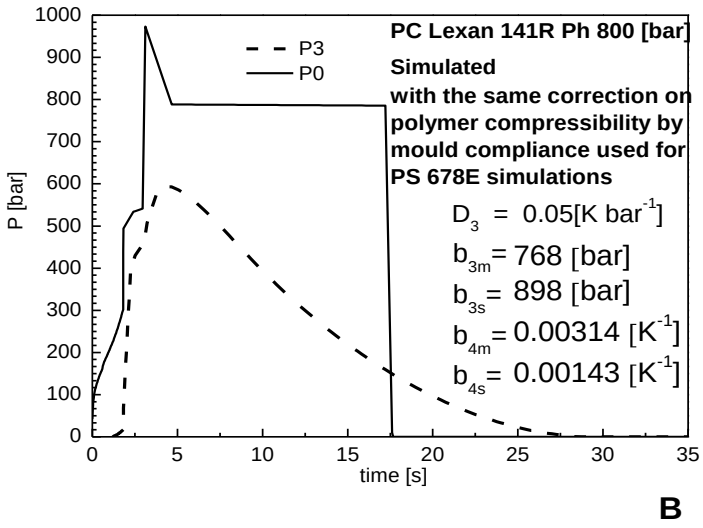

Fig. 67 Comparison between the experimental pressure curve (A), and simulated ones for PC Lexan 141R, using the same correction on polymer compressibility than PS 678E (B)

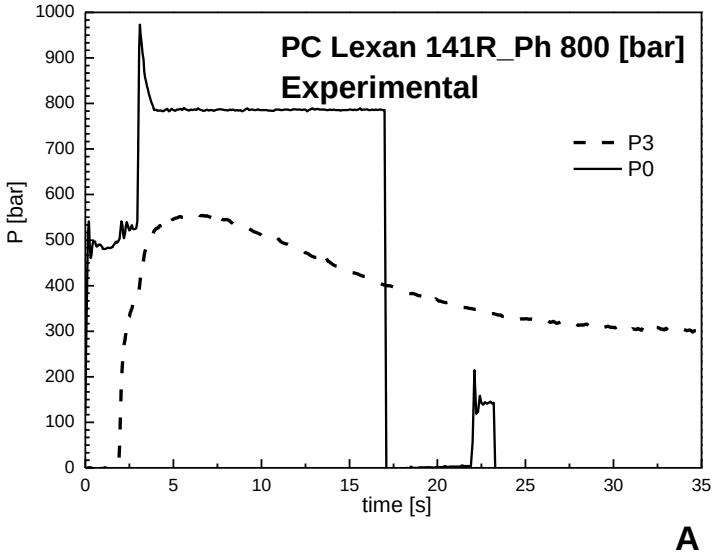

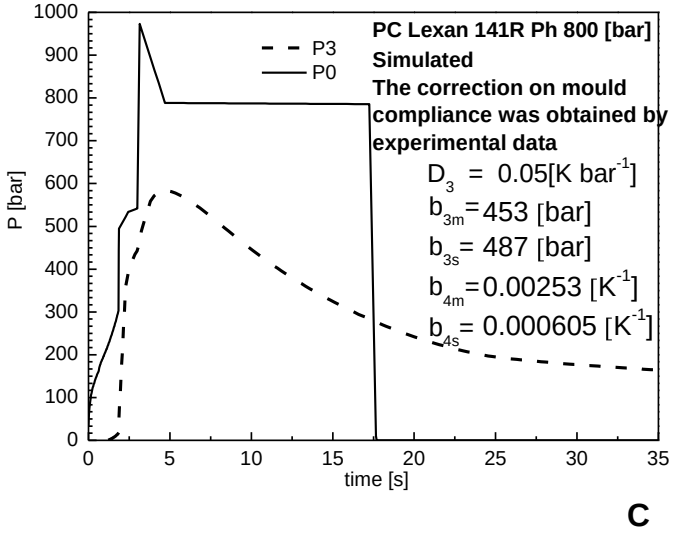

Fig. 68 Comparison between the experimental pressure curve (A), and simulated ones for PC Lexan 141R (C), using the correction on polymer compressibility by adopting a mould compliance estimated by the experimental approach based on the line plot slope, showed in **Fig.65**

VII.4 Relevance of the results of normalized part weight vs pressure at the gate freezs off time for PP BA 238GE.

In **Fig. 69**, the Excess of Normalized part weight (or volumetric shrinkage) vs P_{gf} for PP BA238 GE, are plotted. Except for some data, belonging to shorter post pressure conditions, which, led to lighter samples, (probably due to the backflow of polymer toward the runner), the approach based on the eq (7.12) for part weight data description, led to a satisfactory correlation with P_{gf},. The line slope for estimating the mould compliance (referring to the smaller cavity thickness), gives a value of nearly 1 10^{-3} [MPa^{-1}] which was consistent with the values estimated by considering the PS 678E data.

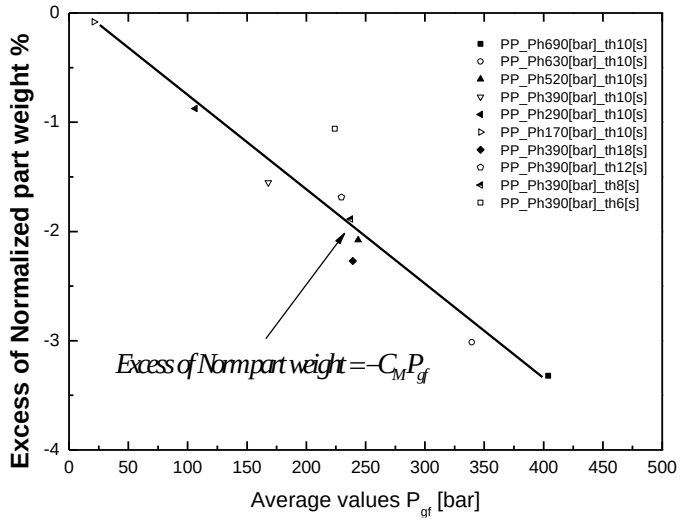

Fig. 69 Normalized part weight percentage (volumetric shrinkage) vs Average values of Pressure at gate freeze off time, for PP BA 238GE series, (referred to M_0=6.5 [g]).

Chapter Eight

Conclusions

This chapter contains a summary of the work done, together with the main conclusions.

In this work an attempt was made to find a single operative process parameter able to describe the effect of processing conditions on product quality, in terms of in-plane shrinkage. For this purpose, a series of injection moulding tests were conducted by adopting a general purpose Polystyrene changing holding pressure and time, injection time, mould and injection temperature, nozzle length, gate and cavity thickness. These tests have been performed using an instrumented research mould, equipped with pressure and temperature transducer, and a DAQ device used for acquiring their signals along the flow path. Furthermore the width dimensions of the moulded specimens were measured for their Position corresponding to the sensors ones, and the width shrinkage values were obtained. Reporting the width shrinkage results versus a single value of pressure such as the hydraulic or the holding pressure, it has been shown that neither the width shrinkage differences inside the cavity nor the effect of the holding time on width shrinkage could be described. The same analysis was extended to the experimental pressure and width shrinkage data referring to Polycarbonate and semi-crystalline material like Polypropylene and the results confirmed what was stated above about Polystyrene data. Therefore it was demonstrated, as generalized results, that no parameter based on the analysis of the pressure curve alone could be adopted to describe in-plane shrinkage, independently of the characteristics of the polymer.

Ulterior research tasks led us to consider a different approach for our purpose, which was based on knowledge of the local pressure history (experimentally obtainable) and knowledge of the local solidification history (not experimentally obtainable), which determine the local average solidification pressure Ps_av. With regard to the local solidification history, a twofold approach was adopted for calculating it, based on its definition. In the first approach, Ps_av was calculated using the experimental pressure curves, jointly with the corresponding simulated solidification history described by Moldflow. Therefore each experimental test, was simulated, and on the basis of a comparison of the pressure curves, a good agreement was observed among them. In order to make an independent assessment using the simulation software, an alternative approach was adopted. A procedure, based on the Labview© platform, not requiring the simulation of the whole injection moulding test and based on the knowledge of the local experimental pressure profile and the polymer thermal diffusivity, was developed to evaluate the local solidification profile, and thus, the Ps_av values. The width shrinkage data reported versus the average solidification pressure Ps_av values (calculated in either way), show the suitability of this parameter in describing in-plane shrinkage in a very wide range of operating conditions. The procedure was also adopted for calculating Ps_av values through experimental pressure data using either Polycarbonate or Polypropylene. Although, the investigated range of operating conditions was smaller, the measurement of the results demonstrates that the Ps_av has a

pivotal role in describing in plane shrinkage of the injected moulded product. As regards the sample weight, it was shown that for samples having a positive average width shrinkage, weight is directly related to width shrinkage, and thus to P_{sav}. However, for samples showing an expansion a further analysis was needed. With regard to this , as was suggested in the literature, it was shown that cavity deformation plays a pivotal role, so the normalized part weight can be directly correlated to the average pressure inside the cavity at the instant when the gate solidifies, namely, P_{gf}. This approach used for analyzing sample weight data was extended to all the polymeric materials considered, and results as being a reliable model for describing the part weight of samples in the injection moulding process.

References

Agralwal, A. R., I. O. Pandelidis, and M. Pecht. "Injection-Molding Process Control-A Review." *Polymer Engineering & Science* 27 (1987): 1345–1357.

Barber Colman Company. "MaCo 485 DDE Server." 2003.

Bushko, W.C., and V. K. Stokes. *Polymerer Engineering & Science* 35, no. 4 (1995): 365-383.

Carpenter et al. "Effect of machine compliance on mold deflection during injection and packing of thermoplastic parts". *Polymer Engineering & Science* 46 no.7 (2006): 844-852.

Carslaw, H. S., and J. C. Jaeger. *Conduction of Heat in Solids.* 2nd. Oxford: Oxford University Press, 1978.

Chen, Z., and L.-S. Turng. "A Review of Current Developments in Process and Quality Control for Injection Molding." *Advances in Polymer Technology* 24, no. 3 (2005): 165-182.

Cheng-H. W., Yu-Jen H.. "The influence of cavity deformation on the shrinkage and warpage of an injection-molded part". *International Journal of Advanced Manufacturing Technology* 32, no.11-12 (2007): 1144-1154.

Delaunay et al. "Nature of contact between polymer and mold in injection molding. Part II: Influence of mold deflection on pressure history and shrinkage". *Polymer Engineer & Science* 40 no 7 (2000): 1692-1700.

De Santis, F., R. Pantani, V. Speranza, and G. Titomanlio. "Analysis of shrinkage development of a semi crystalline polymer during injection moulding." *Industrial Chemical Engineering Research* 49 (2010): 2469–2476.

Flaman, A. A.M. *Build-up and relaxation of molecular orientation in injection molding- PhD. Thesis* . TU Eindhoven, Netherland, 1990.

Gao, F., W. I. Patterson, and M. R. Kamal. "Dynamics and Control of Surface and Mold Temperatures In injection-Molding." *International Polymer Processing* 8, no. 2 (1993): 147-157.

General Electrics Plastic Europe. "A guide to successful injection moulding." 1999.

Harry, D. H. " Injection molding correlation between product properties and process parameters as influenced by random variation ." *Annual Technical Conference - Society of Plastics Engineers 50th(2).* 1992. 2202-2203.

Jansen, K. M.B. "Residual-Stresses in Quenched and Injection – Molded Products." *International Polymer Proccessing* 9, no. 1 (1994): 82-89.
Jansen, K. M.B., and G. Titomanlio. "Effect of pressure history on shrinkage and residual stresses - Injection molding with constrained shrinkage." *Polymer Engineering & Science* 36, no. 15 (1996): 2029-2040.
Jansen, K. M.B., D. J. Van Dijk, and M. H. Husselman. "Effect of processing conditions on shrinkage in injection molding." *Polymer Engineering & Science* 38 (1998): 838-846.
Jansen, K. M.B., R. Pantani, and G. Titomanlio. "As-Molded Shrinkage Measurements on Polystyrene Injection Molded Products." *Polymer Engineering & Science* 38, no. 2 (1998).
Kamal, Musa R.I., Alfredo E. Varela, and W. Ian Patterson. "Control of Part weight in injection molding of amorphous thermoplastics." *Polymer Engineering & Science* 39, no. 5 (1999): 940 - 952.
Kelly, A. L., M. Woodhead, and P. D. Coates. "Comparison of injection molding machine performance." *Polymer Engineering and Science* 45, no. 6 (2005): 857-865.
Laven, J. *Nonisothermal Capdby Flow of Plastics, Ph.D thesis.* Delft University, Netherlands , 1985.
Leo, Cuvelliez. *The effect of the packing parameters, gate geometry, and mold elasticity on the final dimensions of a molded part.* Polymer Engineering & Science 36, no.15, (1996): 1961-1971.
Macfarlane, S., R. Dubay. «The Effect of Varying Injection Molding Conditions on Cavity Pressure.» *SPE ANTEC.* Orlando FLO (USA), 2000. 653-657.
Milacron Inc. "Xtreem XP." 2003.
MoldFlow Plastic Insight . "database ver.6.1." 2006.
Montell Polyolefins. "Development Data." (1998).
Oliveira, P. *Analisi del ritiro di manufatti in Polycarbonato prodotti per stampaggio ad iniezione. Master degree Thesis in Chemical Engineering* . University of Salerno, Italy, 1999.
Pantani, R. *Analysis of Shrinkage Development" Ph.D Thesis¬.* University of Salerno , Italy, 1999.
Pantani, R., G. Titomanlio. «Description of P-V-T behaviour of an industrial Polypropylene-EPR Co-Polymer in process conditions .» *Journal Applied Polymer Science* 81, n. 2 (2001): 267-278.
Pantani, R., F. De Santis, V. Brucato, e G. Titomanlio. «Analysis of gate freeze-off time in injection moulding.» *Polymer Engineering & Science* 44 (2004): 1-17.

Pantani, R., V. Speranza, and G. Titomanlio. "Relevance of mold-induced thermal boundary conditions and cavity deformation in the simulation of injection molding." *Polymer Engineering & Science* 41, no. 11 (2001a): 2022-2035.

Pantani, R., V. Speranza, and G. Titomanlio. "Relevance of Crystallization Kinetics in the Simulation of the Injection Molding Process". Munich: Hanser Publishers, 2001 b.

Pontes, A. *Shrinkage and Ejection Forces in injection Moulded Product- Ph.D Thesis,*. University do Minho, Portugal, 2002.

Pramujati, B., R. Dubay, and C. Samaan. "Cavity pressure control during cooling in plastic injection molding." *Advances in Polymer Technology* 25, no. 3 (2006): 170-181.

Rawabdeh, I. A., and P. F. Petersen. "In-line Monitoring of Injection Molding Operations: A Literature Review." *The Journal of Injection Molding Technology* 3, no. 2 (1999): 47-53.

Sorrentino A., Pantani R. "Pressure dependent viscosity and free volume of atactic and syndiotactic polystyrene." *Rheologica Acta* 48, no. 4, (2009).

Titomanlio, G., and K. M.B. Jansen. "In-mould shrinkage and stress prediction in injection moulding." *Polymer Engineering Science* 36, no. 16 (1996): 2041-2049.

Titomanlio, G., V. Brucato, and M. R. Kamal. "Mechanism of cooling stress build-up in injection moulding of thermoplastic polymers." *International Polymer Process*, 1987: 55-59.

Van Krevelen, D.W. "Properties of Polymers:their correlation with chemical structure, their numerical estimation and prediction from additive group contributions". *Elsevier Amsterdam 3rd edition* (1997).

Wang, K. K., . Zhou, and Y. Sakurai. "An Integrated Adaptive Control for Injection Molding." *SPE ANTEC.* 1999. 611-615.

Wang, K. K., C. A. Hieber, N. Wang, J. Zhou, M. C. Lee, e Y. Sakurai. «In Cornell Injection Molding Program Progress.» Report No. 21 Ch. XI, 2000.

www.materialdatacenter.com. "www.materialdatacenter.com."

Zoetelief. *Multi-component injection moulding Ph.D Thesis.* TU Eindhoven, Netherland, 1995.